DOE/NASA/0167-81/3
NASA CR-167901
GARRETT NO. 31-3725(3)

ADVANCED GAS TURBINE (AGT) POWERTRAIN SYSTEM DEVELOPMENT FOR AUTOMOTIVE APPLICATIONS

8/6/82

THIRD SEMIANNUAL PROGRESS REPORT
(JANUARY 1981 — JUNE 1981)

1/31/83
6/mk3

Engineering Staff of
Garrett Turbine Engine Company
A Division of The Garrett Corporation

December 1981

Prepared for

NATIONAL AERONAUTICS AND SPACE ADMINISTRATION
Lewis Research Center
Cleveland, Ohio 44135
Under Contract DEN3-167

for

U.S. DEPARTMENT OF ENERGY
Office of Vehicle and Engine Research and Development
Technology Development and Analysis Division
Washington D.C. 20585

DOE/NASA/0167-81/3
NASA CR-167901
GARRETT NO. 31-3725(3)

ADVANCED GAS TURBINE (AGT) POWERTRAIN SYSTEM DEVELOPMENT FOR AUTOMOTIVE APPLICATIONS

THIRD SEMIANNUAL PROGRESS REPORT
(JANUARY 1981 — JUNE 1981)

Engineering Staff of
Garrett Turbine Engine Company
A Division of The Garrett Corporation

December 1981

Prepared for
NATIONAL AERONAUTICS AND SPACE ADMINISTRATION
Lewis Research Center
Cleveland, Ohio 44135
Under Contract DEN3-167

for
U.S. DEPARTMENT OF ENERGY
Office of Vehicle and Engine Research and Development
Technology Development and Analysis Division
Washington D.C. 20585

TABLE OF CONTENTS

		Page
1.0	SUMMARY	1
2.0	INTRODUCTION	6
3.0	POWERTRAIN DEVELOPMENT	8
3.1	Mod I Build 1 Engine Fabrication and Test	8
3.2	Performance	8
4.0	COMPONENT/SUBSYSTEM DEVELOPMENT	12
4.1	Compressor Development	12
4.1.1	Compressor Inlet Guide Vane Testing	12
4.1.2	Compressor Rig Testing	13
4.1.3	Powder Metal Aluminum	14
4.2	Turbine	15
4.2.1	Cold Turbine Test Rig	15
4.2.2	Test Procedure	17
4.2.3	Mod I Build 1 Test Results	18
4.2.3.1	Inlet Transition Duct	18
4.2.3.2	Turbine Exhaust System	20
4.3	Combustion	24
4.3.1	Diffusion Flame Combustor Testing	25
4.3.2	Variable Geometry (RPD Combustor)	28
4.4	Regenerator System	31
4.4.1	Ford Regenerator Development	31
4.4.2	Garrett Regenerator Development	33
4.4.2.1	Regenerator LP Cold Rig Testing	35
4.4.2.2	Regenerator HP Cold Rig Testing	36
4.4.2.3	Regenerator Analysis	37
4.4.3	Regenerator Hot Test Rig	42
4.5	Gearbox/Transmission	42
4.6	Ceramic Material and Component Development	42
4.6.1	Ceramic Structures	42

TABLE OF CONTENTS (Contd)

		Page
4.6.1.1	Structures Rig	42
4.6.1.2	Screening Rigs	43
4.6.1.3	Contact Stress Rig	43
4.6.1.4	Ceramic Parts and Testing	43
4.6.1.5	Ceramic Handling Training	46
4.6.2	Ceramic Turbine Rotor	46
4.6.2.1	Simulated Rotors	46
4.6.2.2	Strength of Alternate Carborundum Rotor Materials	49
4.6.3	Subcontractor Ceramic Development	51
4.6.3.1	Ford Motor Company	51
4.6.3.2	AiResearch Casting Company	51
4.6.3.3	Carborundum Company	51
4.7	Foil Gas Bearings	51
4.8	Bearings and Seals	51
4.9	Rotor Dynamics Development	52
4.10	Controls and Accessories	53
4.10.1	Systems Analysis	53
4.10.2	Fuel System	54
4.10.2.1	Outside Supplier Inquiry	54
4.10.2.2	Technical Progress	54
4.10.3	Electrical Accessories	56
4.10.4	Mechanical Accessories	56
4.10.5	Electronic Control	57
Appendix A -	Ford Motor Company Advanced Gas Turbine Powertrain System Development Program Third Semiannual Technical Progress Report	59
Appendix B -	AiResearch Casting Company Advanced Gas Turbine Powertrain System Development Program Third Semiannual Technical Progress Report	67
Appendix C -	The Carborundum Company (Unique Work) Advanced Gas Turbine Powertrain System Development Program Third Semiannual Progress Report	73
References		77

LIST OF ILLUSTRATIONS

Figure	Title	Page
1	AGT101 Powertrain	1
2	AGT101 Power Section Layout	3
3	AGT101 Gearbox and Transmission Layout	4
4	AGT101 Ceramic Evolution	4
5	AGT101 Program Schedule	7
6	Mod I Build I Critical Component Schedule	8
7	Mod I Build 1 Metal Castings	9
8	AGT101 Engine Test Cart	10
9	AGT101 Hydraulic Test Cart	10
10	AGT101 Lubrication Cart	10
11	AGT101 Mod I Build 1 Performance (85°F, Sea Level, DF-2)	11
12	AGT101 Performance Rating Stations	12
13	AGT101 Compressor Inlet Guide Vane Test Rig	12
14	Inlet Guide Vane Flow Tabs	13
15	Inlet Guide Vane Test Results	13
16	Compressor Test Rig Cross Section	13
17	Compressor Test Rig	13
18	Tensile Properties of Forged Alcoa AL-Fe-Ce	14
19	Alcoa AL-FE-Ce Forged Properties (1000 Hour Temperature Exposure)	14
20	Tensile Properties of Aluminum Alloys	15
21	Stress Rupture Properties of Aluminum Alloys	15
22	HCF Properties of Alcoa AL-Fe-Ce	15
23	Performance Prediction Computer Models for the Three AGT101 Turbine Configurations	17
24	Turbine Component Cold Air Test Rig, Instrumentation List and Instrumentation Planes	19
25	Turbine Component Cold Air Test Facility Schematic	19
26	Torquemeter and Readout System	20
27	AGT101 Test Rig Installed in Test Cell	20
28	AGT101 Test Rig Installed in Test Cell	21
29	AGT101 Mod I Build 1 Turbine System Efficiency Characteristics	21
30	AGT101 Turbine Flow Function and Efficiencies at Low Idle (N_{eng} = 50,000 rpm)	21
31	AGT101 Turbine Flow Function and Efficiencies at Design Idle (N_{eng} = 55,000 rpm)	21
32	AGT101 Turbine Flow Function and Efficiencies at Low Cruise (N_{eng} = 60,000 rpm)	22
33	AGT101 Turbine Flow Function and Efficiencies at Design Cruise (N_{eng} = 65,000 rpm)	22
34	AGT101 Turbine Flow Function and Efficiencies at Maximum Power (N_{eng} = 100,000 rpm)	22
35	Inlet Duct P_s Distribution	22
36	AGT101 Turbine Exhaust System Loss Comparisons	23

LIST OF ILLUSTRATIONS (Contd)

Figure	Title	Page
37	Diffusion Flame Combustor	25
38	Combustion Test Rig	25
39	Baseline Combustor	26
40	Diffusion Flame Combustor Predicted Streamlines, Idle Condition	26
41	Diffusion Flame Combustor Predicted Isothermal Lines, Idle Condition	26
42	Diffusion Flame Combustor Predicted Fuel/Air Ratio, Idle Condition	26
43	Diffusion Flame Combustor Mod A Predicted Streamlines, Idle Condition	27
44	Diffusion Flame Combustor Mod A Predicted Isothermal Lines, Idle Condition	27
45	Diffusion Flame Combustor Mod A Predicted Fuel/Air Ratio, Idle Condition	27
46	Diffusion Flame Combustor Mod A Airflow Split	27
47	Diffusion Flame Combustor Mod A Test Results	28
48	Temperature Probe	28
49	Diffusion Flame Combustor Mod A Temperature Data	28
50	Ignition	29
51	Preheater CO Values	29
52	Preheater NO_x Values	29
53	Duplex Airblast Fuel Nozzle	30
54	1.77-Inch Diameter Fuel Nozzle - Effect of Nozzle Inlet Temperature	30
55	1.77-Inch Diameter Fuel Nozzle - Effect of Nozzle Inlet Temperature	30
56	1.77-Inch Diameter Fuel Nozzle - Effect of Pressure Drop	31
57	1.77-Inch Diameter Fuel Nozzle - Effect of Pressure Drop	31
58	2.0-Inch Diameter Fuel Nozzle - Effect of Nozzle Inlet Temperature	31
59	2.0-Inch Diameter Fuel Nozzle - Effect of Nozzle Inlet Temperature	31
60	Crossarm Diaphragm Location	32
61	Static Seal Leakage Test Results	33
62	Regenerator Drive and Support System Bearing Designs	33
63	Regenerator Core Stagnation Pressure Measuring Technique	34
64	Measured LP ΔP Data from Regenerator Cold Rig	35
65	LP Regenerator Cold Rig Upstream Diverter	36
66	LP Regeneration Cold Rig, Effects of Upstream Diverter	36
67	HP Regenerator Cold Rig Flow Effects of Bonnet	36
68	Measured HP ΔP Data from Regenerator Cold Rig with Bonnet	37
69	Measured Analytical Flow Distortion Model	37
70	Measured HP ΔP Data from Regenerator Cold Rig	38
71	Measured LP ΔP Data from Regenerator Cold Rig	38
72	Capacity Rate Ratio and Integrated Mass Flux Versus Radial Position	39
73	AGT101 Mod II Predicted Regenerator Discharge Gas Isotherms for the Cruise Condition Based on Cold Rig Pressure Distortion Patterns	39
74	AGT101 MOD II Predicted Regenerator Local Core Mass Velocities for the Cruise Condition Based on Cold Rig Pressure Distortions	39

LIST OF ILLUSTRATIONS (Contd)

Figure	Title	Page
75	Effect of Linear Radial Distortion on Regenerator HP Effectiveness	41
76	Effect of Measured HP and HP Distortion on Effectiveness and Fuel Flow	41
77	Regenerator Hot Test Rig	42
78	2000°F Structures Rig	43
79	AGT101 Strain Gauged Regenerator Shield and Screening Rig	43
80	AGT101 Screening Rig/Strain Gauged Turbine Backshroud	44
81	NGK Backshroud Strain Gauged for Screen Testing	44
82	ACC RBSN Stators During Cooldown Following Oxyacetylene Torch Heating	45
83	Fracture Faces of Two ACC SNN-502 Test Bars from Rotor S/N 3311 Tested at Room Temperature	47
84	ACC SNN-502 Simulated Rotor S/N 02061-1 After Successful 115,000 RPM Proof Spin	47
85	AGT Simulated Rotor (ACC Si_3N_4) Maximum Principal Stress at 115,000 RPM	48
86	Weibull Flexure Results for Pure Carbon Turbine Rotor S/N 4	48
87	Refel Rotor S/N 4 Microstructure	49
88	Refel Rotor S/N 1	49
89	Carborundum Hot Pressed α-SiC Test Bar Fracture Surfaces	50
90	As-Polished and Etched Microstructure of Carborundum Fine Grain RSSiC (Hexoloy KX-01)	52
91	AGT101 Fuel Control (Breadboard Unit) High Pressure Flowstream Between Pump Discharge and Atomizer Showing Entrained Air and Trapped Air at Top of Tube	55
92	AGT101 Fuel Control (Breadboard Unit) High Pressure Flowstream After Incorporation of Pressurizing Valve Ahead of Atomizer Showing Disappearance of Entrained Air with a Small Bubble Remaining	56
93	Test Bars of RM-1 Material Before and After Oxidation	59
94	Oxidation Weight Gain of RM-1 Material After 300 Hours of Testing	59
95	Strength of RM-1 Material Before and After 300 Hours of Oxidation at 700°C and 1000°C	60
96	Effects of Using of a Slip Suspending Agent on Nitrided Density Gradients in Simulated Rotors	61
97	Sectioned Simulated Rotor Showing Uniform Structure	61
98	Sectioned Simulated Rotor Showing Non-Uniform Structures	61
99	Bladed Rotors After Nitriding	62
100	Sintered Bladed Rotor	62
101	Nitrided Bladed Rotor Incorporating Shrinkage Allowance	62
102	Burst of Simulated Rotor Number 57 at 95,170 rpm	63
103	Simulated Rotor Number 199 After Spin Test to 134,000 rpm	63
104	Principal Stresses in Simulated Rotor Number 199 at 134,000 rpm	63
105	Simulated Rotor Number 201 After Spin Test to 137,000 rpm	64
106	Ceramic Flow Separator Housing Showing Strain Gauges in Place	65
107	Ceramic Flow Separator Housing Mounted in Mechanical Test Fixture	65
108	Stagnant Air Drying Chamber	68

LIST OF ILLUSTRATIONS (Contd)

Figure	Title	Page
109	ACC AGT101 Simulated Rotors of SNN-522 in the Green and Sintered Condition	69
110	Metal AGT101 Turbine Rotor	69
111	ACC AGT101 Bladed Rotor and a Casting Shell	70
112	First Sintered ACC AGT101 SN-522 Bladed Rotor	70
113	ACC RBSN AGT101 Stators and Test Bars in Nitriding Stack-up	71
114	ACC Slip Cast RBSN AGT101 Turbine Shrouds	72
115	ACC AGT101 Turbine Shroud and Section	72

LIST OF TABLES

Table	Title	Page
1	AGT101 Mod II Component Design Summary (Maximum Power)	2
2	AGT101 Powertrain Summary	5
3	AGT101 Turbine Stage Configuration Comparison	16
4	Mod I Build 1 Turbine Cold Rig Versus Engir - Operating Conditions at Critical Engine Operating Points	18
5	AGT101 Mod I Build 1 Turbine Test Data Matrix	20
6	Summary of AGT101 Mod I Build 1 Turbine Exhaust System Performance (Cold Rig Test)	24
7	Comparison of Rig to Engine Combustor Inlet Conditions	25
8	Combustor Inlet Conditions for a 85°F Day Cold Start as a Function of Engine Speed	29
9	Regeneration Analysis Summary	40
10	Results of NGK SN-50 Flexure Testing	45
11	ACC SNN 502 Simulated Rotor Summary	47
12	Pure Carbon Refel Rotor Summary	48
13	Weibull Parameters Obtained from Flexural Tests on Bars Cut from Hot-Pressed Rotor Cores	49
14	Weibull Parameters Obtained from Flexural Tests on Fine Grain Siliconized SiC (Hexoloy KX-01)	51
15	Repeatability Tests 3-Piston and Metering Valve	57
16	Slip Casting Parameters to be Evaluated	69
17	Silicone Carbide Materials Evaluated for Simulated Rotor	74

1.0 SUMMARY

This report describes progress and work performed by the Garrett/Ford team to develop an Advanced Gas Turbine (AGT) powertrain system for automotive applications, for the period January through June 1981. This work was performed for the Department of Energy under NASA Contract DEN3-167. This is the third in a series of semiannual reports. Work performed during the first two periods (References 1 and 2) initiated design and analysis, ceramic development and component testing.

During this reporting period, accomplishments included:

- Completion of all hardware procurement for the Mod I Build 1 metal engine
- Initiation of Mod I Build 1 engine assembly
- Successful cold spin tests of ACC and Ford ceramic simulated rotors to qualification test speed (115,000 rpm)
- Initiation of ceramic bladed turbine rotor development by ACC and Ford
- Completion of diffusion flame combustor and Mod I Build 1 turbine component tests, and initiation of compressor and rotor dynamics component rig tests in support of the Mod I Build 1 metal engine
- Initiation of ceramic structures screening tests
- Continuation of regenerator static seal leakage and seal wear evaluation tests at Ford
- Continuation of ceramic subcontractor efforts to develop material strengths and fabrication processes for the ceramic turbine rotor and ceramic structures
- Priority planning of project work to accommodate budget constraints

The Garrett/Ford project efforts were modified during March 1981 to accommodate imposed budget constraints. The primary changes involved reducing first generation component tests, deferral of gearbox and transmission systems development, and stopping vehicular integration activities. These changes permitted concentration of remaining resources toward continued development of higher technology components and ceramics necessary for the AGT engine. As noted herein, progress through June 1981 indicates that AGT engine performance goals will be achieved. Mod I Build 1 engine tests are scheduled to begin in July 1981.

Salient features of the AGT powertrain system, as noted in References* 1 and 2, are repeated in the remainder of this section as a ready summary for the reader. No significant changes have been made to the design, or performance predictions, during this reporting period.

The AGT101 Powertrain, pictorially shown in Figure 1, consists of a regenerated single-shaft gas turbine engine power section (flat-rated at 100 horsepower), a split differential gearbox, and a Ford Automatic Overdrive (AOD)

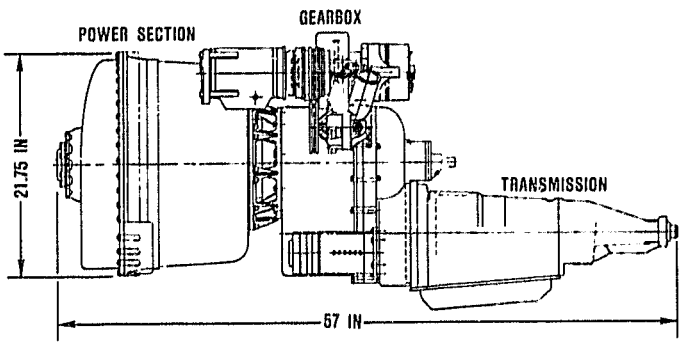

Figure 1. AGT Powertrain.

*A list of references is included immediately following Appendix C.

TABLE I. AGT101 MOD II COMPONENT DESIGN SUMMARY (MAXIMUM POWER)

COMPRESSOR - CENTRIFUGAL	
Material	Aluminum
Design flow, lbs/sec	0.85
Number of blades/splitters	12/12
Backward curvature, degrees	50
VIGV type, number of vanes	Articulated, 17
Diffuser type	2-D vane island, cascade deswirl
Predicted stage efficiency, percent	80.5
TURBINE - RADIAL INFLOW	
Material	SiC or Si_3N_4
Maximum inlet temperature, °F	2500
Maximum tip speed, ft/sec	2300
Number of blades	13
Stator type, number of vanes	Radial, 19
Diffuser type	Radial
Predicted stage efficiency, percent	90.1
REGENERATOR - ROTARY	
Material, fabrication process	AS or MAS, extruded
Active matrix diameter, inches	18.2
Matrix thickness, inches	3.3
Hydraulic diameter, inches	0.020
Support type, drive	Rim, rim drive
Predicted effectiveness, percent	92.9
Predicted seal leakage, percent	3.6
COMBUSTOR - PILOTED, VARIABLE GEOMETRY	
Material	Ceramic
Outlet temperature, °F	2150 to 2500
Maximum primary zone temperature, °F	3000
BALL BEARING - SPLIT INNER RACE, ANGULAR CONTACT	
Material	52100
Size, mm	15
Maximum load - radial/axial, lbs	9/255
FOIL BEARING	
Number of foils	7
Diameter, inches	1.35
Length, inches	1.075
Maximum load - steady state, lbs	3
Maximum load - shock, g's	X6

production transmission. The powertrain is controlled by an electronic digital microprocessor and associated actuators, instrumentation, and sensors. Standard automotive accessories are driven by engine power provided by an accessory pad on the gearbox.

The AGT101 power section, Figure 2, is characterized by a single-stage, 5:1 pressure ratio, backward-swept centrifugal compressor and single-stage ceramic radial inflow turbine mounted on a common shaft. The rotating group is supported by an angular-contact ball bearing at the output pinion gear and an air-lubricated foil bearing located between the compressor and turbine. The AGT101 maximum rotor speed is 100,000 rpm. The combustor, regenerator, and hot-section structural components and radial turbine rotor are made of high temperature ceramic materials. This allows engine operation at turbine inlet temperatures (TIT) of 2500°F (maximum power) and 2150°F (idle) to maintain maximum thermodynamic cycle efficiency over the operating range. Variable geometry is utilized in the compressor and combustion sections to vary engine airflow and control combustion primary-zone temperatures to approximately 3000°F. Table 1 summarizes the power section features.

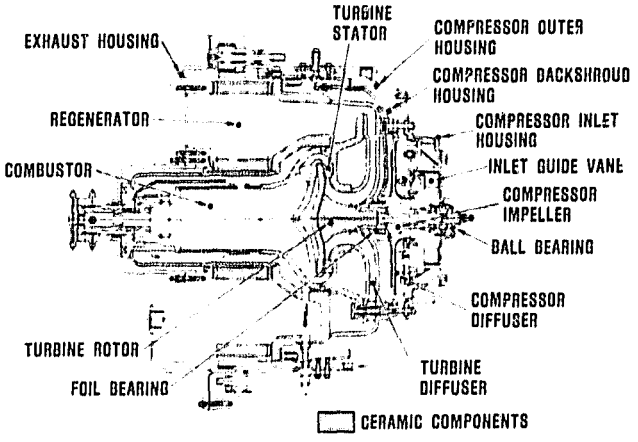

Figure 2. AGT101 Power Section Layout.

The gearbox, Figure 3, is a split-path differential design accepting power directly from the output pinion gear. Power is split in the differential planetary gears with a portion taken through an output gear on the planetary carrier directly to the AOD transmission. The remaining power continues via the same differential planetary to a rotating ring gear and associated gear train to the variable stator torque converter (VSTC). The VSTC provides a variable speed ratio output that is fed back to the planetary carrier and combines with the power delivered to the transmission.

AGT101 powertrain development was initiated in October 1979 through detail design activities based on prior studies. Design efforts on the reference powertrain design (RPD) were approved in January 1980 by NASA. Evolutionary progress toward realization of the RPD continued with design approval of the Mod I powertrain concept in April 1980.

As shown in Figure 4, AGT101 evolution begins with the Mod I Build I all-metallic (except regenerator) engine version. As ceramic hot-section structural components are qualified in dedicated test rigs, the Mod I Build I is selectively upgraded to the Mod I concept (2100°F TIT, metal rotor, ceramic structures). This stepwise evolutionary process enables early verification of component technology development, controls interface, and computer programs used to predict engine performance. In addition, based on "systems design" philosophy, wherein distinct recognition is given to the AGT101 operating range over the combined federal driving cycle (CFDC), an interactive component/engine design feedback loop is established to further optimize program goals (i.e., fuel economy, driveability, emissions, etc). The evolutionary process continues with the introduction of the ceramic radial turbine rotor into the Mod I engine. This configuration, entitled Mod II, currently is equivalent to the RPD. Incorporation of the ceramic rotor will allow TIT to be increased to 2500°F. Table 2 summarizes AGT101 powertrain performance and salient power section features for each configuration.

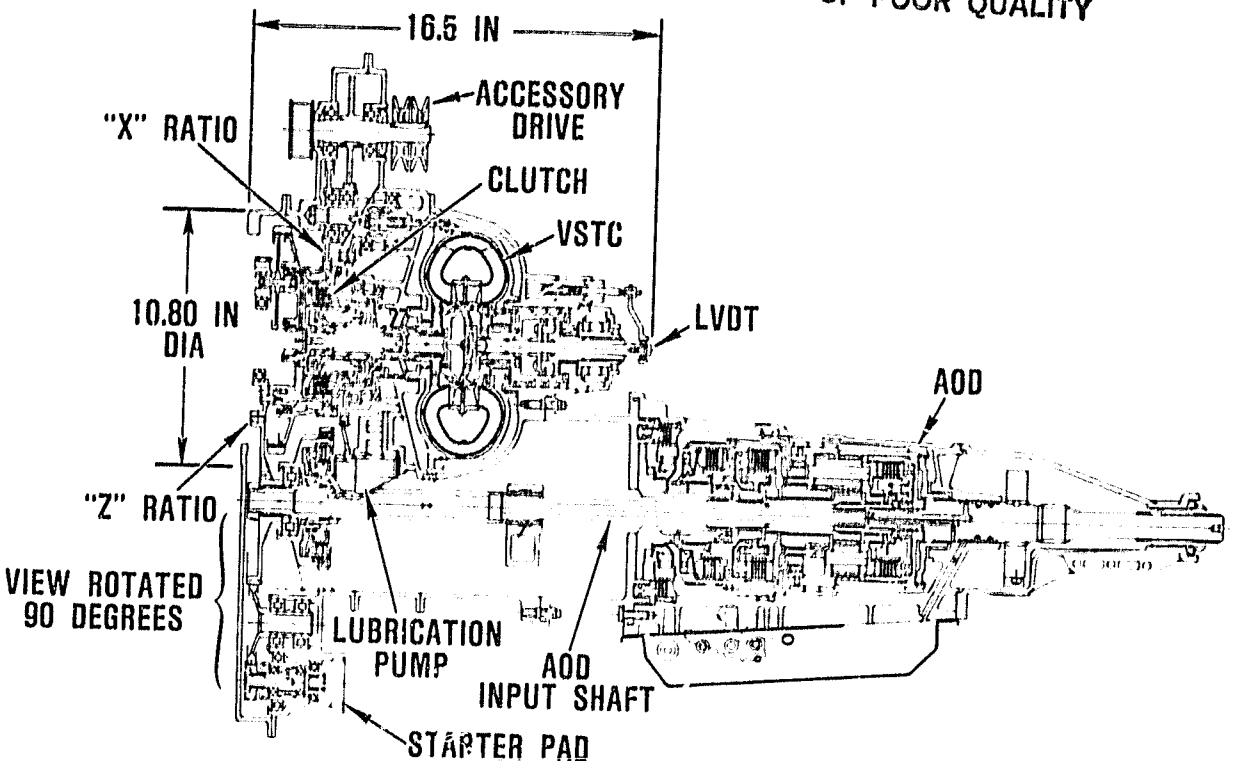

Figure 3. AGT101 Gearbox and Transmission Layout.

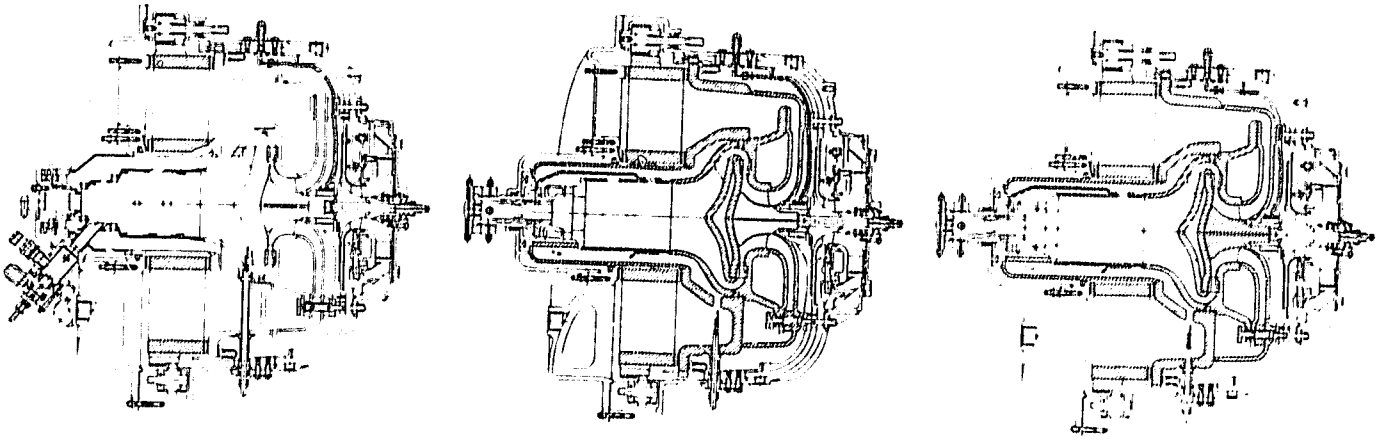

Figure 4. AGT101 Ceramic Evolution.

TABLE 2. AGT101 POWERTRAIN SUMMARY

	Mod I Build 1	Mod I	Mod II	RPD
CFDC (MPG),(DF-2, 59°F, Sea Level 3000 lb, Rear Wheel Drive Vehicle)	N/A	34	42.8	42.8
Cruise SFC	0.503	0.389	0.329	0.329
RPM (Max)	100,000	100,000	86,929	86,929
Maximum Power (HP Net)	50.0	93.6	100.0	100.0
Turbine Inlet Max Temp (°F)	1600	2100	2500	2500
Regenerator Max Temp (°F)	1441	1837	2000	2000
Powersection Configuration				
Compressor	Aluminum 2219T6	Powder Metal Aluminum	Powder Metal Aluminum	Powder Metal Aluminum
Combustor	Diffusion Flame	Variable Geometry	Variable Geometry	Variable Geometry
Turbine	Metal	Metal	Ceramic	Ceramic
Regenerator	Thickwall	Thinwall	Thinwall*	Thinwall*
Structures	Metal	Ceramic	Ceramic	Ceramic
Controls Configuration	Analog	Digital	Digital	Digital

*Extruded Core

2.0 INTRODUCTION

This report is the third in a series of Semiannual Technical Summary reports for the Advanced Gas Turbine (AGT) Powertrain System Development Project, authorized under NASA Contract DEN3-167 and sponsored by The Department of Energy. This report has been prepared by Garrett Turbine Engine Company (hereinafter referred to as Garrett), a Division of The Garrett Corporation, and includes information provided by Ford Motor Company (hereinafter referred to as Ford), The Carborundum Company, AiResearch Casting Company, and The Pure Carbon Company. The project is administered by Mr. Roger Palmer, Project Manager, NASA-Lewis Research Center, Cleveland, Ohio. This report presents progress from January 1981 through June 1981. Brief comments on the effects of budget constraints are also provided, where applicable. The following paragraphs present the original project goals and milestones.

Project effort conducted under this contract is part of the DOE Gas Turbine Highway Vehicle System Program. This program is oriented at providing the United States automotive industry the technology base necessary to produce gas turbine powertrains for automobiles that will have reduced fuel consumption and reduced environmental impact. It is intended that technology resulting from this program be capable of reaching the marketplace by the early 1990's.

The project goal is to develop and demonstrate, by July 1985, an advanced automotive gas turbine powertrain system which, when installed in a 1985 production vehicle of the Ford Fairmont class (3000 pounds inertia weight), meets the following objectives:

- A CFDC fuel economy of 42.8 miles per gallon based on Environmental Protection Agency (EPA) test procedures and diesel No. 2 fuel. The AGT-powered vehicle shall give substantially the same overall vehicle driveability and performance as a comparable 1985 production vehicle powered by a conventional spark-ignition powertrain system (baseline system)
- Gaseous emissions and particulate levels less than:

  NO_X = 0.4 gm/mile
  HC = 0.41 gm/mile
  CO = 3.4 gm/mile

  and a total particulate of 0.2 gm/mile, using the same fuel as used for fuel economy measurements
- Ability to use a variety of alternate fuels

It is intended that AGT powertrains will be demonstrated in dynamometer and vehicle testing at several points during the project. In addition to the demonstratable objectives, the following are system design objectives:

- Reliability and life equal to or better than powertrains currently on the market
- A competitive initial cost and a life cycle cost no greater than that of a comparable conventionally powered vehicle
- Acceleration suitable for safety and consumer considerations
- Noise and safety characteristics that meet currently legislated federal standards and those projected for 1984

Major contract milestones are:

- Complete initial RPD and Mod I powertrain preliminary design review (completed April 30, 1980)
- Complete dynamometer characterization and assessment of first-build Mod I powertrain by July 31, 1982
- Complete dynamometer characterization and assessment of Mod I powertrain by July 31, 1983
- Complete vehicle testing of fuel economy and emissions using the Mod I powertrain system by July 31, 1984 (testing to be performed by the EPA on two vehicles)
- Complete dynamometer characterization and assessment of Mod II powertrain prior to July 31, 1984

- Complete vehicle testing of fuel economy and emissions using the Mod II powertrain system by July 31, 1985 (testing to be performed by the EPA on two vehicles)

The Garrett/Ford Advanced Automotive Gas Turbine Powertrain System has been designated AGT101. The AGT101 represents a significant advancement in gas turbine state-of-the-art. A significant quantity of ceramic parts are employed to enhance high-temperature operation and provide low-cost manufacturing potential for automotive application.

The AGT101 program team is headed by Garrett; the prime contractor responsible for overall powertrain design and development and project management. Ford, as a major subcontractor, is responsible for providing the vehicle-related tasks (i.e., production manufacturing and marketing studies), transmissions, regenerator technology, and major ceramic development efforts. The Corning Company is providing ceramic regenerator cores and one of the major ceramic structural components, under subcontract to Ford. There are three other major subcontractors:

- The Carborundum Company, a Division of Kennecott, located in Niagara Falls, New York, developing and providing ceramic components

- AiResearch Casting Company, located in Torrance, California, also developing and providing ceramic components

- AiResearch Manufacturing Company, located in Torrance, California, developing and providing the electronic control system

The original AGT101 project schedule, shown in Figure 5, includes eight project tasks and six contract milestones with a total project duration of 70 months. A government-directed funding reduction occurred in March 1981 affecting project efforts. A revised schedule will be provided when the funding situation for subsequent years is determined.

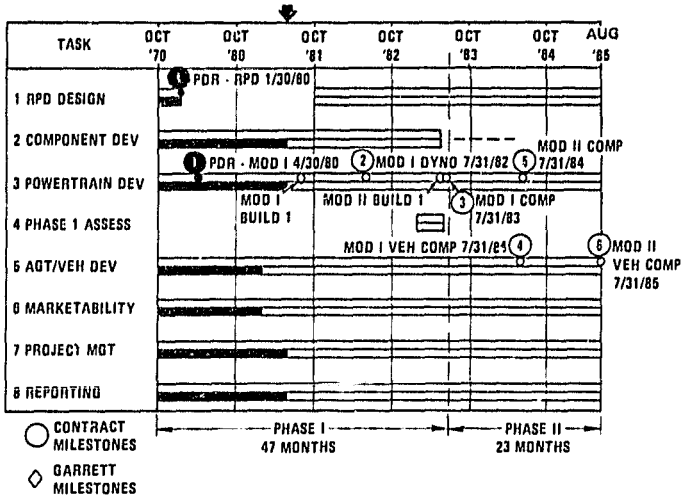

Figure 5. AGT101 Program Schedule.

3.0 POWERTRAIN DEVELOPMENT

As noted in References 1 and 2, AGT101 powertrain development involves numerous sequential and parallel tasks. Powertrain dynamometer and vehicle demonstrations were scheduled at several points throughout the project. However, the aforementioned budget constraints have necessitated a reduction of the planned powertrain development effort. All vehicle activities have been stopped, gearbox and transmission efforts deferred and planned quantities of Mod I and Mod II engines have been reduced.

3.1 Mod I Build 1 Engine Fabrication and Test

During this reporting period, all Mod I Build 1 engine procurement activities have been completed. Figure 6 shows the schedule for each of the eleven major long-lead metal castings, and Figure 7 shows ten of these parts as-received. All hardware, including spares, has been received, inspected and placed in stores.

Assembly of the first Mod I Build 1 all metal engine was initiated in June 1981 and first trial builds have satisfactorily proceeded. Figures 8, 9 and 10 show the engine test cart, hydraulic and lubrication carts, respectively. All activities are on schedule to begin initial cold mechanical checkout tests in July 1981.

3.2 Performance

The predicted Mod I Build 1 (1600°F TIT) engine performance is shown in Figure 11 for idle, cruise and maximum power. Component performance predictions used for Mod I Build 1 cycle analyses were based on 1980 technology levels.

Engine computer programs will be updated as actual component performance data becomes available from rig tests. This will provide the most accurate engine predictions for comparison with actual engine performance.

Also shown in Figure 11 are the SFC curves, as a function of net output horsepower, for the three planned AGT101 engine configurations. As can be seen, improvements in SFC follow the engine evolution (Figure 4) as TIT is increased

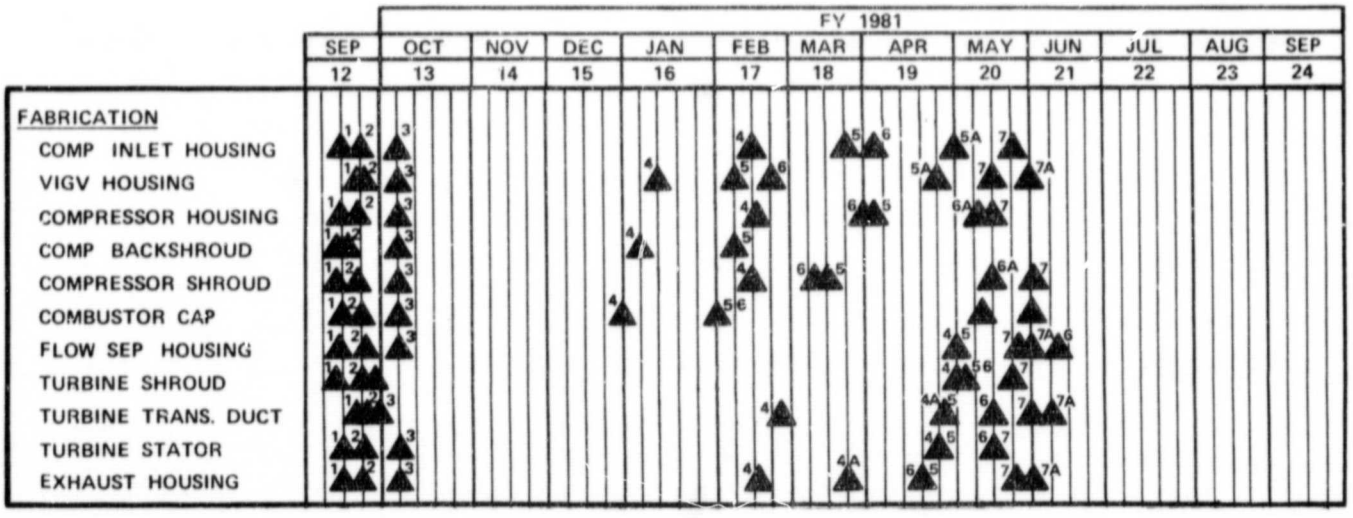

1. DESIGN RELEASE
2. ENGINEERING ORDER
3. TOOL ORDER RELEASED
4. FIRST PARTS
5. MACHINING START
6. CASTING TO SHOP COMPLETE
7. MACHINING COMPLETE

Figure 6. MOD I Build 1 Critical Component Schedule.

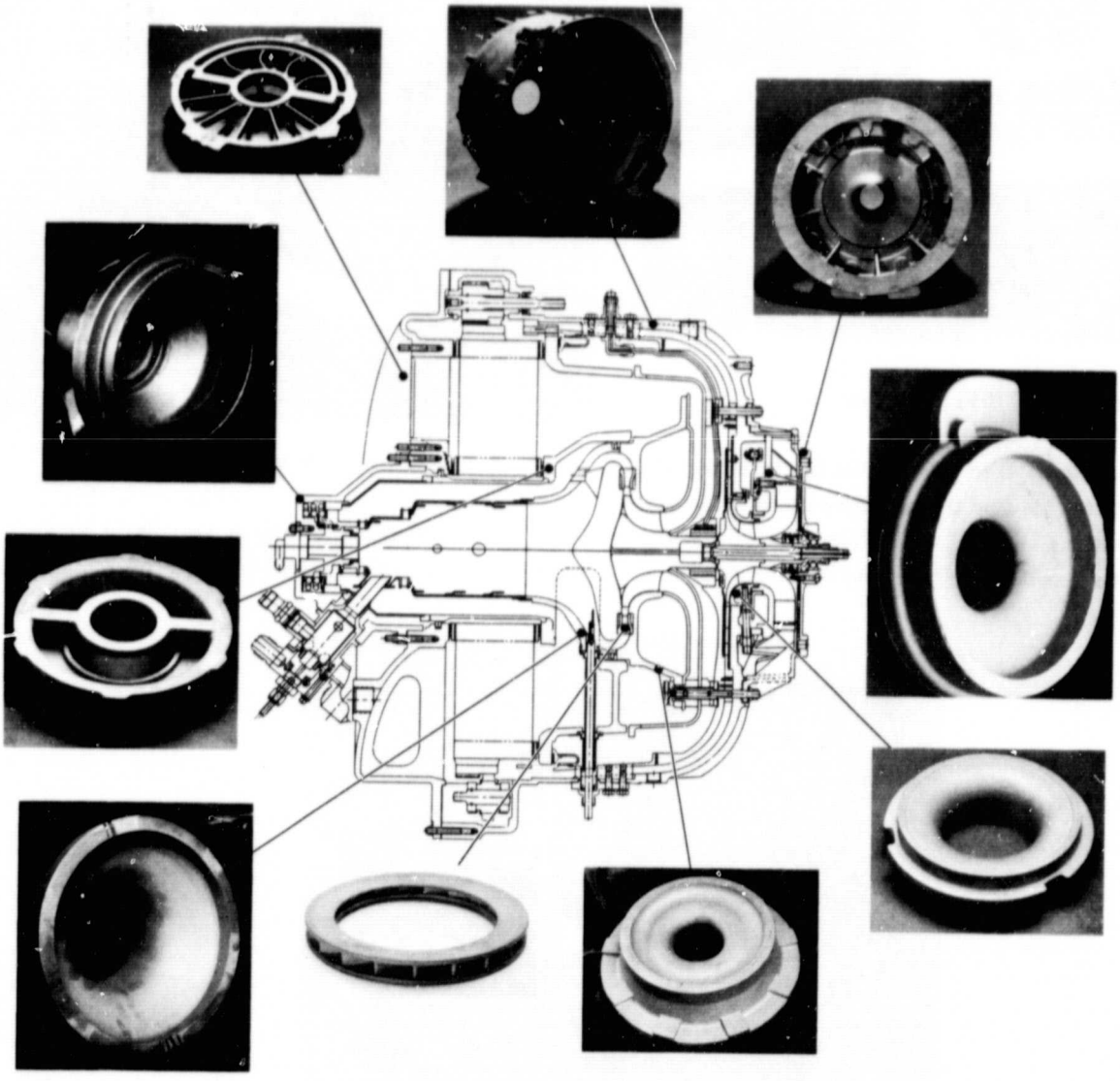

Figure 7. MOD I Build 1 Metal Castings.

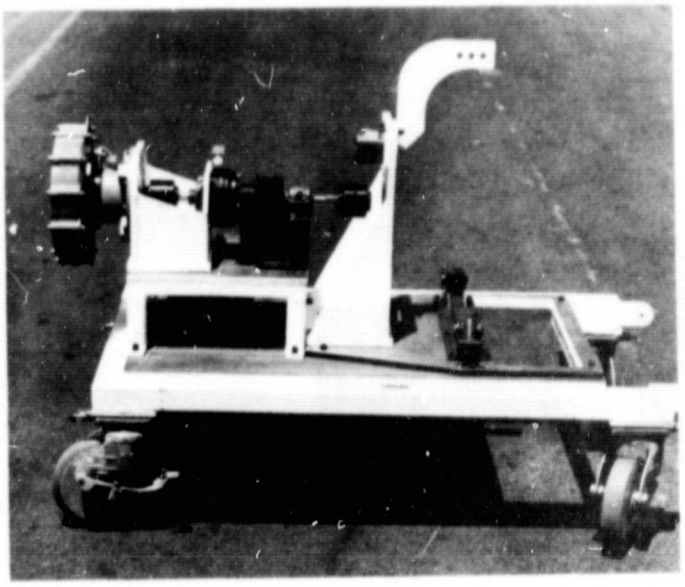

Figure 8. AGT101 Engine Test Cart.

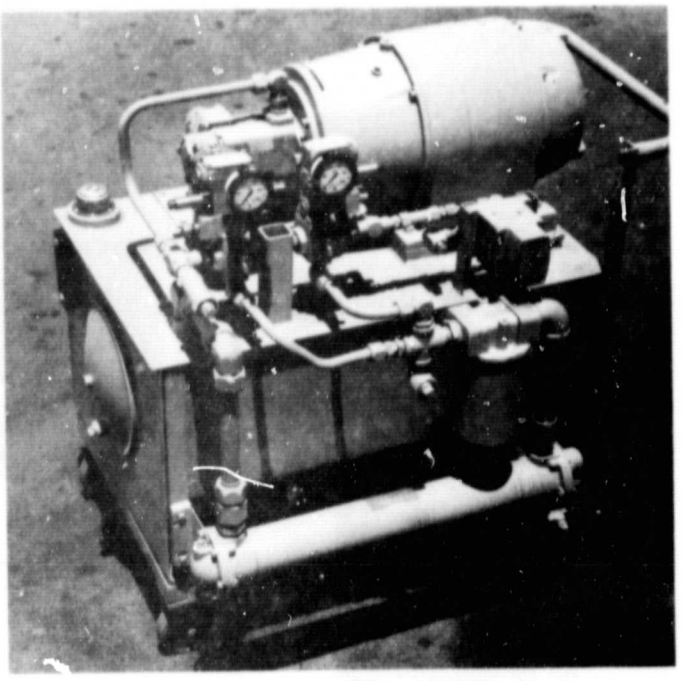

Figure 9. AGT101 Hydraulic Test Cart.

from 1600°F (Mod I Build 1) to 2500°F (Mod II). In particular, the improved SFC for the Mod II is significantly better in the 10-30 hp range where much of the CFDC mileage occurs. This results in the excellent fuel economy of 42.8 mpg with diesel fuel in a 3000-pound vehicle, assuming a warm-up fuel penalty equivalent to a corresponding spark ignition engine.

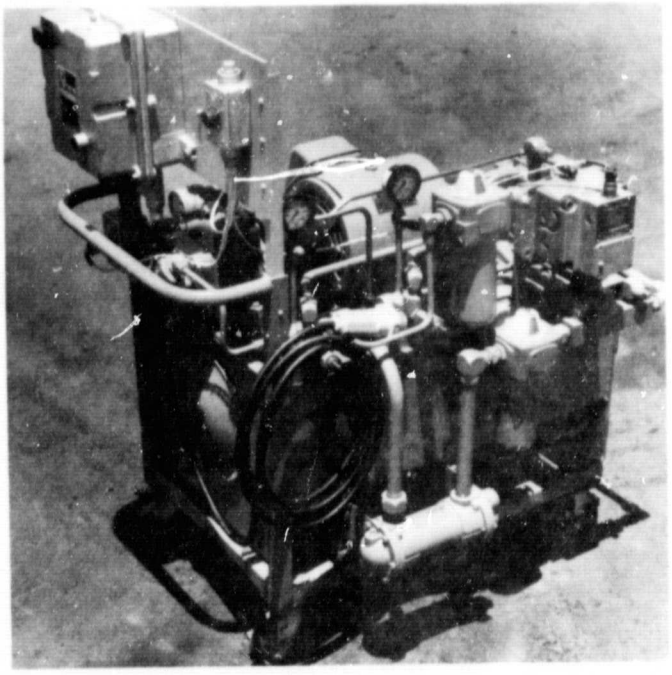

Figure 10. AGT101 Lubrication Cart.

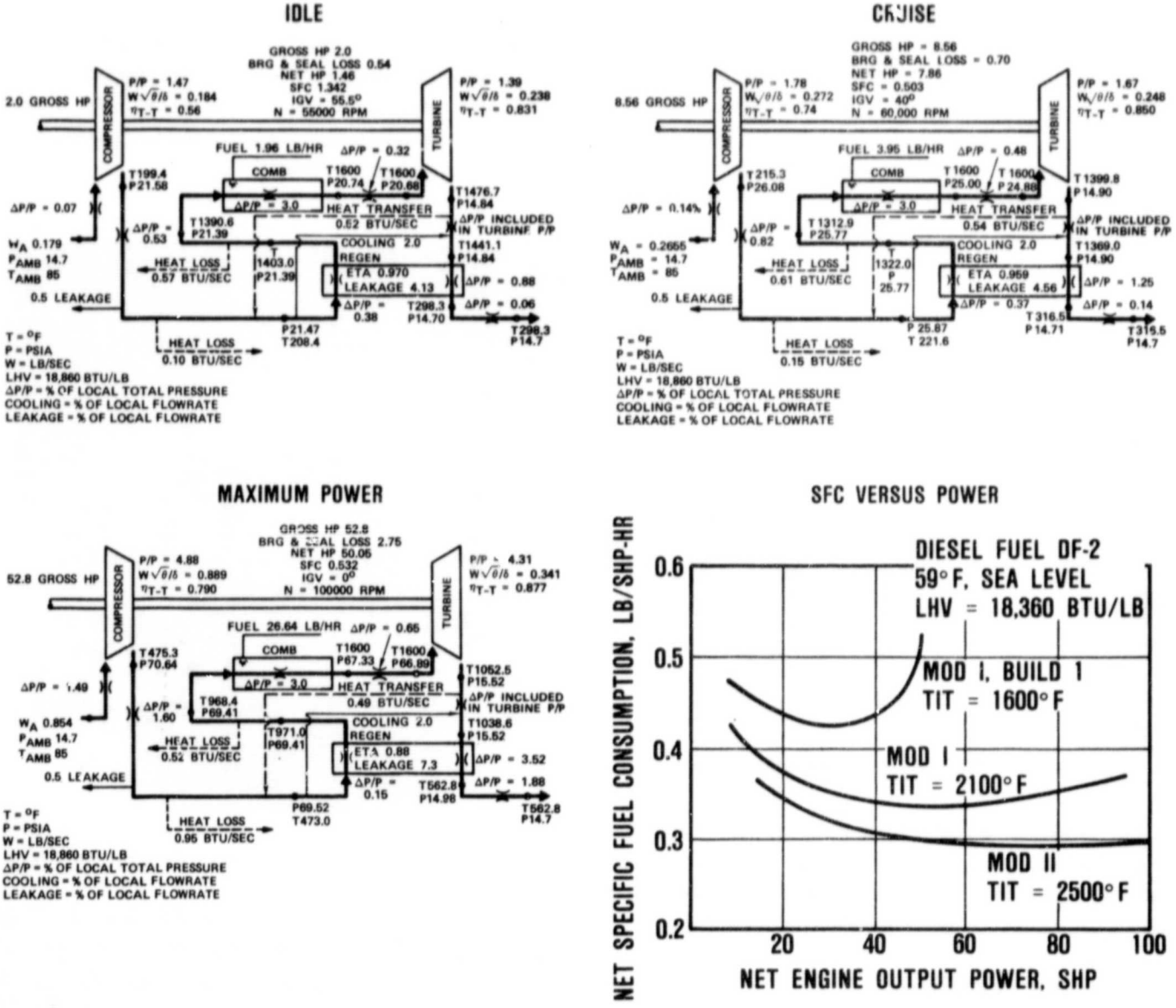

Figure 11. AGT101 MOD I Build 1 Performance (85°F, Sea Level, DF-2).

4.0 COMPONENT/SUBSYSTEM DEVELOPMENT

Task 2.0, Component Subsystem Development, activities during this reporting period entailed completion of component and test rig fabrication, initiation of component development testing and analysis, and continuation of ceramic development activities. The test rigs are specifically designed to fully evaluate the component for performance and, in some cases, mechanical integrity. Figure 12 shows the performance rating stations for the engine and components.

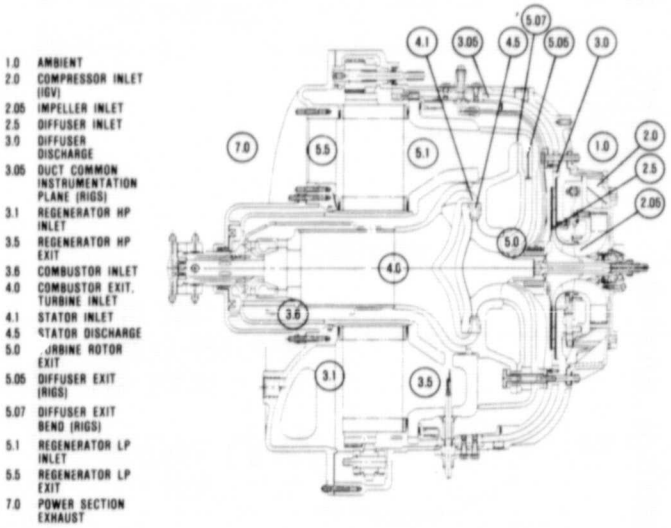

Figure 12. AGT101 Performance Rating Stations.

The following sections discuss the major efforts and accomplishments during the reporting period for each component/subsystem. Due to budget constraints, some planned activities have been revised and/or curtailed.

4.1 Compressor Development

Activities during this reporting period were concentrated on test rig builds, development testing, and powder metal aluminum characterization.

4.1.1 Compressor Inlet Guide Vane Testing

Development testing on compressor stage hardware encompassed inlet guide vane (IGV) acoustic evaluation. The IGV test rig, shown in Figure 13, replicates the IGV aerodynamic flowpath from the inlet housing to the compressor impeller leading edge (station 2.0 to 2.05 in Figure 12). High response acoustic microphones were located upstream of the IGVs. Mass flow rates were set based on inlet instrumentation. Data were taken at selected fixed IGV angles over a range of 0 to 65 degrees closed.

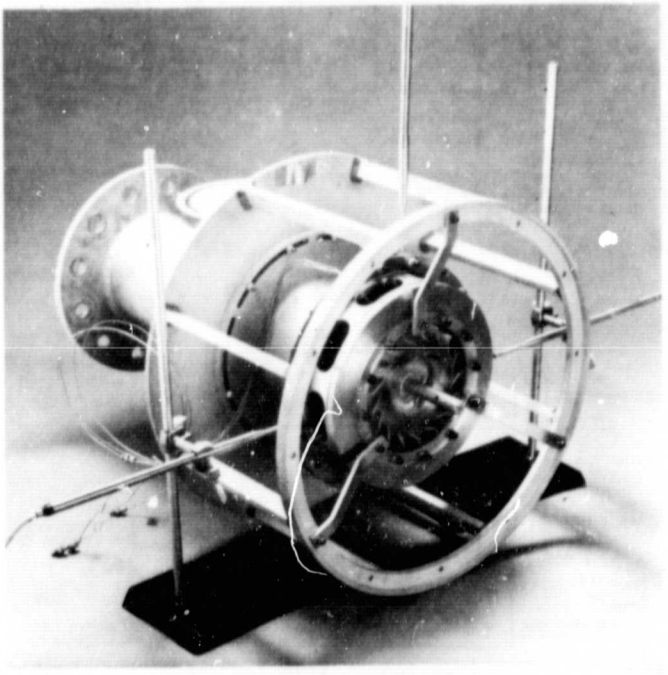

Figure 13. AGT101 Compressor Inlet Guide Vane Test Rig.

Initial testing identified objectionable acoustic noise levels (in the audible range) in excess of 120 dB when the IGVs were closed to 50 degrees or higher. This phenomena is similar in nature to previous Garrett experience on another articulated radial IGV system. Although the exact mechanism generating the tones is not well understood, it is believed that the IGV-induced swirl transfers flow energy to acoustic energy.

This problem was resolved, based on prior Garrett experience, by introducing a minimal disturbance in the flow field. Flow tabs, as shown in Figure 14, were installed on the

fixed leading edge of two IGVs. These flow tabs dramatically reduced the tone amplitude. Figure 15 presents the results of IGV testing with and without flow tabs.

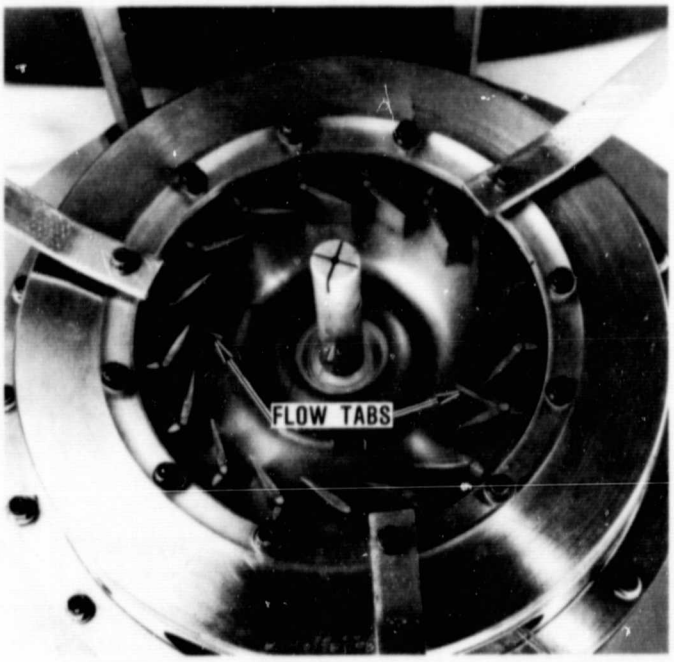

Figure 14. Inlet Guide Vane Flow Tabs.

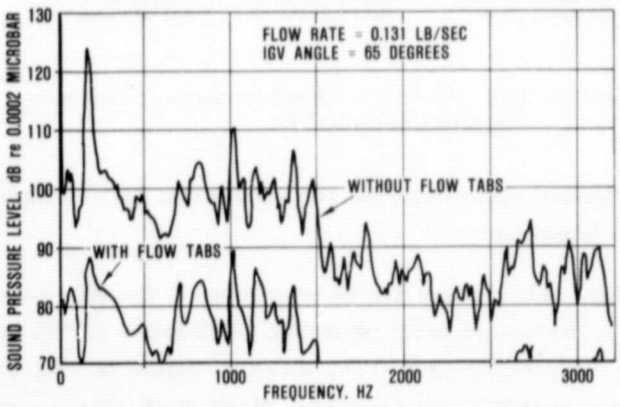

Figure 15. Inlet Guide Vane Test Results.

4.1.2 Compressor Rig Testing

The compressor test rig, shown in Figures 16 and 17, replicates the AGT101 flowpath from the IGV inlet to the

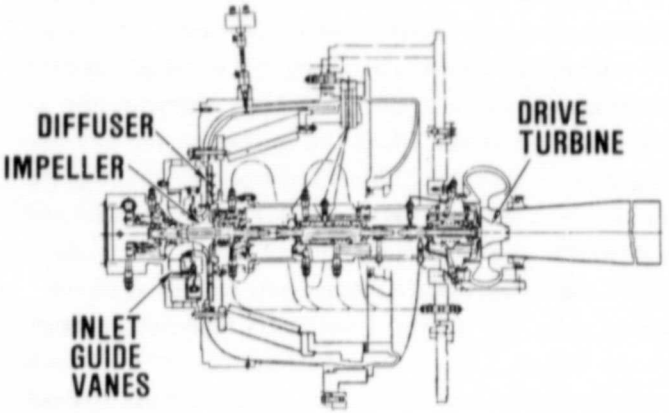

Figure 16. Compressor Test Rig Cross Section.

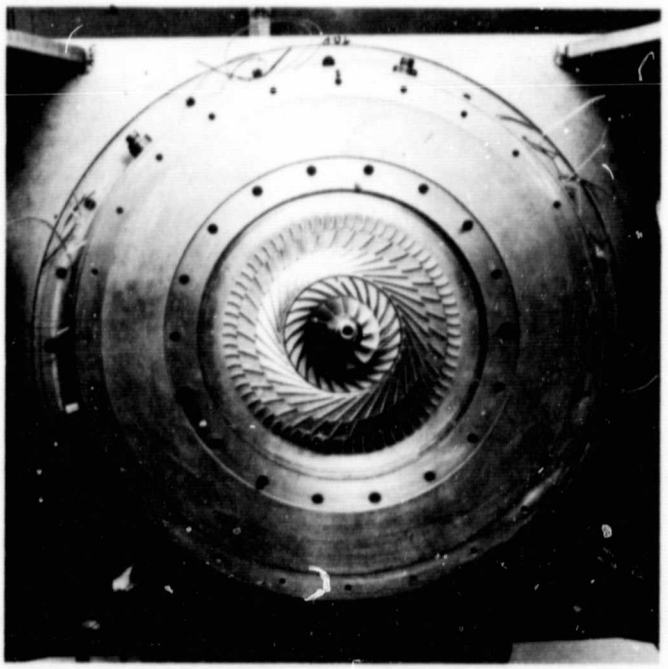

Figure 17. Compressor Test Rig.

regenerator inlet (station 2.0 to 3.1 in Figure 12). The test rig is a straddle-mounted bearing configuration utilizing AGT101 engine high speed ball bearings and is capable of speeds up to 110,000 rpm (110-percent design speed). Power is derived from a drive turbine system composed primarily of the Garrett Model TV81 turbocharger hot flowpath components. Compressor stage hardware (IGVs, impeller, and

diffuser) is utilized in the rig to establish actual performance and verify design predictions.

The rig incorporates the capability for controlling, and evaluating effects of, impeller running clearance. The clearance adjustment mechanism, based on a design concept successfully demonstrated on other Garrett programs, uses an Acme thread to axially adjust the position of the impeller during dynamic operation. This is accomplished by fixing the internal thread and turning the external thread, thus forcing the externally threaded members (impeller shafting) to move axially. Capacitance probe instruments, located at selected stations along the impeller meridional flowpath, measure dynamic impeller clearances. Performance data at each running clearance is recorded after the test rig has reached thermal equilibrium for the speed and pressure ratio selected.

At the close of this reporting period, the unit was being installed in the test facility for mechanical checkout testing and subsequent performance mapping.

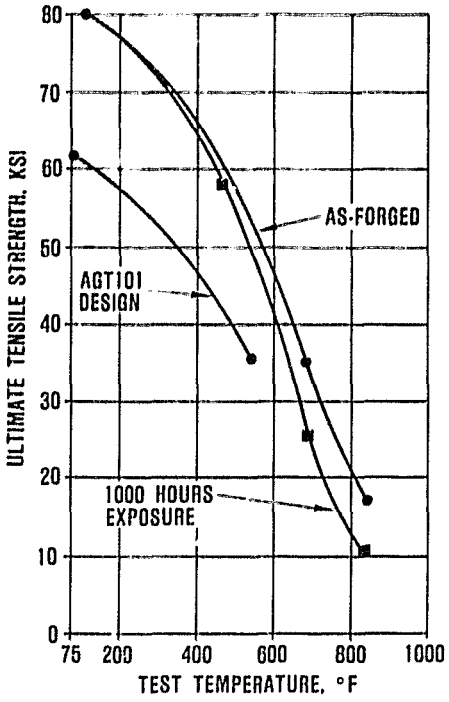

Figure 18. Tensile Properties of Forged Alcoa PM Al-Fe-Ce.

4.1.3 Powder Metal Aluminum

Material characterization and evaluation of the Alcoa Al-Fe-Ce powder metal (PM) aluminum continued. As reported in Reference 2, baseline screening tests on sub-size pancake forgings, indicated the material had the capability to exceed the design goals (Figure 18). Based on these early evaluations, component size pancake forgings were procured (4.5-inches diameter by 3-inches thick). These forgings were thermomechanically processed (TMP) specifically to improve alloy ductility.

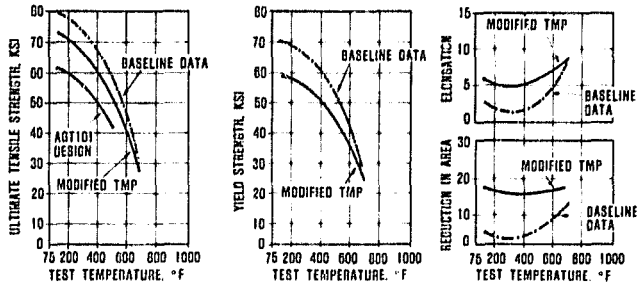

Figure 19. Alcoa Al-Fe-Ce Forged Properties (1000-Hour Temperature Exposure).

Results show (Figure 19) that the ductility improvement goal was successfully met. Tensile strengths, as predicted, are lower than the baseline data but continue to exceed AGT101 design goals. Properties at elevated temperatures, particularly above 550°F, were observed as less sensitive to TMP variables, as evidenced by the convergence of property levels at 650°F. Comparing the tensile strength of PM Al-Fe-Ce with two of the high-strength aluminum alloys commercially available (A2219-T6 and A201-T7), shows it to be superior even after the 1000-hour exposed condition (Figure 20). Stress rupture capability of the alloy also is significantly better than the two commercial high strength alloys (Figure 21).

High cycle fatigue (HCF) properties of the Al-Fe-Ce alloy currently are being generated. Preliminary results at room temperature and 450°F, shown in Figure 22 tend to indicate good HCF life capability. Stress levels of 30 ksi at room temperature resulted in runout at 10^8 cycles while cycles exceeding 10^7 were obtained at stress levels of 25 ksi at 450°F.

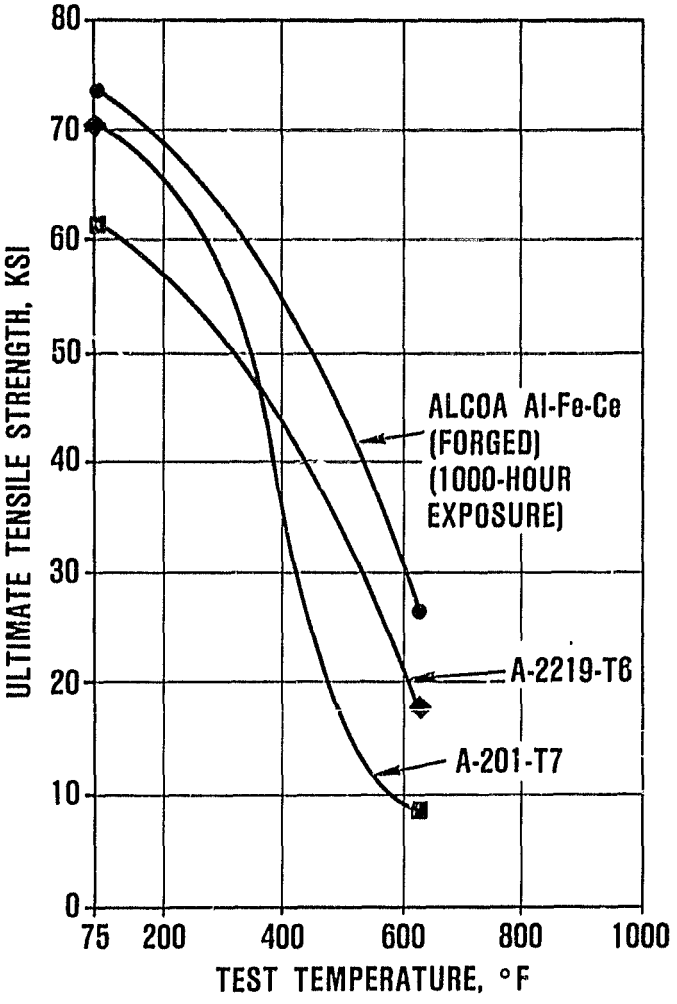

Figure 20. Tensile Properties of Aluminum Alloys.

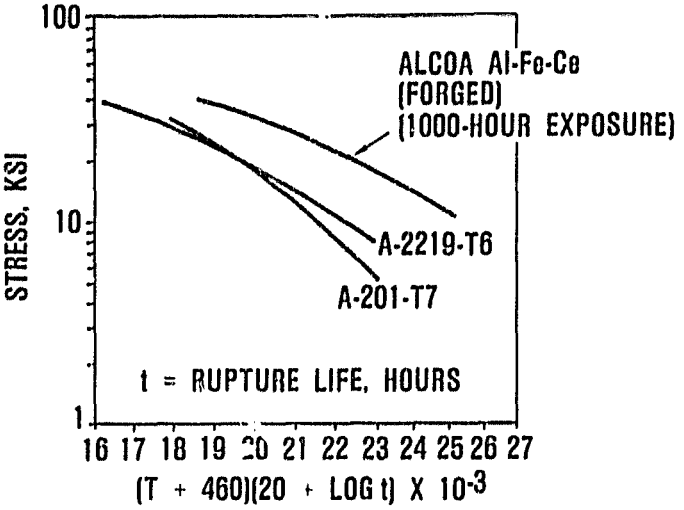

Figure 21. Stress Rupture Properties of Aluminum Alloys.

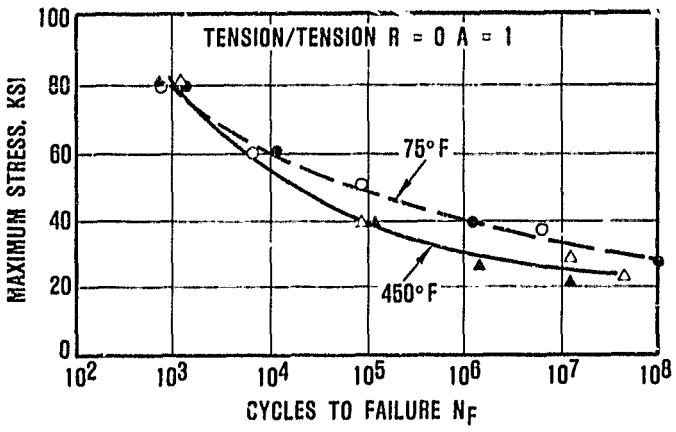

Figure 22. HCF Properties of Alcoa Al-Fe-Ce.

4.2 Turbine

The test plan established for cold-air testing of the turbine stage encompasses aerodynamic evaluation of the three turbine configurations [baseline ceramic Mod II (replicated in metal), Mod I, and Mod I Build 1]. Due to budget constraints, testing was reduced in scope to aerodynamic evaluation of the Mod I Build 1 configuration only. This selection was based on the immediate need to support the Mod I Build 1 engine test program. The remainder of the test program will be accomplished at a later time when adequate funding is restored.

The predicted maximum power design point performance for the three turbine configurations (References 1 and 2) is summarized in Table 3 and Figure 23. Predicted maximum power performance was then used for off-design modeling using established Garrett procedures. Rotor speed, stator and rotor incidence, tip diameter, and mixing losses were included in arriving at idle-to-maximum power performance predictions. The Mod I Build 1 performance predictions are shown in Table 4 along with the equivalent cold-air test rig conditions.

4.2.1 Cold Turbine Test Rig

The test rig, shown in Figure 24, is an overhung bearing system with hydraulic mounts, coupled to a direct reading

TABLE 3. AGT101 TURBINE STAGE CONFIGURATION COMPARISON

	Engine Configuration		
	Mod I Build I (All Metal)	(All Ceramic Except Turbine Rotor)	Mod II (All Ceramic)
MAXIMUM POWER POINT			
o Turbine Inlet Temp (Maximum), °F	1600	2100	2500
o Rotational Speed, rpm	100,000	100,000	100,000
o Corrected Speed, Percent	119.9	107.5	100.0
o Tip Speed, Ft/Sec	2100	2100	2300
TURBINE DESIGN FEATURES			
o Rotor			
- Material	Metal	Dual-Alloy Metal	Ceramic
- Number of Blades	13	13	13
- Diameter, Inches	4.8128	4.8128	5.2712
- Exducer/Shroud Clearance, Inches	0.010	0.010	0.010
o STATOR			
- Material	Metal	Ceramic	Ceramic
- Number of Vanes	19	19	19
- Trailing Edge Thickness, Inches	0.030	0.020	0.020
- Nozzle Area	85% (Vanes Rotated Closed)	100%	100%
- Suction/Pressure Profile	Linear	Linear or* Non-Linear	Linear or* Non-Linear

NOTE: MOD II is the baseline turbine design with the turbine design point at maximum power.

* Dependent on ceramic component development.

high speed torquemeter and reduction gearbox. Engine flowpath geometry is fully replicated from combustor exit-to-regenerator LP exit, including installation of the regenerator core. Test cell installation and facility layout are depicted in Figure 25.

Static and total pressure instrumentation, and total temperature probes were located along the entire flowpath (Figure 24) to determine overall turbine system performance, subsystem component performance (except stator)*, inlet and exhaust parameters and salient diagnostic information. Mechanical integrity instrumentation was appropriately installed to establish vibration levels, bearing temperature and oil flow and temperature.

The test rig was insulated both externally and internally (inlet duct, shroud and exhaust diffuser) to minimize heat transfer.

Due to the very low power levels anticipated during mapping at the idle and cruise power regimes, a direct-reading high-speed torquemeter was purchased from

*No stator instrumentation was available due to project funding constraints

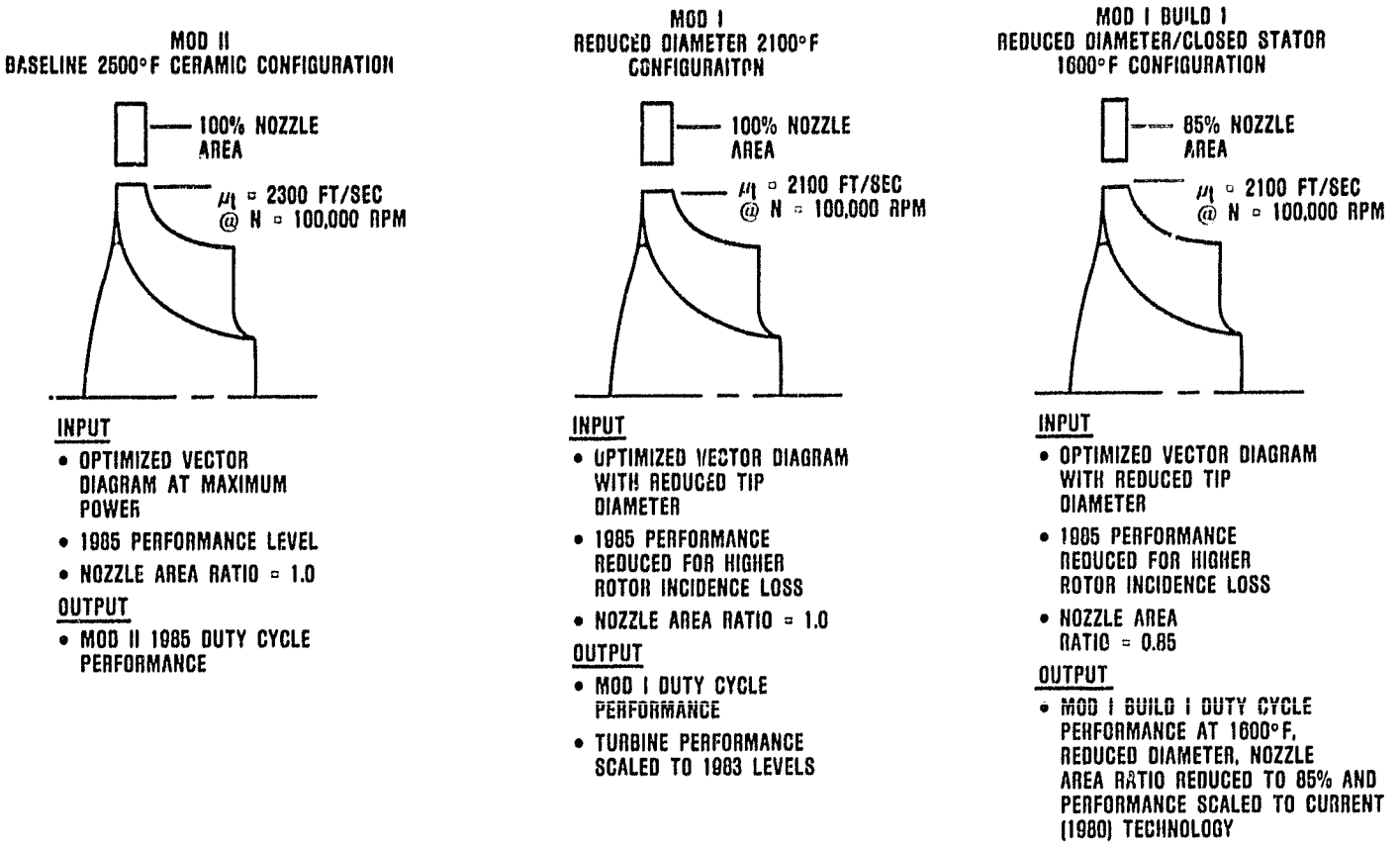

Figure 23. Performance Prediction Computer Models for the Three AGT101 Turbine Configurations.

Torquemeters, Ltd., London, England. The system, shown in Figure 26, consists of a torquemeter and readout system with appropriate calibration hardware and mechanical instrumentation. To maintain the highest potential accuracy from idle-to-maximum power, four torque shafts were procured, rated at 1.4, 7, 18 and 40 in-lbf.

4.2.2 Test Procedure

During mechanical checkout tests the test rig was configured with a "dummy" rotor for tare loss calibration tests. The dummy bladeless rotor was designed with identical mass and inertia characteristics of the bladed rotor. Test rig operation was accomplished to full speed using the dynamometers in the driving mode and under full vacuum to eliminate dummy rotor disk friction characteristics.

The test rig then was assembled with the Mod I Build 1 machined astroloy turbine rotor. Capacitance probes were used in all planes (radial, axial and backface) to assess rotor running clearances during aerodynamic mapping.

The torquemeter was configured with the appropriate shaft depending on the selected mapping range. Prior to each data run, a dead weight calibration was performed. Data records were obtained following an iterative procedure wherein inlet temperature at a desired pressure ratio was adjusted to obtain a rig discharge temperature within several degrees of cell ambient, thereby minimizing heat transfer effects. Speed then was set based on inlet temperature, and inlet pressure (for a given pressure ratio) was adjusted to obtain the desired turbine Reynolds number. This procedure was followed for all performance tests and data records obtained after system stabilization for approximately 10 minutes. The data matrix is shown in Table 5.

Figures 27 and 28 show the unit installed in the test facility.

TABLE 4. MOD I BUILD I TURBINE COLD RIG VERSUS ENGINE OPERATING CONDITIONS AT CRITICAL ENGINE OPERATING POINTS

	Maximum Power		Design Cruise		Low Cruise		Design Idle		Low Idle	
	Cold	Eng	Cold	Eng	Cold	Eng	Cold	Eng	Cold	Eng
N (RPM)	62,522	100,000	36,044	65,000	32,891	60,000	29,438	55,000	26.623	50,000
$N/\sqrt{\theta}$ (RPM)	50,633	50,182	32,913	32,619	30,380	30,109	27,849	27,601	25,317	25,091
$N/\sqrt{\theta}$ (%)	119.1	119.9	77.4	77.9	71.5	71.9	65.5	65.9	59.6	59.9
T_{In} (°R)	790.9	2059.7	622.1	2059.7	608.0	2059.7	579.6	2059.7	573.6	2059.7
PR 4.1 5.1	4.846	4.261	1.881	1.814	1.710	1.664	1.413	1.390	1.344	1.327
PR 4.1 5.0	4.711	4.165	1.817	1.765	1.657	1.625	1.348	1.33	1.293	1.280
PR 4.0 5.0 (Stage)	4.745		1.824		1.662		1.352		1.296	
$\Delta P_T/P_T$ Diffuser	0.028	0.022	0.034	0.027	0.031	0.023	0.046	0.041	0.038	0.035
$R_\epsilon = W/(R_{Tip}\mu)$	130,218	130,218	47,440	47,440	41,622	41,622	34,000	34,000	25,831	25,831
$w\sqrt{\theta}/\delta$ 4.0	0.354	0.348	0.308	0.303	0.292	0.287	0.232	0.228	0.214	0.210
PR 4.0 5.1 (System)	4.880		1.888		1.716		1.417		1.347	
η 4.0 5.0 (Stage)	0.883		0.834		0.828		0.828		0.821	
η 4.0 5.1 (System)	0.871		0.795		0.782		0.721		0.718	
η 4.1 5.1	0.873	0.873	0.799	0.799	0.789	0.789	0.726	0.726	0.724	0.724
$\Delta P_T/P_T$ Inlet	0.0072		0.0038		0.0030		0.0030		0.0023	

NOTE: Efficiencies shown are predicted values

4.2.3 Mod I Build 1 Test Results

Overall turbine system performance, based on torquemeter measurement, for the Mod I Build 1 configuration is shown in Figure 29. All data were corrected to engine Reynolds number and design clearance using existing Garrett correlations. At maximum power, a η_{T-SYS} of 86.5 percent was achieved; the predicted value was 87.1 percent. An idle efficiency of 76.3 percent was achieved; 71.8 percent was predicted. At cruise condition, the performance measured was 79.6 percent; 78.2 percent was predicted.

Figures 30 through 34 present test results for the Mod I Build 1 turbine as a function of system efficiency versus pressure ratio for the five speed conditions tested.

4.2.3.1 Inlet Transition Duct

The inlet transition duct depicted in Figure 24, (station 4.0 to 4.1) represented a complex design problem due to the

COMBUSTOR EXIT (4.0)	T_T · 6 THERMOCOUPLES · 3 ROSEMONT PROBES P_T · 8 KIEL PROBES
TRANSITION DUCT (4.0) TO (4.1)	P_S · HUB, SHROUD
ROTOR SHROUD (4.5) TO (5.0)	P_S · SHROUD
ROTOR EXIT (5.0)	P_T · 8 KIEL PROBES
EXHAUST DIFFUSER (5.0) TO (5.05)	P_S · HUB, SHROUD
DIFFUSER EXIT BEND (5.05) TO (5.07)	P_S · HUB, SHROUD
REGENERATOR INLET (5.1)	T_T · 9 THERMOCOUPLES · 3 ROSEMONT PROBES P_S · SHROUD
ROTOR CLEARANCE PROBES	4 RADIAL PROBES 4 AXIAL PROBES
MECHANICAL INSTRUMENTATION (A)	BEARING TEMPERATURE, VIBRATION, OIL FLOW, OIL TEMPERATURE
TORQUEMETER (B)	TORQUE
MASS FLOW (C)	SONIC NOZZLE

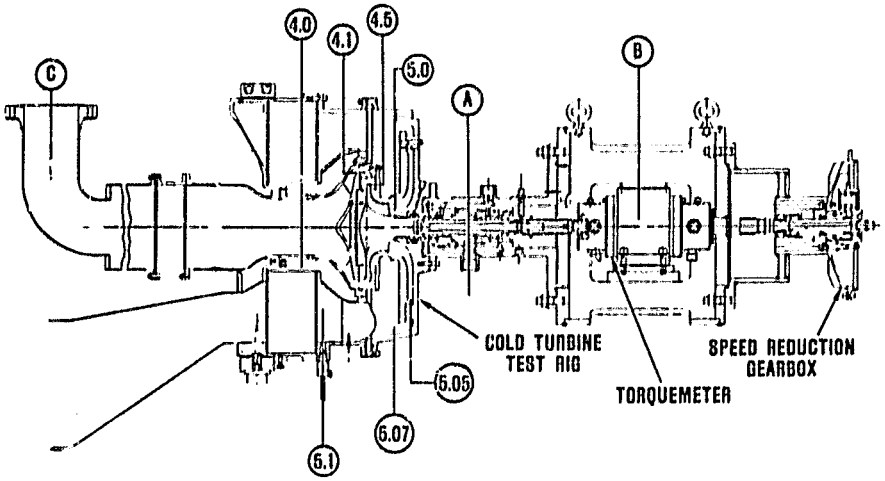

NUMERICAL STATION DESIGNATIONS ARE CONSISTENT WITH ENGINE PERFORMANCE RATING STATIONS ON FIGURE 12.

Figure 24. Turbine Component Cold Air Test Rig, Instrumentation List and Instrumentation Planes.

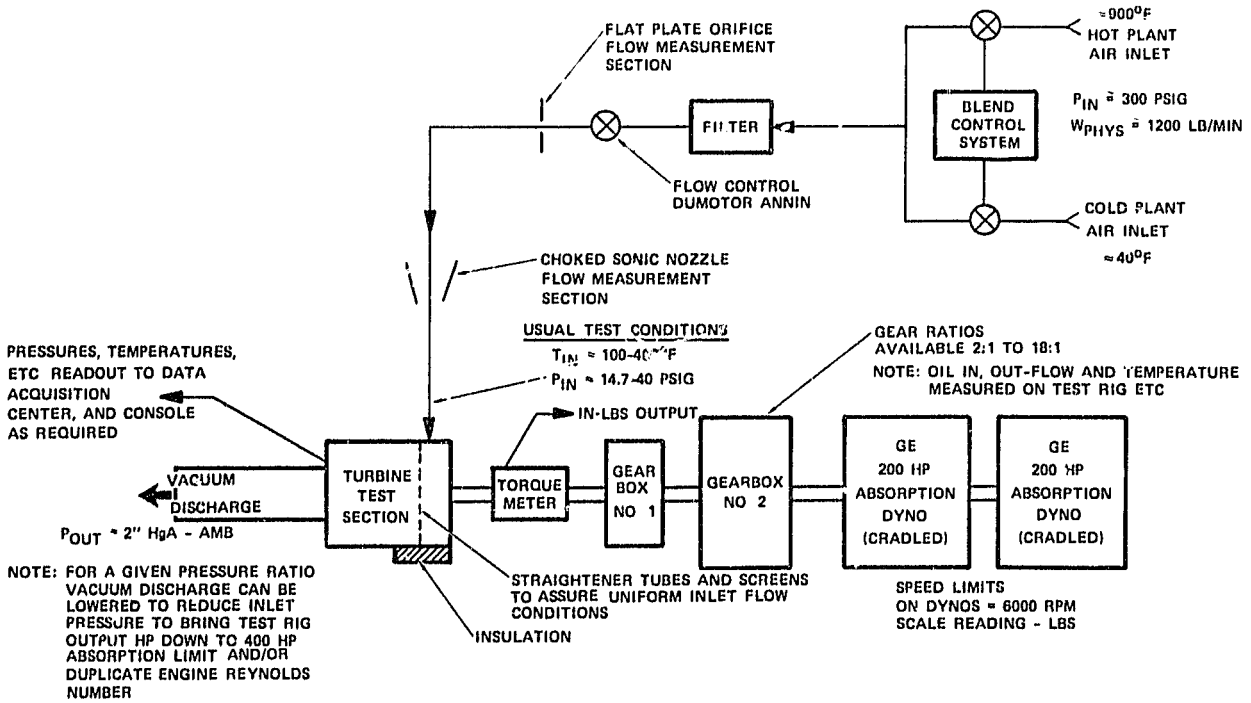

Figure 25. Turbine Component Cold Air Test Facility Schematic.

Figure 26. Torquemeter and Readout System.

high flow turning required (approximately 230 degrees). Design objectives for the duct were to minimize the hub and shroud diffusion rate and magnitude arriving at a non-separated flow design. Design details are reported in Reference 1.

During the test program, the duct flow characteristics were obtained from static pressure instrumentation located along the inlet transition duct endwalls. The measured hub and shroud static pressure distribution is shown in Figure 35 for the Mod I Build 1 configuration. In general, excellent agreement was obtained between predicted and measured characteristics.

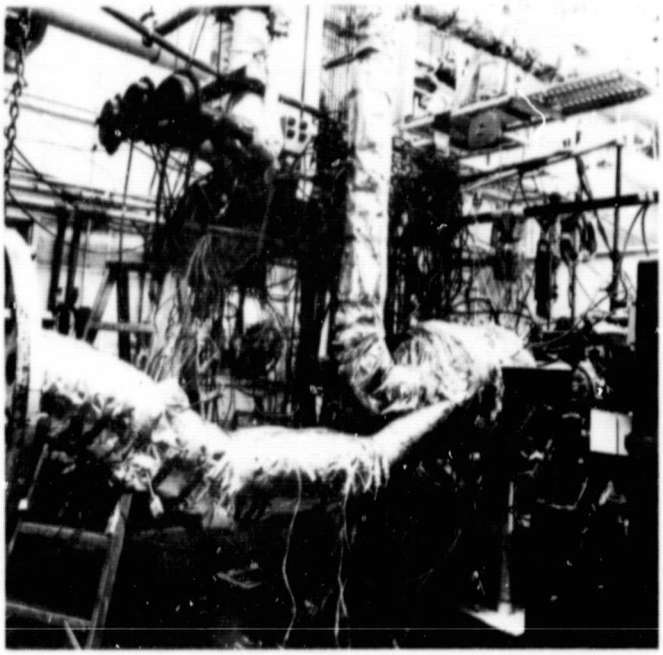

Figure 27. AGT101 Test Rig Installed in Test Cell.

4.2.3.2 Turbine Exhaust System

The turbine exhaust system is shown in Figure 24 (stations 5.0 to 5.1). The system includes: a radial exhaust diffuser (5.0 to 5.05), diffuser exit dump and 90 degree bend (5.05 to

TABLE 5. AGT101 MOD I BUILD 1 TURBINE TEST DATA MATRIX

	$N/\sqrt{\theta}$, Percent				
PR_{TT} 4.0 5.0	Low Idle 59.6	Design Idle 65.5	Low Cruise 71.5	Design Cruise 77.4	Max Power 119.1
1.232					
1.296	X	X			
1.352					
1.450	X	X			
1.662			X	X	
1.824			X	X	
2.315			X	X	
2.960					
4.745					X

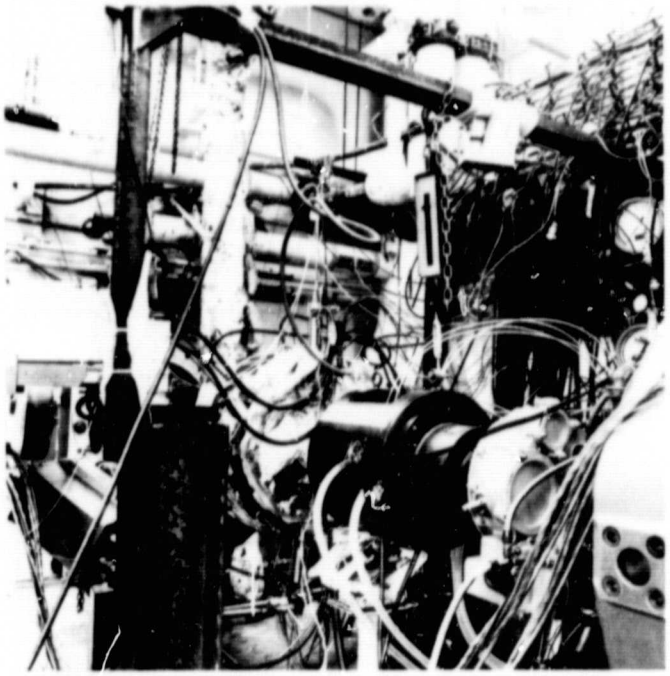

Figure 28. AGT101 Test Rig Installed in Test Cell.

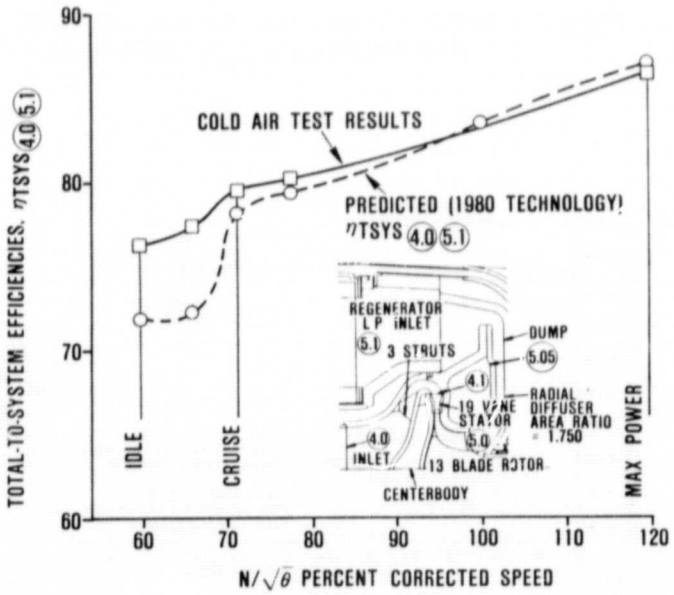

Figure 29. AGT101 Mod I Build 1 Turbine System Efficiency Characteristics.

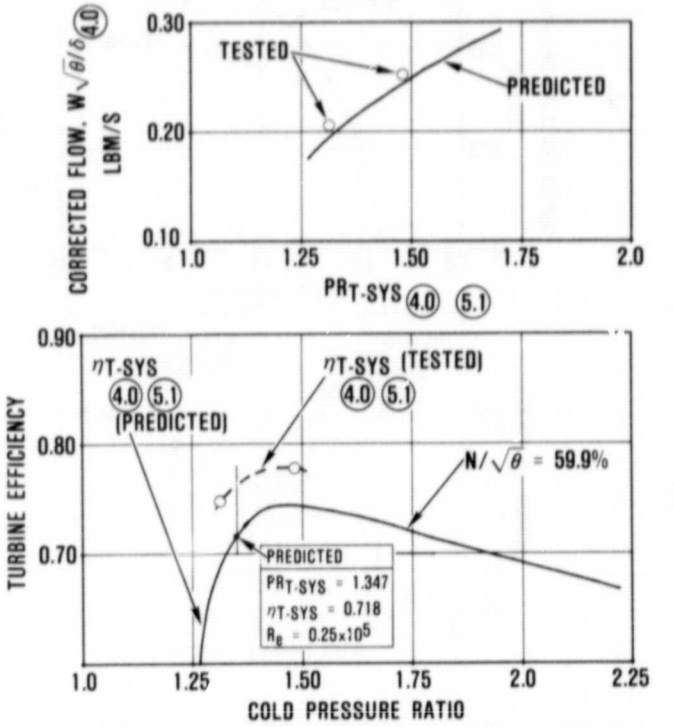

Figure 30. AGT101 Turbine Flow Function and Efficiencies at Low Idle (N_{eng} = 50,000 rpm).

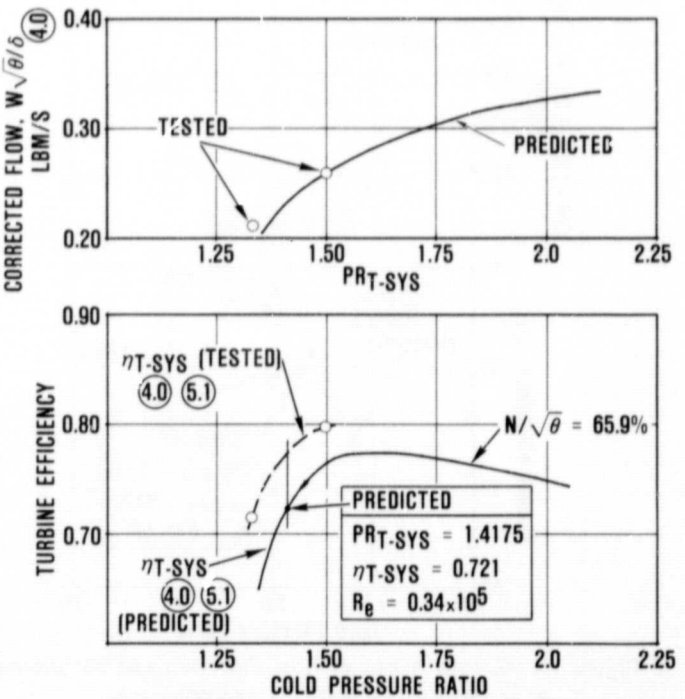

Figure 31. AGT101 Turbine Flow Function and Efficiencies at Design Idle (N_{eng} = 55,000 rpm).

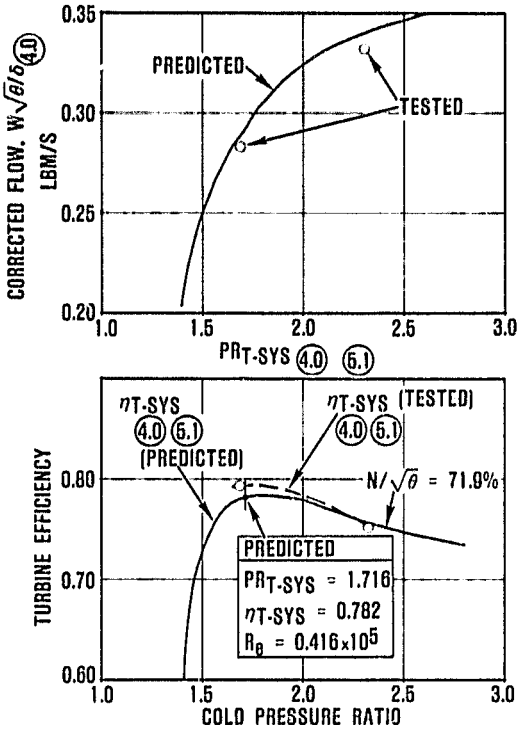

Figure 32. AGT101 Turbine Flow Function and Efficiencies at Low Cruise (N_{eng} = 60,000 rpm).

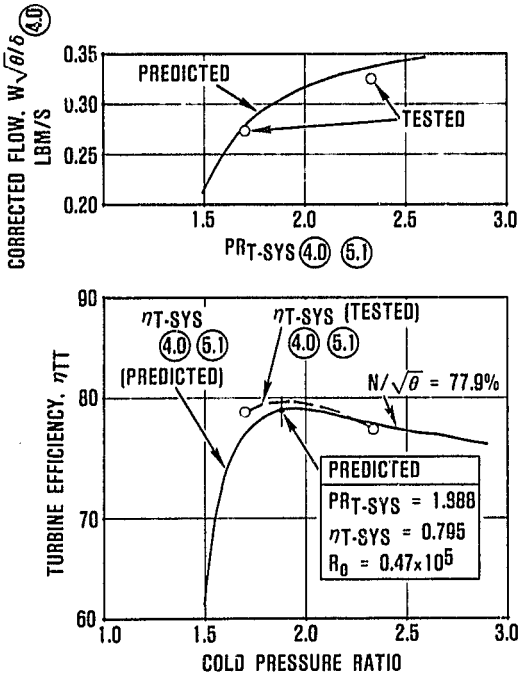

Figure 33. AGT101 Turbine Flow Function and Efficiencies at Design Cruise (N_{eng} = 65,000 rpm).

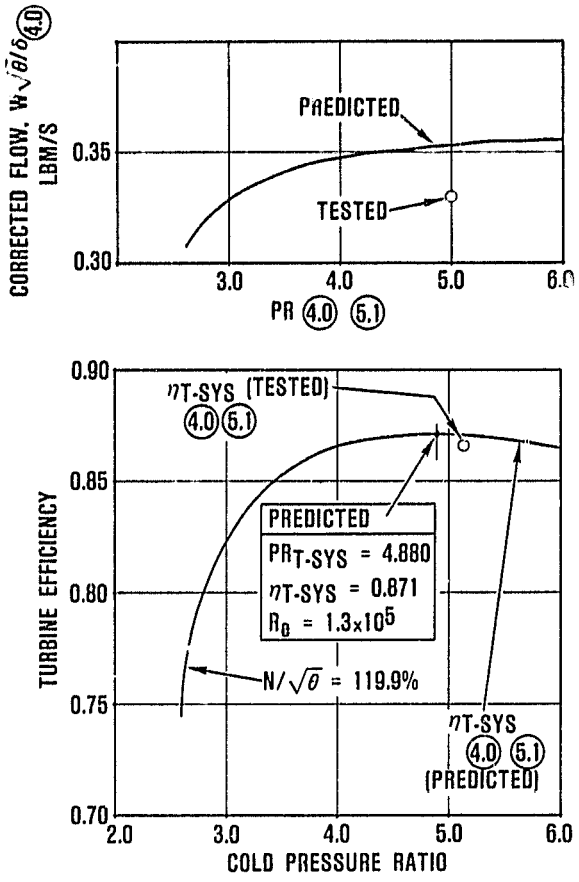

Figure 34. AGT101 Turbine Flow Function and Efficiencies at Maximum Power (N_{eng} = 100,000 rpm).

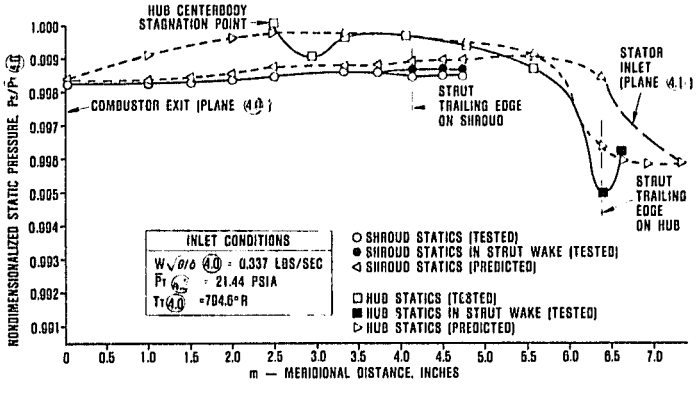

Figure 35. Inlet Duct P_s Distribution.

5.07) and a sudden expansion to the LP regenerator inlet (5.07 to 5.1). Objectives of the design were to: minimize system total pressure drop, maximize static pressure recovery, and provide a uniform velocity profile at the regenerator LP inlet.

The selection of a single shaft regenerated engine for the automotive duty cycle results in a broad speed, flow and pressure ratio requirement for the radial turbine. As a result, the rotor exit flow experiences significant variations in swirl angle. Although available data for radial exhaust diffusers indicate that the loss coefficient is relatively insensitive to inlet swirl angle, the sensitivity of the regenerator to swirl and large velocity gradients was not known. If deswirl vanes or other devices were required to improve the flow uniformity at the regenerator inlet, then the exhaust system loss coefficient would be a function of a swirl angle.

An exhaust system loss coefficient, therefore, was established (from Garrett correlations), which would account for regenerator inlet deswirl vanes or other flow straightening devices where the tangential component of velocity would be lost over the majority of the engine duty cycle. This approach resulted in a minimum loss coefficient ($\bar{\omega}_{MIN}$) at zero swirl of 0.30 and a variation of loss coefficient with diffuser inlet swirl described by the following empirical relationship:

$$\frac{\bar{\omega}}{\bar{\omega}_{MIN}} = 2.554\alpha^2 + \frac{1}{\cos\alpha}$$

where:

α = diffuser inlet (rotor exit) swirl angle, radians

$$\bar{\omega} = \frac{P_{T5.0} - P_{T5.1}}{P_{T5.0} - P_{S,5.1}}$$

Initial evaluation of the turbine exhaust system and its impact on regenerator performance with swirl and non-uniformities was established with the LP regenerator cold air test rig. Detailed results of this test program are described in Section 4.4, herein, and Reference 2. From a turbine exhaust system standpoint, the important result was that the regenerator performance was relatively insensitive to the range of swirl angles experienced over the engine operating points. Therefore, major modification to eliminate the residual swirl at the regenerator inlet is not necessary. The LP regenerator test program also showed that the radial exhaust diffuser performance actually improved with high inlet swirl.

The preliminary radial exhaust diffuser design used in the LP regenerator test program was based on an area ratio (5.0 to 5.05) of 1.85. However, further detail design and analytical evaluation of the radial exhaust diffuser reduced the area ratio to 1.75. This selection was considered the baseline configuration, since detailed analysis indicated that separation would occur along the diffuser shroud line even at an area ratio of 1.65. Therefore, it was concluded that the final diffuser area ratio must be determined from experimental evaluation of a range of diffuser designs.

The baseline (1.75 area ratio) diffuser design was evaluated in the Mod I Build 1 cold rig test over the range of duty cycle operation and with actual turbine exit gradients. Test results at the engine operating points are presented in Figure 36.

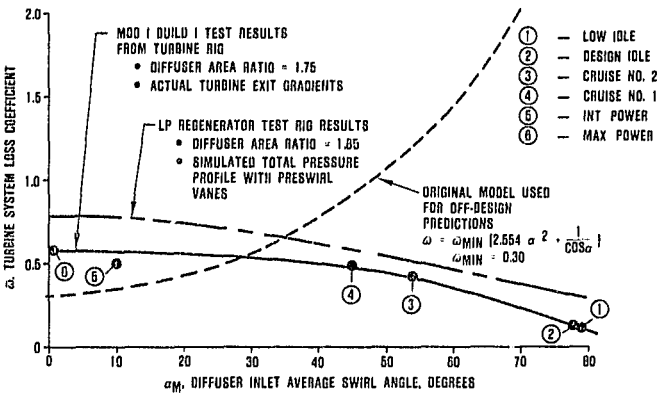

Figure 36. AGT101 Turbine Exhaust System Loss Comparisons.

The results again show that the exhaust system loss characteristics are actually improved and confirms the characteristics established from the LP regenerator test rig. It is not known at this time whether the change in loss level between the 1.85 area ratio diffuser (LP regenerator rig) and the 1.75 area ratio diffuser (Mod I Build I turbine rig) is due to the area ratio change or possible differences in inlet flow conditions between the two tests. Nevertheless, the important results from the two test programs are:

- Major modifications to the exhaust system to eliminate regenerator inlet swirl are not required. Therefore, the original loss model, which severely penalizes the exhaust system at high swirl levels, can be modified to the measured loss coefficient. This significantly increases the turbine system performance potential at the engine idle and cruise conditions

- Further optimization of the radial exhaust diffuser to reduce losses at the low swirl operating point (due to high diffuser shroud curvature effects) can be accomplished without significant impact on the diffuser performance at high swirl where the dominant effect is diffuser radius ratio (i.e., the major recovery with high swirl is due to conservation of the angular momentum)

A summary of turbine exhaust system performance with the 1.75 area ratio diffuser is included in Table 6.

4.3 Combustion

Effort during the early part of this reporting period continued toward evaluation of fuel nozzles for the Mod II variable geometry design, and establishment of diffusion flame combustor performance needed to support the operation of the Mod I Build I engines. Budget constraints had a significant affect on combustion system activities, with all effort replanned in support of Mod I Build I engine testing. Variable geometry design and testing and pilot combustor work was deferred to a later date.

Section 4.3.1 describes test activity conducted on the diffusion flame combustor. Section 4.3.2 describes the test results from the fuel nozzle evaluation for the variable geometry (RPD) combustor before that effort was deferred.

TABLE 6. SUMMARY OF AGT MOD I BUILD I TURBINE EXHAUST SYSTEM PERFORMANCE (COLD RIG TEST)

ENGINE CONDITIONS		TURBINE RIG OPERATING CONDITIONS			PERFORMANCE PARAMETERS							
Engine Operating Points	Engine Rotation Speed,	System Pressure Ratio $PR_{T\text{-}SYS}$ 4.0 5.1		Percent Corrected, Speed	Inlet Critical Velocity Ratio, V/A_{cc} 5.0		Inlet Swirl Angle, α 5.0 deg		Overall Tot. P. Loss, $\Delta P/P$ 5.0 5.1	Overall Loss Coeff. ω 5.0 5.1	Overall Pressure Recovery, C_p 5.0 5.1	Diffuser Alone C_p 5.0 5.05
		Tested	Design		Tested	Predicted	Tested	Predicted				
Low Idle	50,000	1.312	1.347	59.9	0.179	0.184	79	65	0.0019	0.102	0.900	0.525
Design Idle	55,000	1.329	1.417	65.9	0.193	0.210	78	67	0.0035	0.116	0.885	0.625
Cruise No. 1	60,000	1.697	1.716	71.9	0.180	0.197	45	50.5	0.0091	0.481	0.646	0.503
Cruise No. 2	65,000	1.862	1.888	77.9	0.221	0.2125	54	49	0.0119	0.421	0.579	0.470
Intermediate Power	83,963	3.037	3.050	100.0	0.280	0.269	10	26.5	0.0224	0.492	0.508	0.434
Maximum Power	100,000	5.124	4.880	119.9	0.404	0.390	NOT AVAIL	-1.0	0.0528	0.574	0.426	0.263

NOTES: V/A_{cc} 5.0 "tested" was calculated from averaged rotor test static pressures (hub and shroud) and total pressures

α 5.0 "tested" represent the rotor exit swirl determined during test

α 5.0 and V/A_{cc} 5.0 "predicted" were interpolated from off-design model

4.3.1 Diffusion Flame Combustor Testing

The diffusion flame combustor (DFC) described in References 1 and 2 is shown in Figure 37. Testing was conducted in a specially designed test rig replicating engine flowpath geometry and sufficient instrumentation to measure inlet and discharge combustor quantities. Installation of the test rig in the combustion test facility is shown in Figure 38.

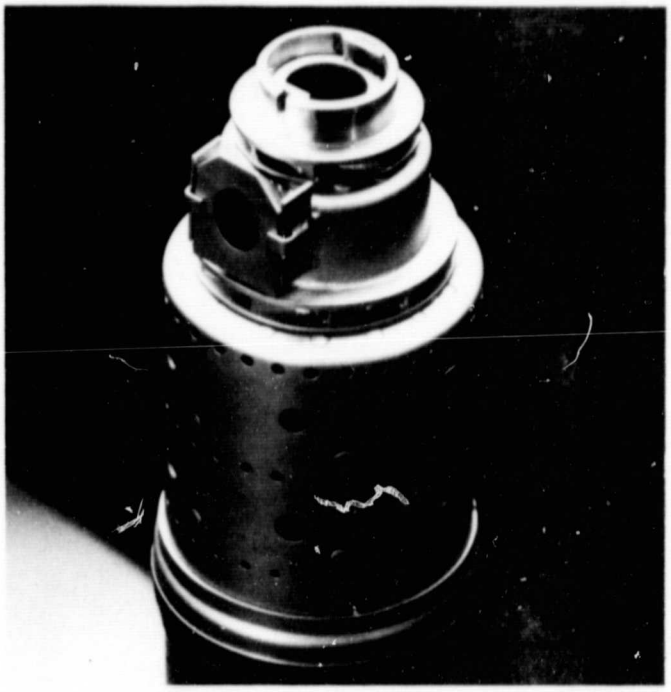

Figure 37. Diffusion Flame Combustor.

Initial testing of the DFC consisted of a cold flow test to determine any leakages present and to measure pressure variation at the inlet flow annulus immediately upstream of the combustor. Pressure variations were measured at a number of axial and circumferential locations over a range of corrected flow conditions from idle to maximum power. Measured variations were less than 5 percent and no significant leakages were noted.

Following cold flow testing, hot testing was conducted at conditions as near engine conditions as possible. Due to test facility hardware limitations, inlet air temperatures were limited to 1000°F maximum. Airflow and fuel flow rates, therefore, were adjusted. Table 7 lists the Mod I Build 1, engine combustor inlet conditions and corresponding rig conditions for idle, cruise and maximum power. The majority of testing was conducted using JP-5 fuel. Lightoff and lean blow-out tests were conducted with both JP-5 and DF-2. Results were essentially the same.

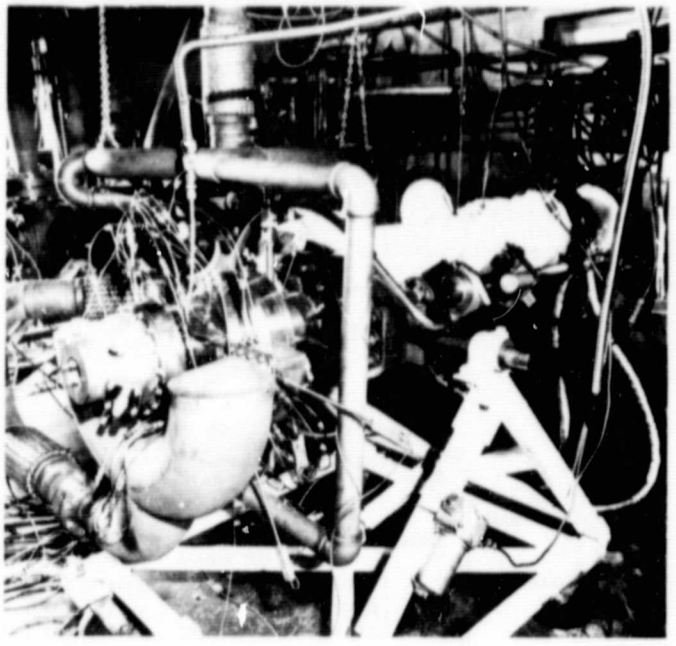

Figure 38. Combustion Test Rig.

TABLE 7. COMPARISON OF RIG TO ENGINE COMBUSTOR INLET CONDITIONS

ENGINE CONDITIONS	IDLE	CRUISE	MAX
Temperature (°F)	1391	1312	968
Pressure (psia)	21.4	25.8	69.4
Fuel/Air Ratio	0.0030	0.0041	0.0089

RIG CONDITIONS	IDLE	CRUISE	MAX
Temperature (°F)	1000	1000	1000
Pressure (psia)	21.8	27.0	63.0
Fuel/Air Ratio	0.0031	0.0043	0.0087

Initial test results at idle and cruise conditions indicated an unacceptable lean blow-out fuel-air ratio, as shown in Figure 39. In an effort to better understand this problem, the DFC was analytically modeled using a 2-dimensional elliptic reacting flow model. Figures 40 through 42 show the predicted streamlines, isothermal and total fuel-air ratio plots for the engine idle case at rig adjusted inlet conditions. As can be seen in these figures, the cup portion of the combustor is very lean. The resulting predicted combustion efficiency was on the order of 25 percent. Garrett experience has shown that predicted low combustion efficiency is indicative of lean blow-out problems.

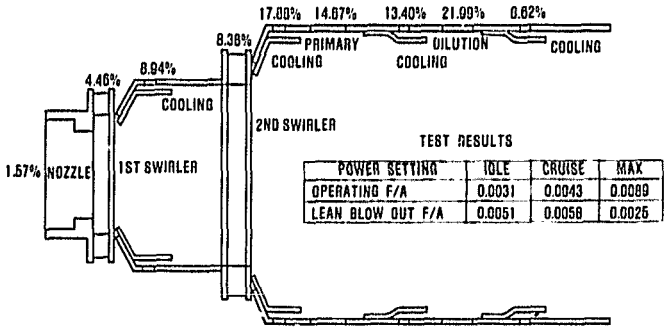

POWER SETTING	IDLE	CRUISE	MAX
OPERATING F/A	0.0031	0.0043	0.0089
LEAN BLOW OUT F/A	0.0051	0.0058	0.0025

Figure 39. Baseline Combustor.

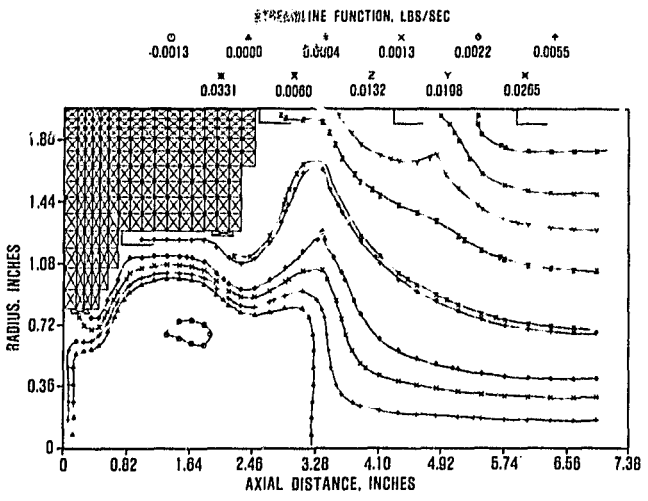

Figure 40. Diffusion Flame Combustor Predicted Streamlines, Idle Condition.

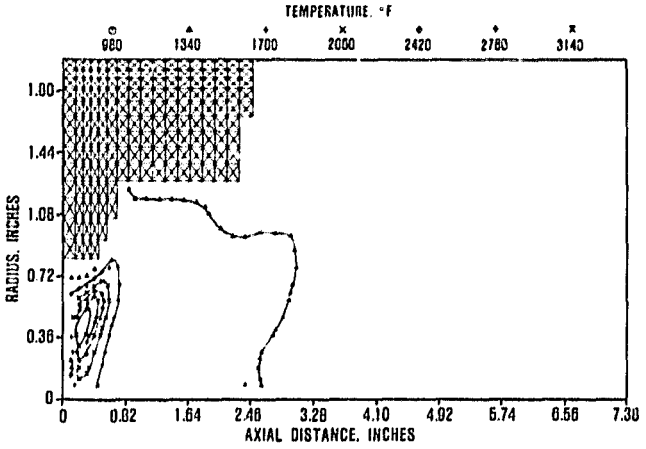

Figure 41. Diffusion Flame Combustor Predicted Isothermal Lines, Idle Condition.

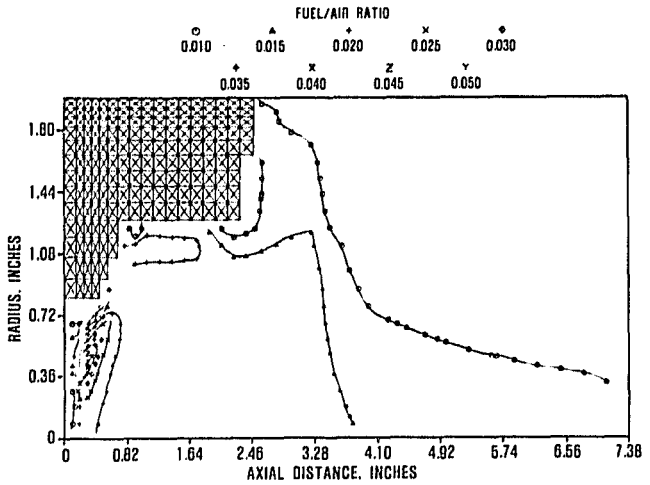

Figure 42. Diffusion Flame Combustor Predicted Fuel/Air Ratio, Idle Condition.

Based on these early test results and subsequent analyses, several potential modifications to the DFC were evaluated. Figures 43 through 45 show predicted results of the selected modifications. This design configuration, denoted Mod A, is configured to richen the cup portion and allow the fuel to burn more completely.

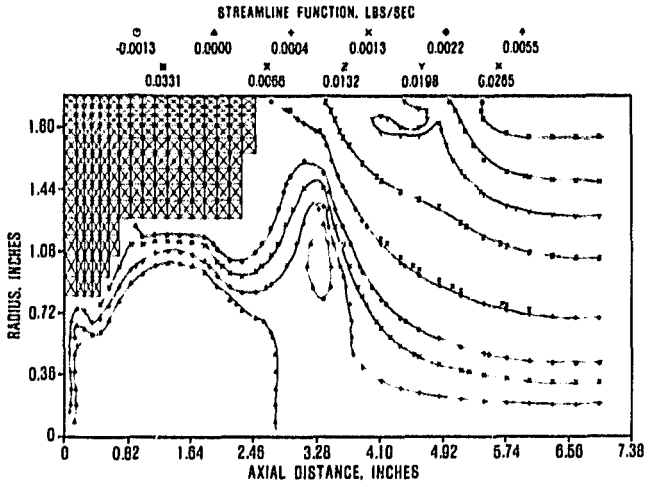

Figure 43. Diffusion Flame Combustor Mod A Predicted Streamlines, Idle Condition.

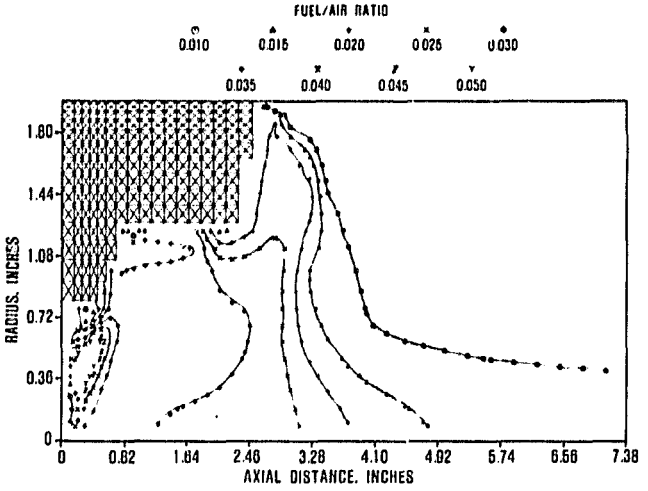

Figure 45. Diffusion Flame Combustor Mod A Predicted Fuel/Air Ratio, Idle Condition.

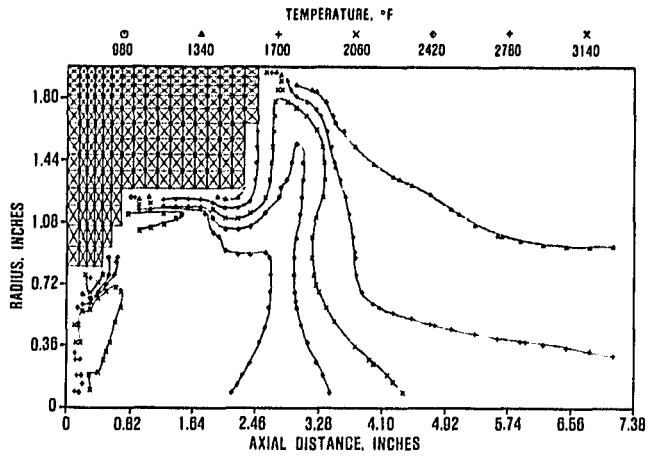

Figure 44. Diffusion Flame Combustor Mod A Predicted Isothermal Lines, Idle Condition.

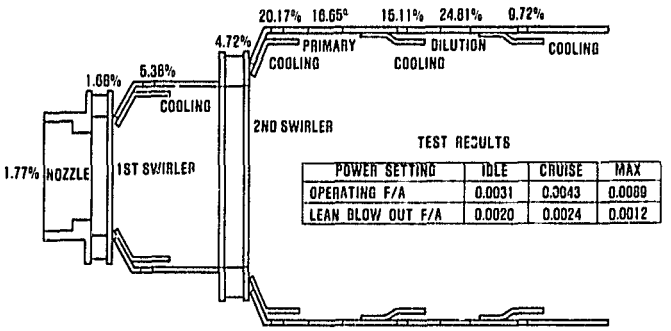

Figure 46. Diffusion Flame Combustor Mod A Airflow Split.

The hardware was modified by reducing the amount of airflow in the cup region as shown in Figure 46. Testing was resumed and resulted in substantially better lean blow-out fuel-air ratios. Figure 47 presents the Mod A combustor test results (see Figure 39 for comparison).

Temperature scans were taken at a location simulating the turbine stator inlet (station 4.1, Figure 12), denoted as the four-inch location, for each of the three power points. The sampling probe, Figure 48, comprises 3 legs (temperature, pressure and emissions) with 5-radial elements each. The probe was rotated through a 160-degree arc in 10 degree increments with zero degrees noting top dead center. The results of the temperature scans are shown in Figure 49. As can be seen, the temperature profiles and resulting pattern factors are quite low, indicating symmetrical burning and inlet air flow distribution. Measured pressure drop ranged

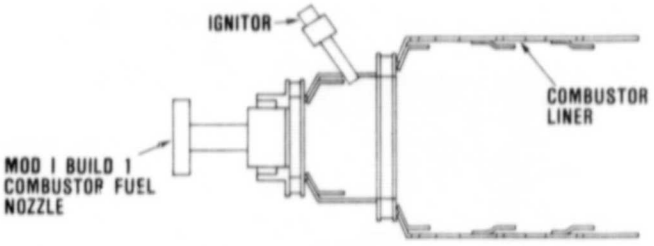

OPERATING CHARACTERISTICS

POWER SETTING	IDLE	CRUISE	MAX
OPERATING F/A	0.0031	0.0043	0.0089
LEAN BLOW OUT F/A	0.0020	0.0024	0.0012
PATTERN FACTOR	0.215	0.130	0.103
MAX RECORDED WALL TEMP (°F)	1167	1237	1332

IGNITION CHARACTERISTICS

ENGINE SPEED (%)	20	30	40
MAXIMUM ALLOWABLE F/A	0.022	0.022	0.022
MINIMUM LIGHT OFF F/A	0.0139	0.0091	0.0076

Figure 47. Diffusion Flame Combustor Mod A Test Results.

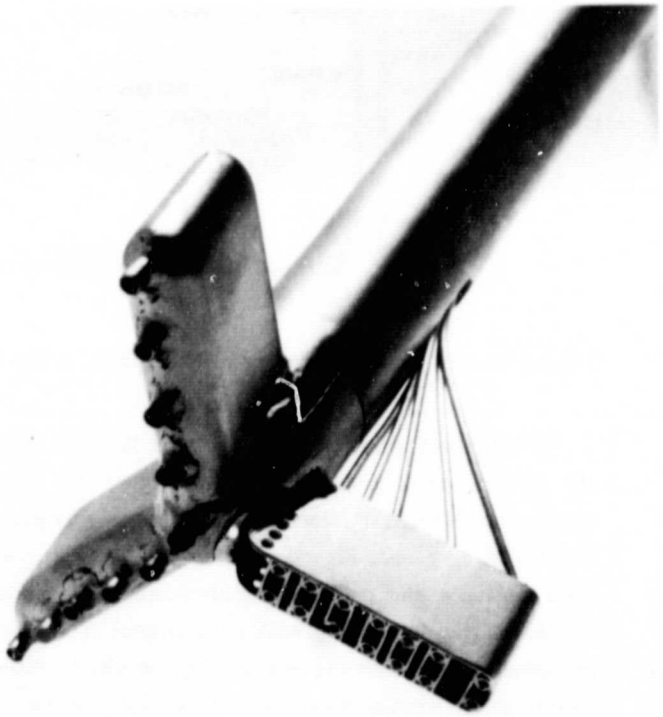

Figure 48. Temperature Probe.

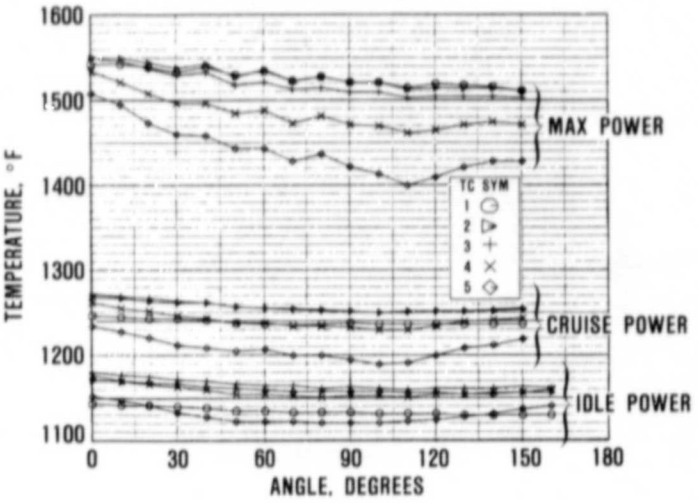

Figure 49. Diffusion Flame Combustor Mod A Temperature Data.

from 1.8 to 3.8 percent for idle to maximum power respectively, compared to predicted values of 2.34 and 3.76 percent, respectively.

Combustor wall temperatures were recorded at 8 locations. The maximum wall temperature was 1332°F at maximum power conditions. Thermopaint tests will be conducted and reported in subsequent reports.

Combustor lightoff characteristics were evaluated as a function of engine cranking speeds. Combustor inlet air flow rate, pressure, and temperature were analytically determined for an 85°F, sea level, cold regenerator start for engine cranking speeds between 20- and 60- percent engine speed in 10- percent increments (see Table 8). Testing was conducted by first setting the combustor inlet conditions and varying fuel flow. For a given inlet condition, the lightoff fuel-air ratio was defined by obtaining two fuel flow test points; one in which ignition and sustained combustion occurred, and one where ignition did not occur. Figure 50 presents the results of this testing.

4.3.2 Variable Geometry (RPD Combustor)

Element testing was continued, with ninety-four emission points obtained. Of the 94 points, 24 represent emission

TABLE 8. COMBUSTOR INLET CONDITIONS FOR A 85°F DAY COLD START AS A FUNCTION OF ENGINE SPEED

Engine Cranking Speed (percent)	20	30	40	50	60
Combustor Air Flow (lb/sec)	0.068	0.112	0.168	0.231	0.302
Combustor Pressure (psia)	14.7	15.2	15.9	16.7	17.6

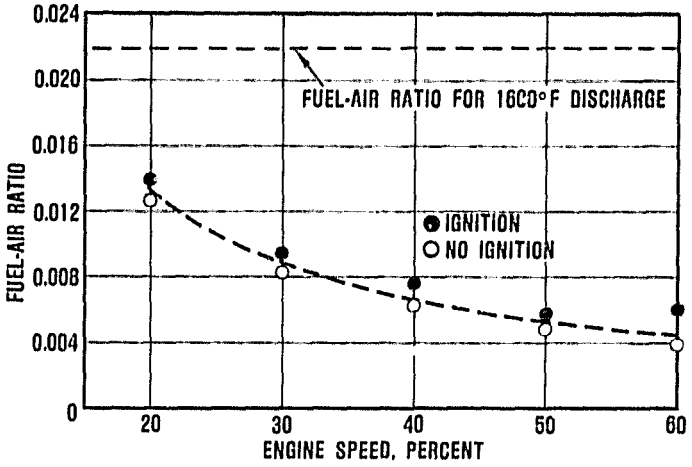

Figure 50. Ignition.

levels of the inline gas-fired preheater to assure that profiles downstream of the preheater were uniform. Figures 51 and 52 show fuel-air ratio and NO_x as a function of radial position at two axial locations (0.5 and 4 inches) for three nozzle inlet temperatures (1500, 1600 and 1700°F). As shown, the fuel-air ratio and NO_x values are uniform for the preheater; therefore, any deviation noted during subsequent testing will be attributed to the liquid fuel injection systems.

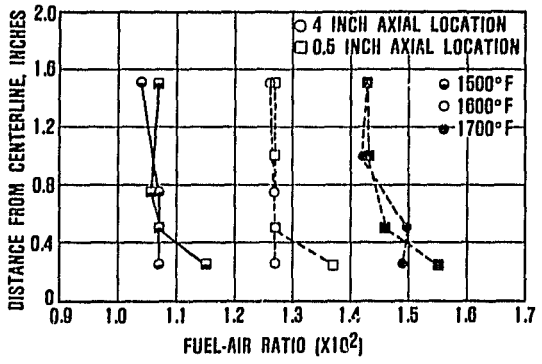

Figure 51. Preheater CO Values.

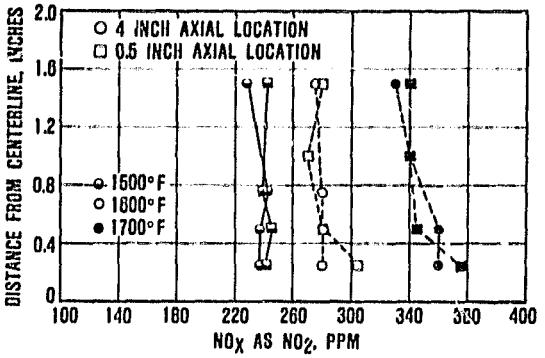

Figure 52. Preheater NO_x Values.

Two duplex airblast liquid fuel injector systems were evaluated: a 1.77-inch diameter and a 2-inch diameter system. A nozzle schematic is shown in Figure 53. As shown, three flow swirlers are incorporated; an outer swirler, inner swirler and central swirler. Airflow entering through the outer swirler interacts and atomizes the secondary fuel while air entering the inner swirler atomizes the primary fuel. Central swirler air flow is utilized to enhance the radial fuel-air mixing intensity in an effort to produce a more uniform fuel-air ratio distribution. Both the 1.77- and 2-inch diameter nozzles were fabricated using modular construction techniques so that the different swirl angles could be evaluated. Swirl angles of 0-, 15-, and 30-degrees counterclockwise and clockwise can be accommodated. For initial test purposes, a 30-degrees counterclockwise configuration was selected for the inner, outer, and central swirler passages.

Testing was divided into the following major categories:

- 1.77-inch diameter duplex nozzle--inlet temperature effects and pressure drop effects
- 2-inch diameter duplex nozzle--inlet temperature effects

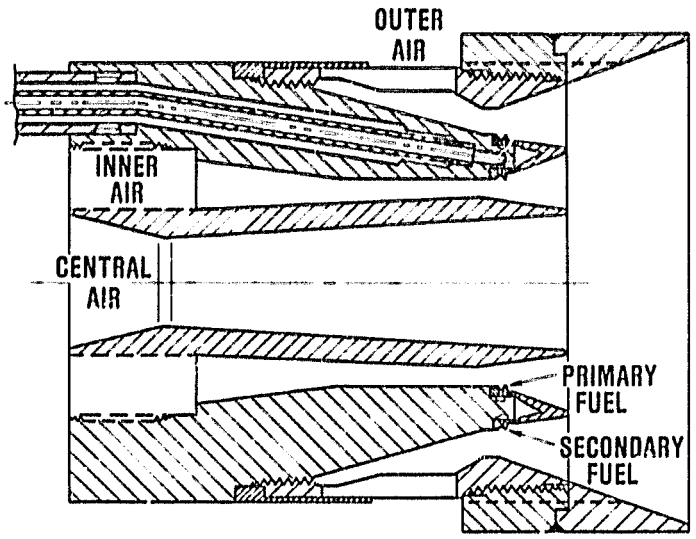

Figure 53. Duplex Airblast Fuel Nozzle.

For each test category, emissions were measured at two axial and six radial locations for each condition. Testing was conducted at a constant liquid fuel-air ratio with the nozzle positioned axially at the maximum power location (outer radial inflow swirler uncovered). Fuel was introduced through the secondary (outer) passages only.

The major differences between the 1.77- and 2-inch diameter duplex nozzles is the effectiveness of outer airblast swirl imparted to the flow. Due to the limited thickness on the 1.77-inch diameter outer airblast radial inflow swirler, the actual swirl imparted to the outer airblast air is minimal. On the 2-inch diameter nozzle, sufficient wall thickness can be accommodated and the 30-degree swirl is present.

Test results for each category are presented for carbon monoxide (CO) and oxides of nitrogen (NO_x) as a function of radial position for the two axial sampling stations (2- and 4-inches downstream of the prevaporizer discharge plane). Test conditions were maintained at 46.5 psia rig inlet pressure and a fuel-air ratio of 0.020. Figures 54 and 55 present test results for the 1.77-inch diameter nozzle for CO and NO_x, respectively. Carbon monoxide levels (Figure 54) at the 2 inch location indicate that fuel is still near the combustor centerline, whereas, at the 4-inch location, the fuel has had sufficient time to diffuse radially outward thereby flattening this profile. Increasing the temperature from 1600 to 1700°F reduces the CO spike diameter, but not significantly. At the 0.25-inch radial sampling point, CO values were greater than instrumentation capabilities.

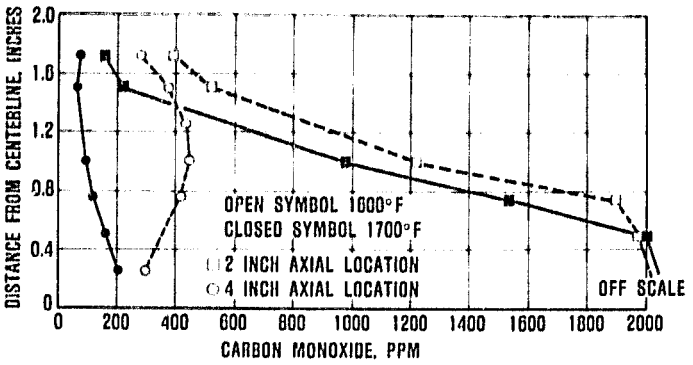

Figure 54. 1.77-Inch Diameter Fuel Nozzle - Effect of Nozzle Inlet Temperature.

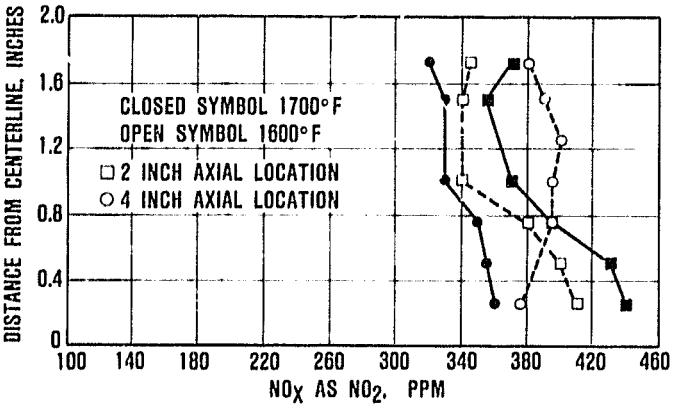

Figure 55. 1.77-Inch Diameter Fuel Nozzle - Effect of Nozzle Inlet Temperature.

Figures 56 and 57 present test results for the 1.77-inch diameter duplex nozzle pressure drop effects. Inlet temperature was held at 1600°F and two corrected flows were

valuated (0.275 and 0.190 lb/sec) corresponding to a doubling of the pressure drop. As shown, the increase in pressure drop reduces the radial width, and magnitude, of the CO and NO_x spikes near the centerline.

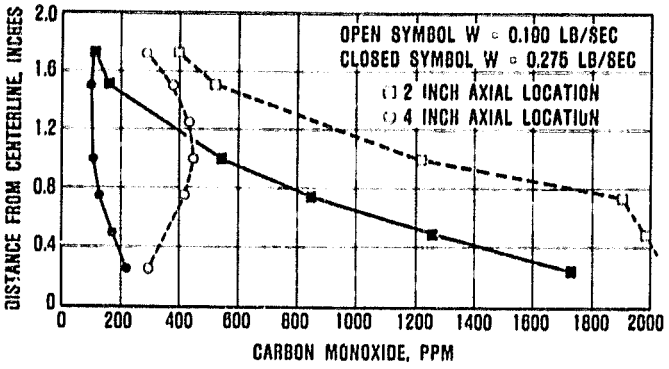

Figure 56. 1.77-Inch Diameter Fuel Nozzle - Effect of Pressure Drop.

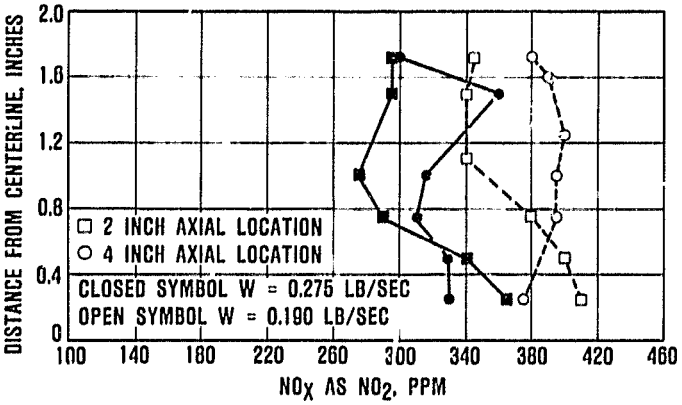

Figure 57. 1.77-Inch Diameter Fuel Nozzle - Effect of Pressure Drop.

Figures 58 and 59 present test results for the 2-inch diameter nozzle inlet temperature effects. In general, radial profiles were improved for the 2-inch diameter nozzle compared to the 1.77-inch diameter nozzle (Figures 54 and 55).

In summary, test results confirmed analytical predictions in that increased mixing yielded more uniform profiles. Pressure drop increases improved the profiles for the 1.77-inch diameter nozzle as did the effective outer airblast swirl imparted with the 2-inch diameter nozzle.

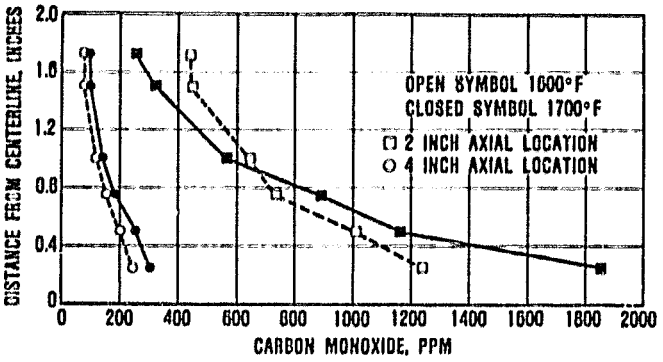

Figure 58. 2.0-Inch Diameter Fuel Nozzle - Effect of Nozzle Inlet Temperature.

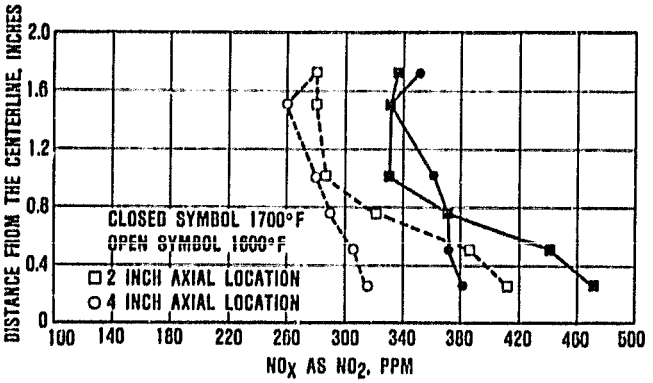

Figure 59. 2.0-Inch Diameter Fuel Nozzle - Effect of Nozzle Inlet Temperature.

4.4 Regenerator System

4.4.1 Ford Regenerator Development

Two regenerator seal wear test rigs are currently being utilized to evaluate the seal coatings. The low temperature (1400°F) rig is used to determine coefficient of friction for comparison with baseline data established on previous Ford seal systems. A second rig, capable of 2000°F operation, is used to determine wear and wear-rate data of different supplier coating samples. A total of 991 test hours has been accumulated on the wear rigs.

During initial checkout of the high temperature rig, an instability or "chatter" condition occurred at temperatures between 1000 and 1400°F with and without load on the coating test bar (noted in Reference 2). This condition was traced to the torque measurement system; modifications were incorporated and testing resumed.

Initial testing in the high temperature rig established correlation with previous Ford test rig data. A test plan then was initiated to evaluate three different versions of the crossarm coating (I-112) supplied by Ferro Corporation to determine an optimum process. In addition, wear test specimens from three different suppliers were received for evaluation.

A torque capacity test was completed on a LAS regenerator with the ring gear attached using the AGT diagonal bond elastomer configuration. Separation of the elastomer did not occur after 750 lb-ft applied torque; three times the maximum torque expected for the AGT regenerator.

New extrusion dies at NGK produced a matrix sample having isosceles triangular flow passages with 0.003-inch wall thickness, which is the 1985 program objective. Cores for the seal wear rig have been ordered. A full-size core for evaluation in the hot regenerator test rig should be available during the fourth quarter.

The original version of the "core position" analysis, written specifically for the Ford 707 regenerator seal system utilizing welded diaphragms associated with the AGT regenerator system, was revised during this reporting period. The core position analysis determines the operating plane of the regenerator by an iterative method that performs a summation of forces and moments imposed on the regenerator. Once this operating plane is determined, the variation in force and stress distribution for each component of the regenerator seal system can be defined.

Evaluation of the initial AGT101 regenerator seal system was completed utilizing this core position analysis. This analysis establishes a baseline for future design changes based on actual hardware experience in the hot regenerator test rig. Based on the core position analysis, the location of the hot and cold side crossarm diaphragm, with respect to the low pressure edge of the rubbing shoe, must be mismatched as shown in Figure 60. This requirement is necessitated by the difference in undershoe pressure distributions between the high and low pressure carryover halves of the crossarm.

Design changes have been initiated to accommodate the mismatched diaphragm locations for the hot and cold side

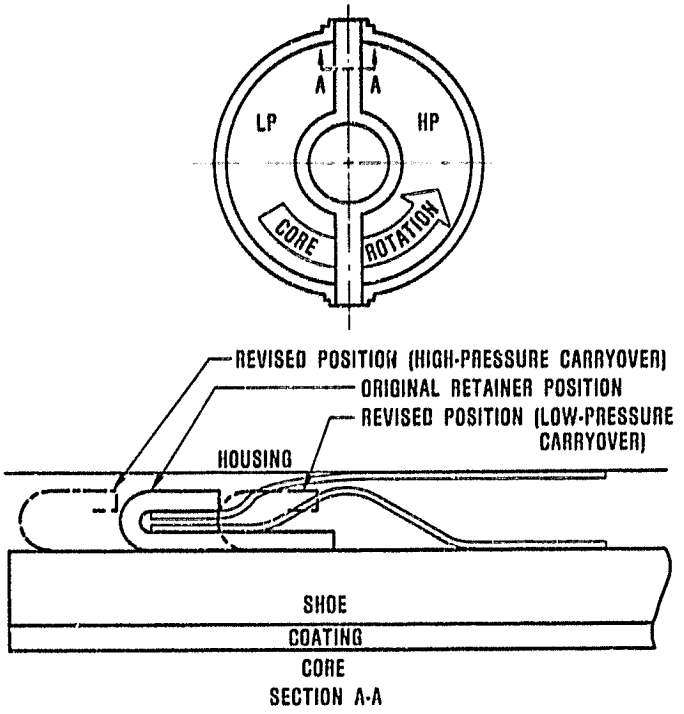

Figure 60. Crossarm Diaphragm Location.

crossarms. New keyways must be machined in the rubbing shoe to properly locate the modified retainers. Existing diaphragms will be adjusted at assembly to accommodate these changes.

The static seal leakage rig is being utilized extensively to evaluate regenerator seal assemblies to identify locations where further leakage reductions can be made. Alterations in diaphragm design and tooling have produced significant reductions in seal assembly leakage. The improvements have been progressive and consistent as illustrated in Figure 61.

During this reporting period, the initial two complete engine sets of regenerator system hardware were shipped to Garrett. The leakage level for each regenerator seal assembly was approximately 5 percent. This represents a significant reduction from the first seals evaluated in the static seal leakage rig, which were slightly above the state-of-the-art objective of 7.2 percent. These seals do not have the mismatched diaphragm locations for the hot and cold side crossarms dictated by the core position analysis. Tooling

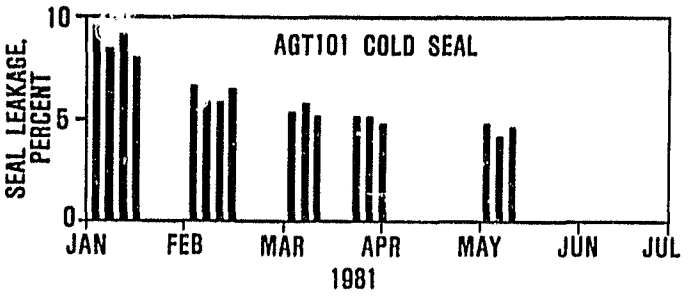

Figure 61. Static Seal Leakage Test Results.

required to accommodate the mismatched diaphragm locations will be available during the next report period.

Efforts also have been concentrated on improving the graphite bearing design for the regenerator drive and support system. The revised design, based on the Ford 707 engine design, successfully replaced the grease-packed ball bearing system, and is shown in Figure 62. The revised design illustrated in Figure 62 features the following improvements:

- o Elimination of costly shoulders
- o Total compressive support for the bearing
- o Simplified roller support design
- o Steel-backed pinion bearings can be press fit without preheating the housing
- o Multiple-bonded graphite buttons, which utilize a highly developed bonding procedure, are used as the pinion thrust surface

Hardware for the modified drive and support system will be available during the next reporting period.

4.4.2 Garrett Regenerator Development

Two cold flow regenerator test rigs, low pressure (LP) and high pressure (HP), were designed and fabricated for purposes of evaluating the quality of flow (distortion) entering the regenerator core. Details of the rig design activities were discussed in References 1 and 2.

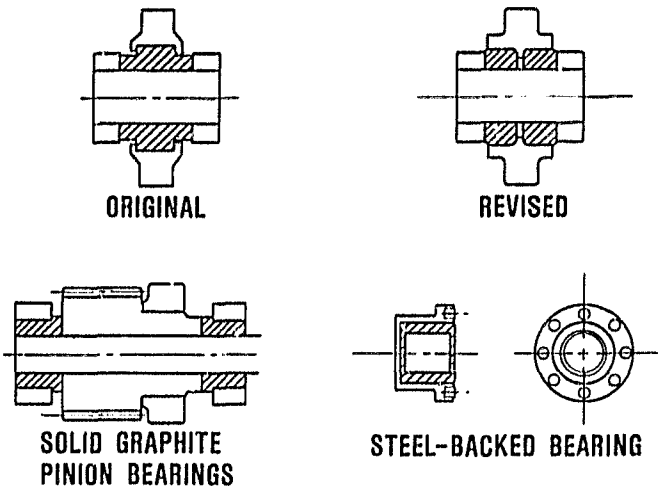

Figure 62. Regenerator Drive and Support System Bearing Designs.

The objectives of the LP and HP cold flow test programs focused on:

- o Determination of circumferential and radial pressure distortion profiles imposed on the core inlet faces by engine flowpath geometry
- o Evaluation of distortion influencing/controlling mechanisms
- o Generation of data to allow analytical prediction of the installed regenerator effectiveness

Based on duty cycle histograms for the reference vehicle on the combined federal driving cycle (CFDC), the aggregate fuel consumed in the upper 60-percent power range is negligible; therefore, regenerator cold flow testing was focused on the cruise power conditions.

Initially, testing was conducted using hot-wire anemometry techniques to determine the velocity profiles near the core face. During the course of testing a second measurement system was employed which involved using pressure probes at the respective core faces and essentially measuring core inlet stagnation or exit static pressure (see Figure 63). Data obtained by the second measurement technique were

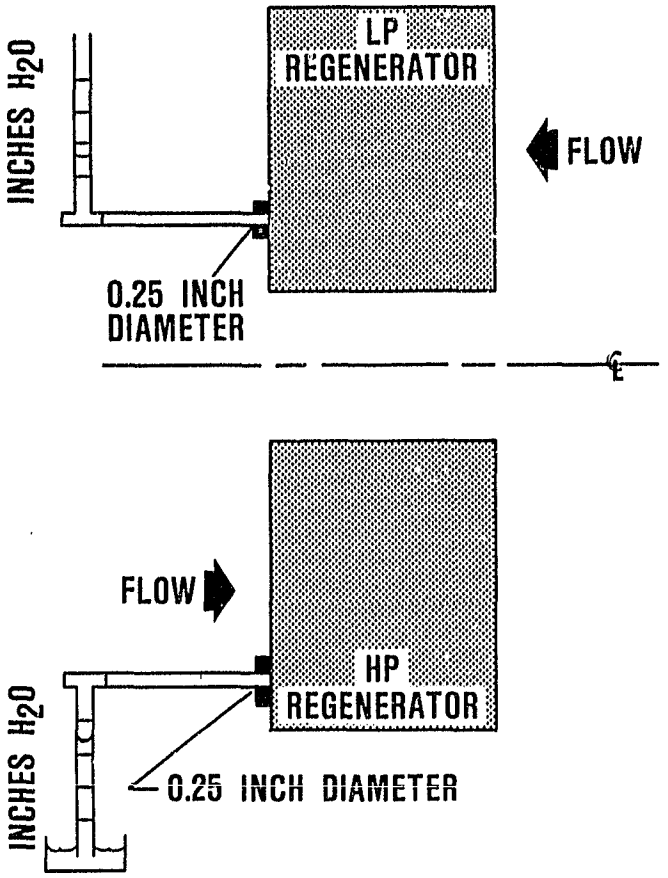

Figure 63. Regenerator Core Pressure Drop Measuring Technique.

utilized for all performance calculations. Hot-wire data was effectively utilized during test to evaluate different flow influencing mechanisms on a gross basis and to gain understanding of the flow acceleration patterns within the HP and LP plenums.

It should be noted that the regenerator analytical model and test activities were undertaken concurrently; therefore, a distinct interplay evolved between analyses and tests. This interplay has revealed several phenomena, some of which may be contrary to reader intuition. Therefore, to assist the reader, a summary of these phenomena are listed below and should be borne in mind during review of the regenerator flow test results and subsequent discussion, herein.

a) Pressure distortion profiles under evaluation are primarily the result of the flow acceleration/deceleration components in the LP-inlet and HP-discharge plenums. The magnitude of the axial velocity head ($Q = \rho V_a^2/2g$) at the core faces is of the order of 1 percent of the core pressure drop and, therefore, is considered a negligible factor. Therefore, measured core pressure drops may be considered indicative of either total or static core pressure drops.

   Of significantly more importance are the static pressure gradients related to fluid acceleration/deceleration forces in the plenum areas. These accelerations are estimated on the order of 25 g's.

b) Pressure distortion is manifested by asymmetric redistribution of gas flow through the regenerator in an engine environment. The resultant flow pattern may, in turn, significantly affect regenerator effectiveness.

   The regenerator may be viewed as a series of parallel heat exchangers divided into concentric cylindrical segments, each essentially independent from the others. Flow distortion may result in significant variation of the flow ratio of LP and HP sides of a segment and, hence, variation in the effectiveness. The combined effectiveness of the segments will always be less than or equal to the undistorted case.

c) Analysis (discussed later) shows that the effect of turbine exit swirl (imposed circumferential pressure distortion) does not materially affect performance (effectiveness) while radial distortions may have a significant impact.

d) The cold rig test data was compiled with rig corrected flow and Mach number equal to the corresponding engine operating condition at the distortion station. Therefore the absolute magnitude (in terms of pressure ratio) of the pressure distortion is identical at cold rig and engine conditions.

e) Detected areas of high core pressure drop, in the LP core matrix during cold test, analytically may translate into areas of low mass velocity ($G = \rho V = \dot{\omega}/A$) when rotational and thermal effects are introduced.

f) Engine performance predictions are based on the assumption that a complete dump pressure loss is taken at the turbine diffuser exit. The 3-D analysis also predicts that an increase of only 0.07 percent total pressure loss (1 percent of the fractional pressure loss) occurs in the presence of distortion at maximum power. The LP distortion, which has the greatest effect on performance, therefore, is derived from kinetic energy that is already considered lost. The effect of such small increases in presure drop on engine performance is considered negligible.

With these statements in mind, the following paragraphs describe the test rig results and subsequent analyses.

4.4.2.1 Regenerator LP Cold Rig Testing

The main objectives of the LP cold flow rig tests were as follows:

- o Determine circumferential and radial pressure distortion profiles imposed on the LP inlet core face by engine flowpath geometry
- o Investigate and evaluate different flow influencing devices and the effect on overall regenerator performance

Test rig configuration and instrumentation are defined in References 1 and 2. As previously stated, hot wire anemometry techniques were employed during initial testing. However, due to the geometry of the 3-D hot wire probe sensing elements, wherein, discrete (matrix cell) velocity jets could impinge on an individual probe element, the results of testing were highly suspect. Therefore, hot wire anemometry data was used to ascertain flow trends within the plenums, and core pressure drop data (Figure 63) was used during later testing for obtaining raw test data to be used in the analysis.

A series of tests were conducted at simulated turbine rotor exit swirl angles and respective flows to determine the effect of swirl on regenerator LP inlet pressure distortion. Swirl angles of +55 degrees (idle), 0 degrees (cruise), and -27 degrees (maximum power) were induced at the rotor exit plane (station 5.0, Figure 12). Concurrent 3-D analysis showed that circumferential distortion of comparatively large magnitude has a negligible effect on regenerator effectiveness when gas/matrix heat transfer and core rotation effects are considered. Data to support this contention is supplied in Section 4.4.2.3.

Tests also were conducted at various mass flows [hence Mach number and plenum head Q ($\rho V^2/2g$)] and 0 degrees swirl. These tests were conducted to determine effects of mass flow variations on regenerator LP-inlet pressure distortion. Results indicate that the pressure distortion magnitude remains approximately linear with inlet Q as mass flow rates increase.

Based on the above test results and the fact that the aggregate fuel consumed over CFDC in the upper 60-percent power range is negligible, all remaining cold flow pressure distortion testing (LP and HP) was conducted at cruise conditions.

Figure 64 presents the observed inlet pressure distortion (local cold core pressure drop) for the LP core face imposed by engine flowpath geometry at the simulated cruise condition.

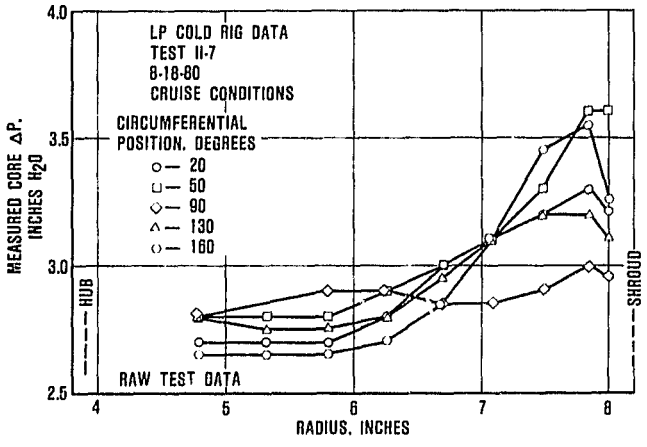

Figure 64. Measured LP ΔP Data From Regenerator Cold Rig.

Several flow influencing devices were evaluated to determine the potential of reducing LP inlet flow distortion. Downstream devices (baffles) showed limited potential for

reducing LP inlet flow distortion. An upstream "diverter", Figure 65, showed good potential for redistributing the flow, as noted in Figure 66. The parameter U/V_{REF} seen in Figure 66 is based on 3-element anemometer data and is the ratio of local to average axial velocity at core inlet.

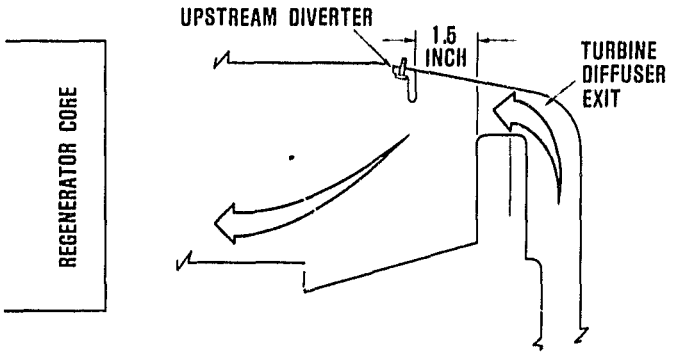

Figure 65. LP Regenerator Cold Rig Upstream Diverter.

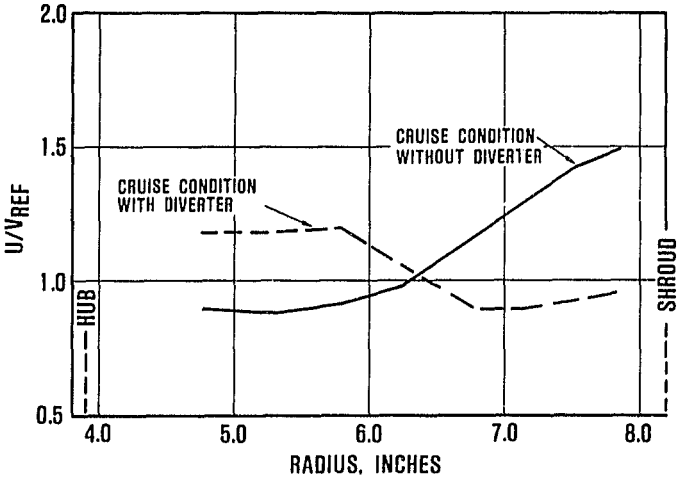

Figure 66. LP Regeneration Cold Rig, Effects of Upstream Diverter.

For the ceramic engines, placement of the upstream diverter requires ceramic fabrication tooling changes. Therefore, it was decided to await hot regenerator rig test results prior to any further evaluation or adoption of this upstream diverter for AGT101 application.

Data obtained from LP and HP cold rig testing were used to predict regenerator performance in the engine as described in Section 4.4.2.3.

4.4.2.2 Regenerator HP Cold Rig Testing

Main objectives for the HP cold flow rig tests were the same as the LP cold flow rig tests and test rig design and instrumentation details also are reported in References 1 and 2.

Testing was initiated to determine HP inlet flow distortion at engine cruise operating conditions. Radial distortion (from hub to shroud) was measured for a bare, untreated HP flowpath.

Several flow influencing devices (bonnets) were evaluated on the downstream HP flowpath utilizing hot-wire anemometry. Figure 67 shows the dramatic influence of one of the bonnets on HP-flow conditions in terms of HP-discharge velocity ratios (U/V_{REF}).

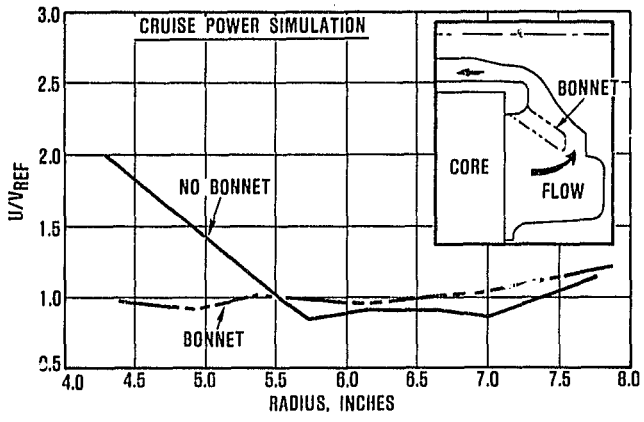

Figure 67. HP Regenerator Cold Rig Flow Effects of Bonnet.

Figure 68 shows the HP regenerator cold rig test data used for subsequent analyses. Testing was conducted both with and without the HP-inlet housing (exhaust housing) and confirmed that HP-inlet flow distortion is dominated almost solely by hot face geometry (downstream bonnet).

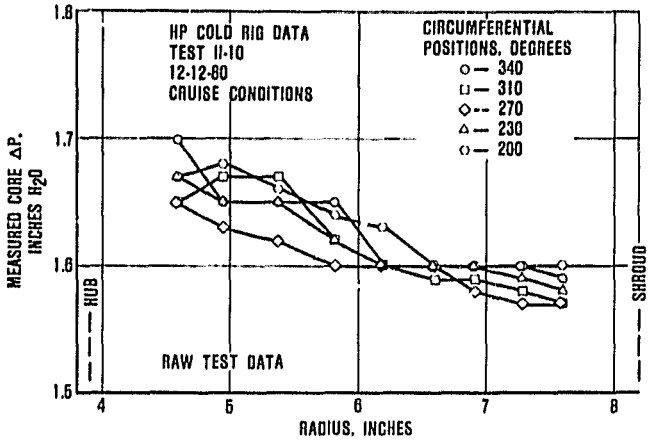

Figure 68. Measured HP ΔP Data From Regenerator Cold Rig With Bonnet.

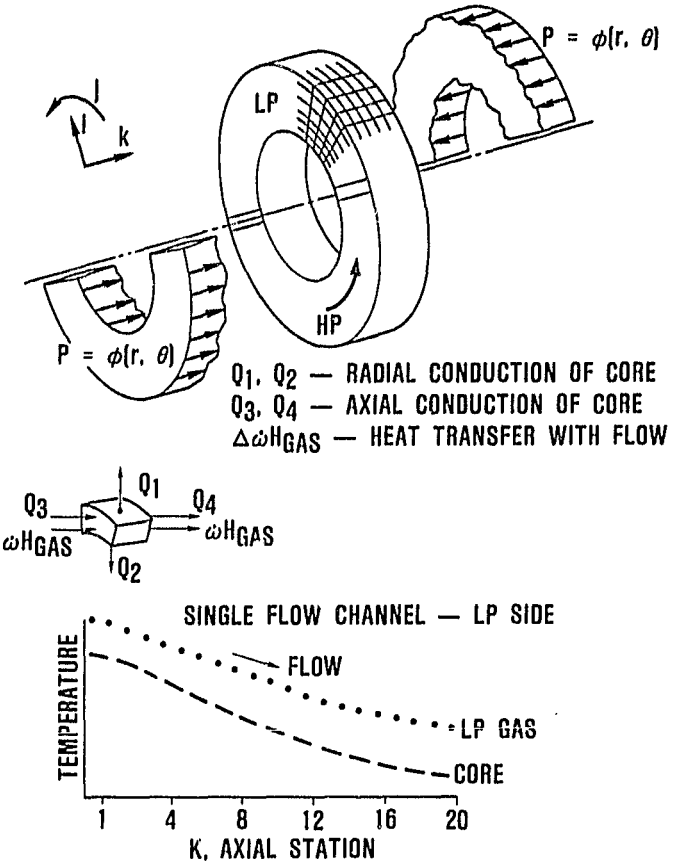

Figure 69. Measured Analytical Flow Distortion Model.

4.4.2.3 Regenerator Analysis

To predict regenerator effectiveness based on cold flow test data, an analytical model using 3-dimensional finite element techniques was used. The core matrix was divided into 10-radial stations, 20-axial stations and 360-rotational increments. Core matrix geometry and pressure drop/heat transfer characteristics are program inputs.

Care should be exercised when comparing quoted regenerator effectiveness associated with engine performance (Section 3.2) to results presented herein. Performance discussed in Section 3.2 includes effects of regenerator seal leakage and, therefore, represents the mixed flow effectiveness for the entire regenerator system. The results described in Section 4.4 refer only to core effectiveness. Mass flows used in the 3-D analysis for both the LP and HP flowpaths have been adjusted for predicted seal leakages.

4.4.2.3.1 Analytical Model

Regenerator core effectiveness was analytically predicted by imposing measured or prescribed core inlet face pressure distortion profiles on the rotating 3-dimensional heat transfer model. Figure 69 shows the principle features of the analysis wherein matrix geometry, Colburn number characteristic, Fanning friction factor characteristic and core rotational speed are program inputs. Heat transfer and core pressure drop calculations, within the core matrix, are determined using local properties (i.e., local Reynold's Number, viscosity, etc). The analytical model also includes effects of local radial and axial conductive heat transfer to neighboring elements. Individual elements are analyzed for heat transfer along five paths (four core conduction and one gas convection path). Time integration is used to arrive at a steady-state heat transfer solution that is consistent with this pressure distortion profile imposed at the HP and LP inlet planes.

Sample Procedure

As an aid in explaining the test and analytical procedures, the following paragraphs describe the steps involved in obtaining an analytical prediction of regenerator performance in the engine. Since the cruise condition is of most interest, it is the subject of the example case.

Step 1; Cold Rig Testing

Cold rig tests were performed using the LP and HP cold flow rigs. The salient corrected flows (and therefore the Mach numbers) predicted for engine operation at cruise were supplied to the respective rigs. The corrected flows simulated were LP inlet and HP discharge since these are the locations generating the bulk of the pressure distortion.

Data were taken in the form of core pressure differential. Data for the LP rig were obtained by stagnating small core areas (0.25 inch diameter) from the exhaust side. The upstream stagnation pressure was then measurable through the core matrix. Static pressure data from the HP cold rig were obtained in similar fashion from the HP inlet core face.

It is assumed that the core face stagnation pressure is essentially unaffected by the instrumentation measurement technique since the axial velocity through the core corresponds to only about 0.01-inch H_2O velocity head (approximately one percent of the peak-to-peak distortion level).

Figures 70 and 71 describe the raw cold rig ΔP (local cold core pressure drop) data for the HP and LP rigs. Note the excellent agreement between the theoretical (calculated from the core matrix Fanning friction factor data) ΔP for uniform flow and the average measured ΔP in both cases.

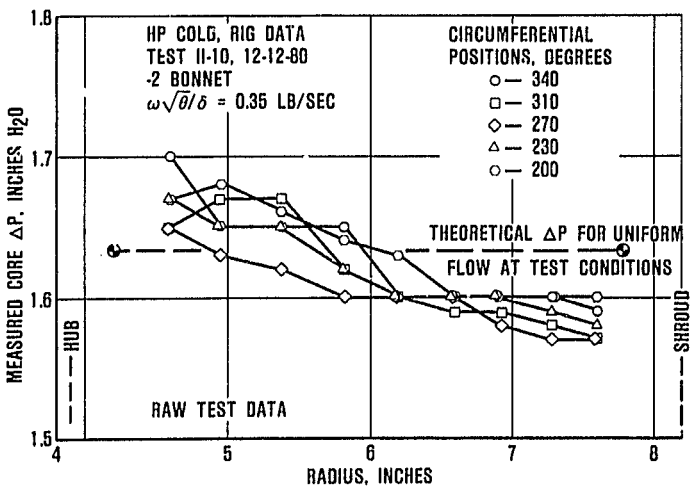

Figure 70. Measured HP ΔP Data From Regenerator Cold Rig.

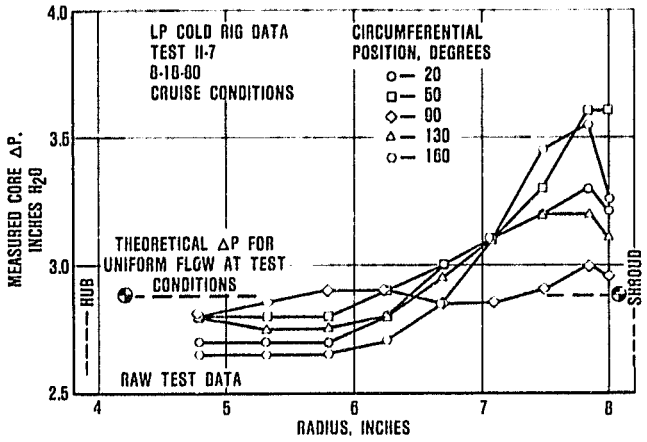

Figure 71. Measured LP ΔP Data From Regenerator Cold Rig.

Step 2; Test Data Preparation

The P data shown was scaled slightly upward [by the ratio of $P(\omega\sqrt{\theta}/\sigma)^2$] to match the latest predicted engine hot face corrected flow and Mach number at the cruise condition. This step is required solely because engine predicted state points had changed slightly between test and analysis stages.

Step 3; Analytical Input

The scaled HP and LP pressure field data were input to the 3-dimensional analysis as hot face pressure boundary conditions. The analysis allows a uniform pressure drop bias to pass the required flow rates. However, the variable portion of the pressure profile is preserved. The gross level of pressure drop is a result of core matrix pressure drop while the variable (profile) portion is the result of flowpath geometry and flow redistribution patterns.

Step 4; 3-Dimensional Analysis

The analysis was run with the above pressure profiles as boundary conditions and the predicted engine flow, temperature and pressure data as input. The analysis iteratively arrives at a heat transfer solution and HP- and LP-flow profiles, which satisfy the heat transfer, energy balance, and pressure drop boundary conditions.

Step 5; Interpretation of Analysis

Figure 72 shows the analytical prediction of capacity rate ratio (CRR) and LP and HP mass velocities (G = ρV), which result from the imposed (test) pressure fields and flow conditions. The mass velocities and CRR are circumferentially averaged at each radial station in Figure 72. Note that CRR is defined here as the ratio of LP-capacity rate divided by HP-capacity rate and is not necessarily equal to C_{Min}/C_{Max}. Figures 73 and 74 summarize the analytically predicted cruise discharge face gas isotherms and mass flux contours.

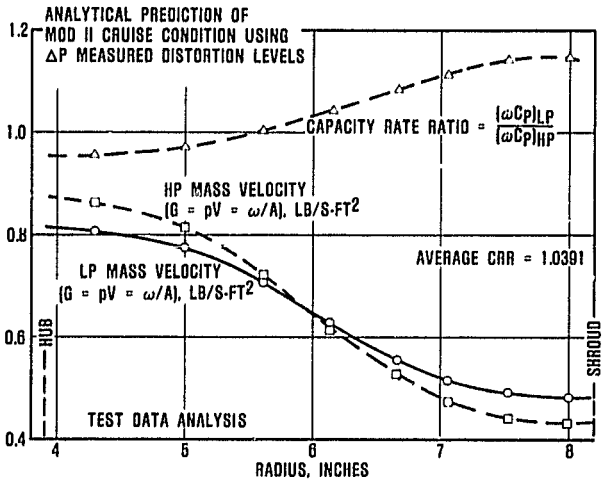

Figure 72. Capacity Rate Ratio and Integrated Mass Flux Versus Radial Position.

Observe that even nominal distortion generates a significant (100°R/inch) radial discharge gas temperature gradient at the LP and HP carryover points (about 170- and 350-degrees angular position). The idealized case (no pressure distortion) yields essentially radial isotherms (no radial gradient) except for slight asymmetry introduced by the cross arm seals.

The analysis predicts an HP-side temperature effectiveness of 0.9662 with the imposed distortion levels. This compares with the ideal effectiveness of 0.9779 in the absence of pressure distortion. The predicted loss in effectivess due to distortion is, therefore, 0.0117 at the cruise condition. No significant effect on performance is antici-

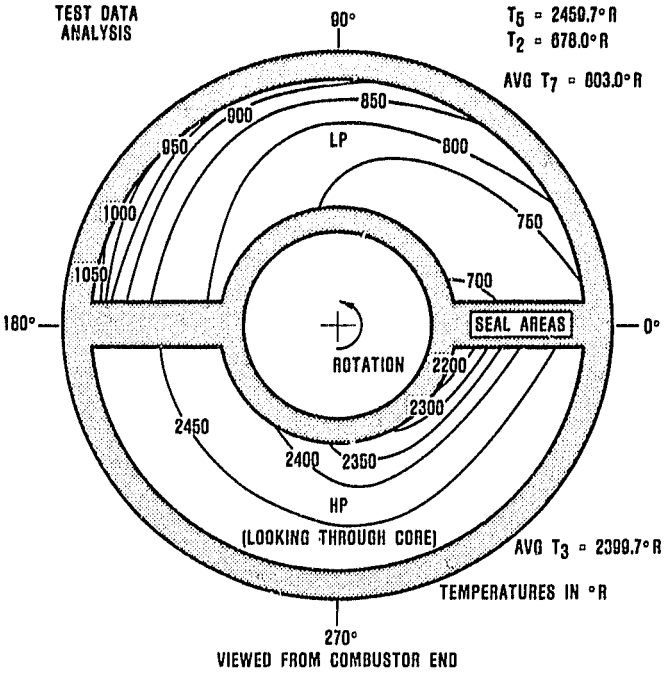

Figure 73. AGT101 Mod II Predicted Regenerator Discharge Gas Isotherms for the Cruise Condition Based on Cold Rig Pressure Distortion Patterns.

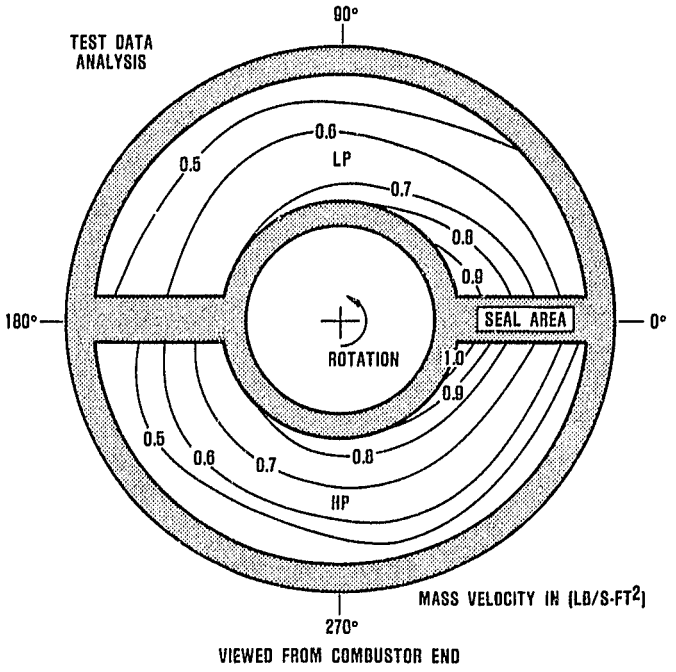

Figure 74. AGT101 Mod II Predicted Regenerator Local Core Mass Velocities for the Cruise Condition Based on Cold Rig Pressure Distortions.

pated from the slight predicted increases in core pressure drop. These small increases in pressure drop are manifestations of residual flow kinetic energy which is already considered lost in the engine performance predictions.

Analysis of distortion effects was similarly accomplished for operating points along the engine operating line from idle to maximum power. The penalty, in terms of fuel flow, was then correlated to engine output power as described in the following section.

4.4.2.3.2 Analytical Results

Table 9 summarizes the regenerator analysis results. Cases 1 through 7 and 14 are hypothetical cases using prescribed distortion profiles. Cases 9 through 13 and 15 through 18 are evaluations with measured distortion profiles based on LP and HP testing. Initial work (cases 1 through 8) was conducted using early engine cycle statepoint data corresponding to a low cruise (15 hp) condition. Subsequent work (cases 9 through 18) was performed using current Mod II engine statepoints (References 1 and 2).

TABLE 9. REGENERATOR ANALYSIS SUMMARY

Case	Engine Power	LP Core Inlet Distortion	HP Core Inlet Distortion	Effectiveness ($\Delta T/\Delta T_{MAX}$)	
				E_{HP}	E_{LP}
1	Low Cruise	1-D Ideal	1-D Ideal	0.9823	-
2		Ideal (3-D)	Ideal (3-D)	0.9837	0.9473
3		0.42 in-H_2O Radial**	Ideal	0.9810	0.9445
4		1.00 in-H_2O Radial**	Ideal	0.9734	0.9359
5		1.95 in-H_2O Radial**	Ideal	0.9607	0.9212
6		Ideal	0.21 in-H_2O Radial**	0.9814	0.9449
7		Ideal	0.976 in-H_2O Radial**	0.9648	0.9259
8		ΔP MAP 8-18-80	Ideal	0.9794	0.9426
9	Idle	1-D Ideal	1-D Ideal	0.9849	-
10	Idle	Ideal (3-D)	Ideal (3-D)	0.9841	0.9632
11	Idle	ΔP Map 8-18-80*	ΔP Map 12-12-80*	0.9808	0.9603
12	Cruise	1-D Ideal	1-D Ideal	0.9750	-
13	Cruise	Ideal (3-D)	Ideal (3-D)	0.9779	0.9430
14	Cruise	2.23 in-H_2O Circumferential	Ideal (3-D)	0.9778	0.9429
15	Cruise	ΔP Map 8-18-80*	ΔP Map 12-12-80*	0.9662	0.9299
16	Max	1-D Ideal	1-D Ideal	0.9506	-
17	Max	Ideal (3-D)	Ideal (3-D)	0.9549	0.8996
18	Max	ΔP Map 8-18-80*	ΔP Map 12-12-80*	0.9421	0.8858

*ΔP maps scaled from cold flow rig for appropriate corrected flow
** Linear variation of (P_{SHROUD}-P_{HUB}) in inches H_2O

Results of case studies showed good agreement between the traditional 1-dimensional (1-D) solution* and the 3-dimensional (3-D) finite element solution for undistorted cases.

Figure 75 presents results of cases 2 through 8. These case studies, with hypothetical distortion were configured to evaluate and quantify the effect of radial inlet distortion profiles. The prescribed inlet distortion profile for these cases is linear with radius from hub to shroud. Note the difference in LP and HP sensitivity.

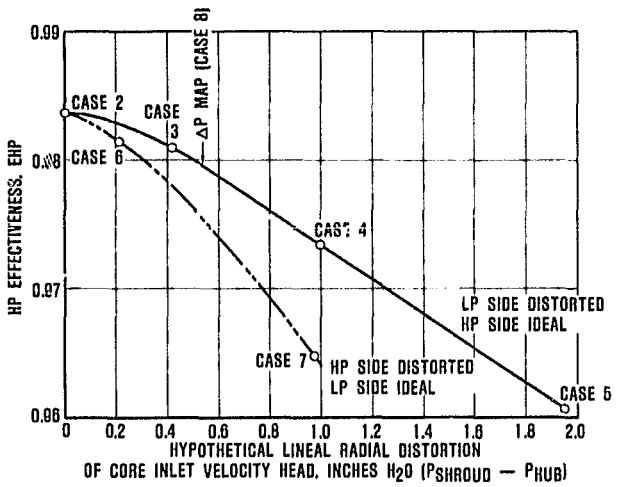

Figure 75. Effect of Linear Radial Distortion on Regenerator HP Effectiveness.

Early measured LP-cold flow data for the low cruise condition was analyzed with a uniform (ideal) HP inlet flow. Case 8 results, shown in Figure 75, indicates that the distortion measured on the LP rig yields an effectiveness degradation of (0.0043) equivalent to a linear radial LP inlet distortion profile of 0.56-inch H_2O.

Cases 9 through 18 summarize the analysis for idle, cruise and maximum power using current Mod II engine cycle statepoints. Cases 13 and 14 can be used to evaluate the effects of LP-circumferential pressure distortion. Case 14 is a case with a hypothetical circumferential pressure distortion of 2.23 inches H_2O (positive gradient in direction of rotation). This magnitude is two to ten times greater in peak-to-peak magnitude than the observed cold flow radial distortions, and yet results in a negligible (Δ = 0.0001) degradation of effectiveness. Other cases (HP side and negative gradients), not included in Table 9, show equal or lesser impact. Circumferential distortion of any reasonable magnitude is not considered to impact regenerator performance.

Cases 9, 12 and 16 are traditional 1-dimensional analyses and are provided for comparison with Cases 10, 13, and 17, which are 3-dimensional analyses. Cases 11, 15, and 18 are analytical evaluations using distortion profiles measured during LP and HP cold flow testing. Both the LP and HP inlet flowpaths are untreated (no baffles or flow diverters) and the magnitude of distortion is corrected from cold test conditions to engine operating conditions by the ratio of $P\dot{\omega}\sqrt{\theta}/\delta)^2$.

Cases 11, 15, and 18 results are utilized in the construction of Figure 76, where effectiveness and fuel flow penalties are projected as a function of engine horsepower. These projections are determined through the use of engine performance and CFDC computer models. Since the majority of fuel consumed over the CFDC occurs in the 0 to 40 hp range, the expected fuel consumption penalty for an engine without regenerator distortion treatment is predicted to be approximately 3.5 percent.

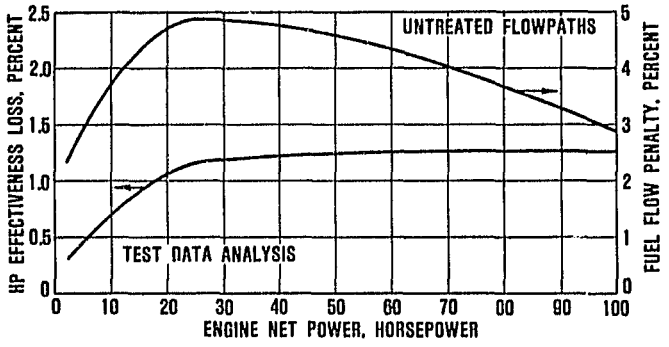

Figure 76. Effect of Measured HP and LP Distortion on Effectiveness and Fuel Flow.

*Kays and London

4.4.3 Regenerator Hot Test Rig

The regenerator hot test rig objectives are summarized below:

- o Determination of regenerator seal leakage by the use of an inert gas (helium) seeding/detection system
- o Optimization of flow distortion treatment geometry
- o Determination of the matrix effectiveness at optimum core rotational speeds for idle, cruise, and maximum power simulated conditions. Seal leakage is automatically factored into the core performance
- o Determination of core drive torque under the following conditons:
  - New seal breakaway torque
  - New seal break-in interval (idle conditions for approximately 10 hours)
  - Core drive torque during engine start sequencing
  - Steady-state torque at idle, cruise, and maximum power simulated engine conditions
  - Verify matrix $\Delta P/P$ (HP and LP) at idle, cruise, and maximum power simulated engine conditions
  - Measure bore cavity pressure at core ID under idle, cruise, and maximum power simulated engine conditions, and size the bleed orifice to LP discharge to limit pressure in this area

The regenerator hot test rig design is shown in Figure 77. The rig is designed to minimize extraneous leakage paths (at seal locations) by eliminating all seals not required for unit assembly. Braze joints replace seal joints so that leakage from the HP side of the rig to the LP side can only occur across the static side of the regenerator seal, flipper seal, and the dynamic face of the regenerator seals. The rig will operate initally with an NGK core and first-generation, Ford-designed/fabricated, seal assembly. Core performance will be evaluated at idle, cruise, and maximum power Mod I Build 1 simulated engine conditons (except swirl entering the LP cavity).

Figure 77. Regenerator Hot Test Rig.

4.5 Gearbox/Transmission

All gearbox and transmission activities at Garrett and Ford (procurement and fabrication of hardware and test rigs) were deferred to a later time due to budget constraints. Existing hardware was placed in storage and outstanding hardware orders were cancelled, where applicable, to conserve project funds.

4.6 Ceramic Material and Component Development

4.6.1 Ceramic Structures

4.6.1.1 Structures Rig

The structures rig (illustrated in Figure 78) was designed and fabrication initiated. This rig will test all the Mod I and Mod II ceramic static structures to 2000°F. A ceramic deswirl "rotor" was designed and fabricated to deswirl the turbine nozzle discharge to radial diffuser inlet flow. With the absence of a turbine rotor, the rig is limited to 2000°F, which is the maximum regenerator inlet temperature limit.

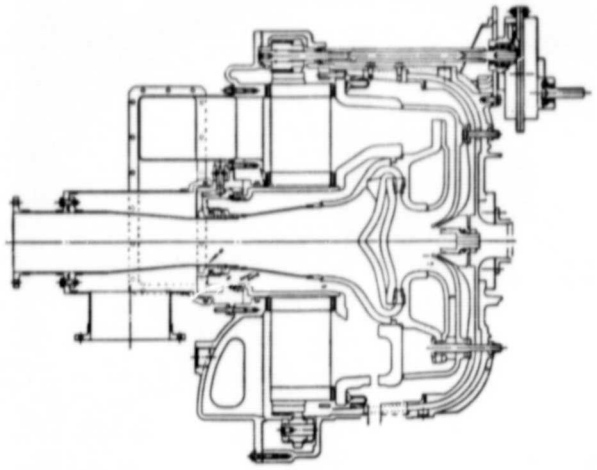

Figure 78. 2000°F Structures Rig.

Thermal transients and maximum regenerator temperature testing will be possible in this rig.

4.6.1.2 Screening Rigs

Fabrication of five ceramic screening rigs was completed during this reporting period. These rigs were designed to mechanically load, in the direction indicated by analysis, the highest stressed ceramic components to a predetermined material stress to screen parts with gross imperfections.

Additional discussions of the ceramic screening rig tests are provided in Section 4.6.1.4, below.

4.6.1.3 Contact Stress Rig

A ring-type ceramic contact stress rig was fabricated to determine the effects of circular ceramic geometries in contact under various steady-state and cyclic thermal and pressure load conditions. Rings of α-SiC, RBSN, LAS, and Haynes 188 have been fabricated for these tests. Respective material interfaces will be evaluated on the basis of surface condition (40X magnification) with variables of: interface geometry (i.e., planer or radius) and compliant coatings as a function of load and temperature.

4.6.1.4 Ceramic Parts and Testing

Regenerator Shields - Carborundum

Four regenerator shields received from Carborundum (α-SiC material) were inspected, heat treated, and have undergone screening tests. Strain gauges were installed on the first part as shown in Figure 79. The part was installed in the screening rig and hydraulically pressure tested to 20 ksi peak stress. Three of the four shields successfully passed this test while the fourth fractured at 18 ksi.

Figure 79. AGT101 Strain Gauged Regenerator Shield and Screening Rig.

Turbine Backshrouds - NGK

Two turbine backshrouds of SN-50 sintered Si_3N_4 material (isopressed and green machined) were received from NGK Insulators, Japan at no cost to the program. These backshrouds passed dimensional, dye penetrant and microfocus X-ray inspections. Both backshrouds were successfully screen tested in a hydraulic pressure test fixture, illustrated

in Figure 80. Testing was initially performed by applying strain gauges to one shroud surface analytically predicted to be stressed in tension (see Figure 81). This shroud was pressurized to obtain a hydraulic pressure versus peak stress calibration to be used for screening both parts. Pressure loading to a peak stress of 20 ksi was successfully performed on both components without damage, confirming suitability for additional evaluation.

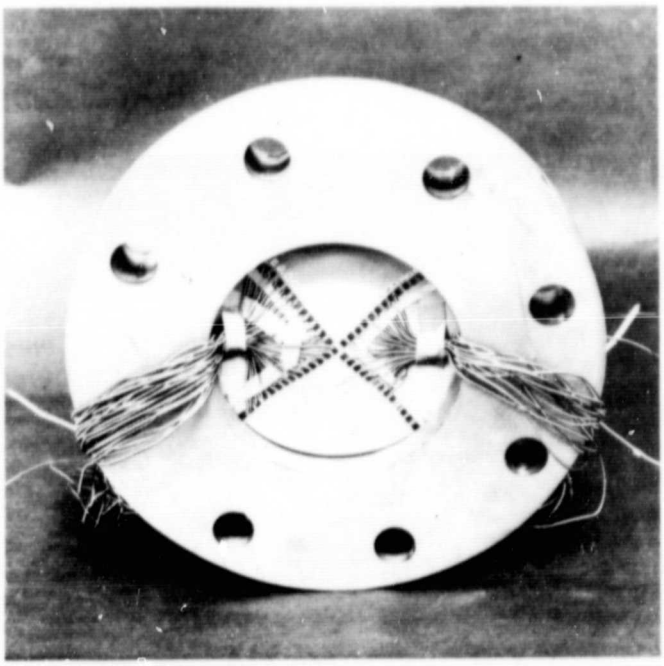

Figure 80. AGT101 Screening Rig/Strain Gauged Turbine Backshroud.

Also, several billets of SN-50 sintered Si_3N_4 have been received for evaluation from NGK. The billets were machined into test bars and evaluated in four-point flexure at room and elevated temperatures. Test bars measuring 0.125 by 0.250 inch in cross section were machined and tested in quarter-point flexure with a 1.5-inch outer span and a crosshead speed of 0.02 inch/minute. Results, summarized in Table 10, indicate that NGK SN-50 may be suitable for AGT components operating below 2000°F, and thus is suitable for backshroud application. At 2200°F, significant slow crack growth was observed. None were observed at 2000°F in fast fracture.

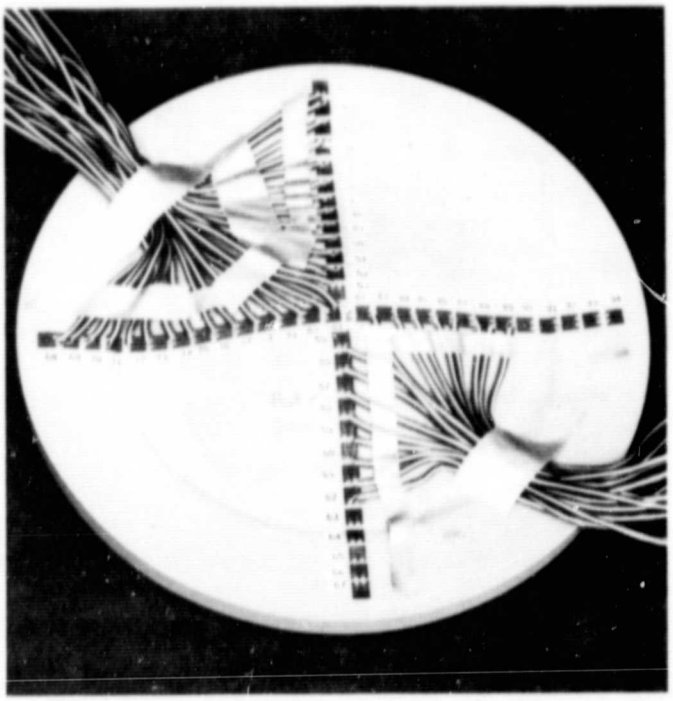

Figure 81. NGK Backshroud Strain Gauged for Screen Testing.

Flow Separator Housings - Corning

Several LAS flow separator housings were successfully screened without failure by Corning Glass. These major ceramic components were pressure tested to 1.25 times the analytically predicted engine pressure loads. Further details of this effort are presented in Appendix A.

Duct Spacers - Carborundum

Thirty ceramic duct spacers were received from Carborundum and have completed Garrett inspection. These spacers are the original bolted ceramic interface configuration. An interface rig to test duct spacer interfaces was fabricated; however, testing has been deferred due to evaluation of an alternate configuration.

This alternate design provides a technique for alignment of the ceramic turbine shroud and compressor housing while removing the sliding surfaces between the adjacent ceramic parts. Details of this configuration will be presented in the next semiannual report.

TABLE 10. RESULTS OF NGK SN-50 FLEXURE TESTING

	Room Temperature	2000°F	2200°F*
Characteristic Stress, ksi	87.6	47.1	Approx 31
Weibull Modulus	10.5	13.6	Not Determined
Population	10	7	4
Test Bar Size: 0.125 x 0.25 x 2 inches			
Test Span: 0.75 x 1.50 inches, quarter-point loading			

*Slow crack growth occurred at 2200°F

Turbine Shrouds - ACC

A greenware Si_3N_4 turbine shroud (P/N 101) from ACC was partially machined. The shroud was returned ACC for further casting process development. Minor modifications were made to the casting fixtures to add corner radii and fillets as required.

Stator Vanes - ACC

Initial deliveries of stator vane sets have been received from ACC. Deliveries have included potential engine quality hardware as well as approximately 44 stator segments, rejected by ACC prior to shipment due to visual or X-ray indications. These reject stators will be used to verify machining fixtures and to establish screening test parameters.

The first ACC stators received were rejected by ACC due to X-ray indications in the platform area. During initial screening test evaluations, three such stators were sandwiched between two contoured cast alumina refractory plates, simulating engine mounting, and subjected to oxyacetylene flame thermal cycling (see Figure 82). Although no instrumentation was used during this preliminary trial, all three "reject" Si_3N_4 stators survived multiple heat up and forced air cooldown cycles used to evaluate the test setup. Peak flame temperatures achieved, although not measured, were adequate to produce local surface melting of the cast alumina refractory plate leading edges. Although no quantitative conclusions can be made from this initial study, it is encouraging that the Si_3N_4 stator design and material were capable of surviving severe thermal shock conditions. Additional testing is planned for stator evaluation to provide quantitative screening test results.

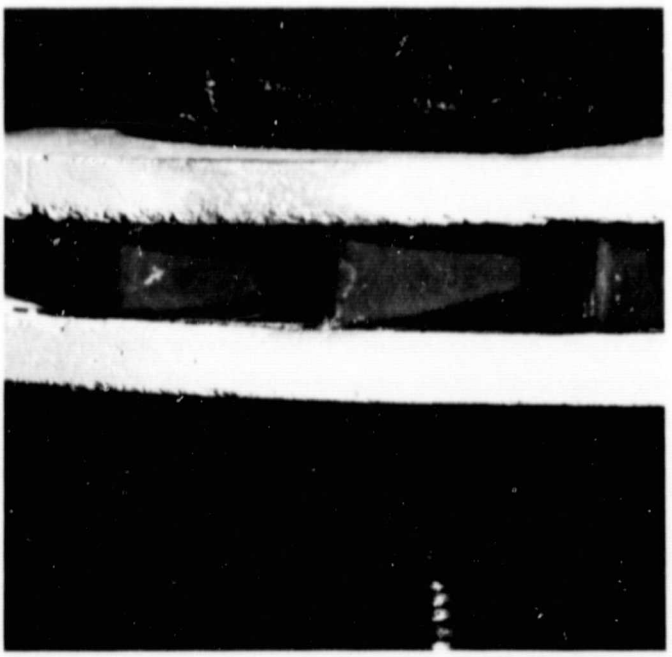

Figure 82. ACC RBSN Stators During Cooldown Following Oxyacetylene Torch Heating.

4.6.1.5 Ceramic Handling Training

To assure that proper care is taken in handling the critical, fragile ceramic parts, a comprehensive Garrett ceramic handling program was initiated for AGT101 ceramic hardware. Component travelers were designed to accompany each ceramic part through the Garrett inspection cycle, with specific personnel in each cognizant department designated to handle the components. Traceability is accomplished through serialization of individual components, which is recorded on the component traveler. Records of each part then are filed by supplier name. A video tape on ceramic handling also was compiled for personnel training.

4.6.2 Ceramic Turbine Rotor

4.6.2.1 Simulated Rotors

Simulated rotor development is being pursued by AiResearch Casting Co (ACC), Pure Carbon Co, Carborundum and Ford. These suppliers have been requested to provide bladeless simulated rotor hubs for evaluation at Garrett to demonstrate that thick section rotor hubs of the required strength can be fabricated. Once required strengths are demonstrated, based primarily on rotor spin tests to 115,000 rpm, suppliers will be released to pursue bladed rotor development. During this reporting period, rotors were received from ACC and Pure Carbon.

4.6.2.1.1 Simulated Rotor

Six SNN-502 Si_3N_4 simulated rotors have been received from ACC for evaluation. Rotor densities varied from 2.85 to 3.15 g/cc, and acceptability of the surface finish varied. Upon receipt, all rotors were evaluated using visual, dye penetrant, microfocus X-ray and 25 MHz ultrasonic inspection techniques. Results of these inspections were used to determine the subsequent use of each rotor (i.e., cut-up evaluation or spin test). A summary of these inspections and subsequent utilization is presented in Table 11. Two rotors were selected for cut-up evaluation. Rotor S/N 03311 has been cut up and machined into test bars with 0.10 x 0.20 inch cross sections. All test bars (31) were tested in room temperature quarter-point flexure using an outer span of 1.5 inches and a cross head speed of 0.02 inch/minute. Testing resulted in a characteristic strength of 52.5 ksi and a Weibull modulus of 7.5. The highest strength bar fractured at 61.9 ksi, the lowest at 34.9 ksi. The low strength and wide scatter, when compared with previously tested ACC sintered Si_3N_4, is attributed to porosity, as illustrated in Figure 83. Flexure results of cut-up rotor S/N 04221-02-II are expected to be better since no porosity has been visually observed in the cutup rotor segments or test bars.

Rotor S/N 02061-I was selected for spin testing based on favorable inspection results. However, prior to testing, balancing required that the entire rotor be lathe ground. The rotor was assembled into a shrink fit metal sleeve and tested. The desired 115,000 rpm proof-test speed was obtained without failure. The post-test rotor is shown in Figure 84. An analytical stress analysis of this rotor at peak speed indicated a maximum principle stress of 44.0 ksi at the rotor hub, as shown in Figure 85. This successful spin test verified the feasibility of ACC slipcast SNN-502 Si_3N_4 as a rotor material.

Additional evaluation of ACC SNN 502 simulated rotors is in progress to determine the reproducibility of the demonstrated rotor integrity. ACC has been approved for bladed rotor development.

4.6.2.1.2 Evaluation of Pure Carbon Refel Rotors

Four simulated rotors, fabricated from reaction sintered silicon carbide, "Refel", by British Nuclear Fuels, Ltd and provided through Pure Carbon Company were received for evaluation. The four rotors were fabricated in two batches by isopressing and green machining prior to the siliconation process.

Upon receipt, the four rotors were dimensionally inspected and evaluated for defects using visual, dye penetrant, microfocus X-ray and 25 MHz ultrasonic inspection techniques. Based on these results, one rotor was selected for cut-up evaluation and the remaining three rotors were spin tested to failure. A summary of these activities is presented in Table 12.

TABLE 11. ACC SNN 502 SIMULATED ROTOR SUMMARY

S/N	Density g/cc	Visual Inspection	Dye Penetrant	Microfocus X-ray	Ultrasonic	Disposition
02061-I	3.10	Good	Porous surface - penetrant not effective	Good	Good	Spin tested to 115K rpm - no failure
02121-I	2.85	Fair - bubbles in in base; bubble on rim		High density spheres near shaft end	Indications 1/2-1 inch from shaft end	To be spin tested
03041-II	2.86	Poor - unbalanced, irregular; metallic inclusion		Low density near shaft end		Not determined
03311	3.08	Good		Indications	Not performed	Cut-up σ_θ = 52.5 ksi, m = 7.5 porous interior
04221-02-II	3.11	Good	Small crack in base	High density near shaft	Indications 1/2-1 inch from shaft end	Cut-up evaluation in progress--no interior porosity
04251-II	3.15	Good	Small surface indications	OK		To be spin tested

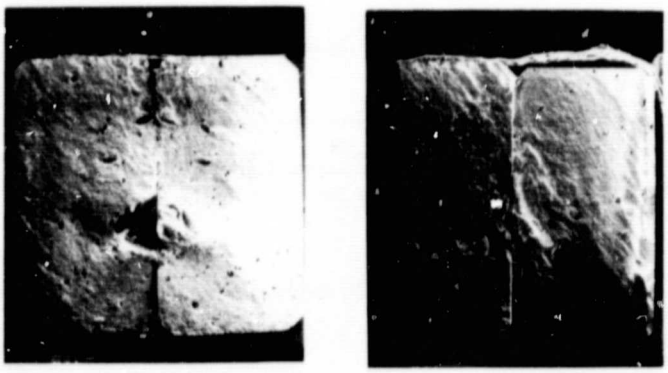

(a) 34.9 KSI (b) 61.9 KSI

Figure 83. Fracture Faces of Two ACC SNN-502 Test Bars From Rotor S/N 03311 Tested at Room Temperature.

As indicated in Table 12, rotor S/N 4 (3.12g/cc), was cut into two test bar groups for evaluation. One group was tested in the as-machined condition, and the second group was tested in the as-heat treated condition after a 2200°F/3 hour heat treatment. Test bar cross sections were 0.100 by 0.200 inch. All test bars were fractured at room temperature using an outer span of 1.50 inches, an inner span of 0.75 inch

Figure 84. ACC SNN-502 Simulated Rotor S/N 02061-I After Successful 115,000 RPM Proof Spin.

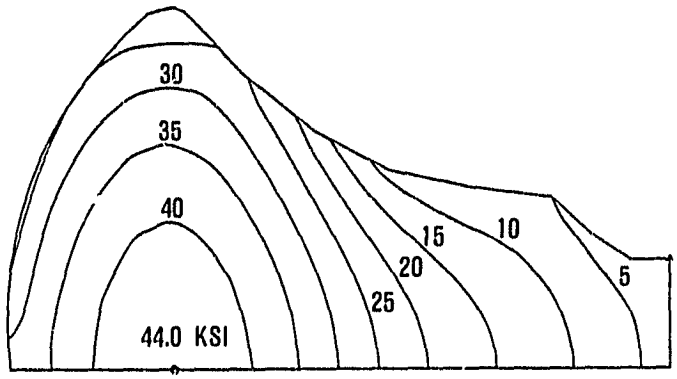

Figure 85. AGT Simulated Rotor (ACC Si_3N_4) Maximum Principal Stress at 115,000 RPM.

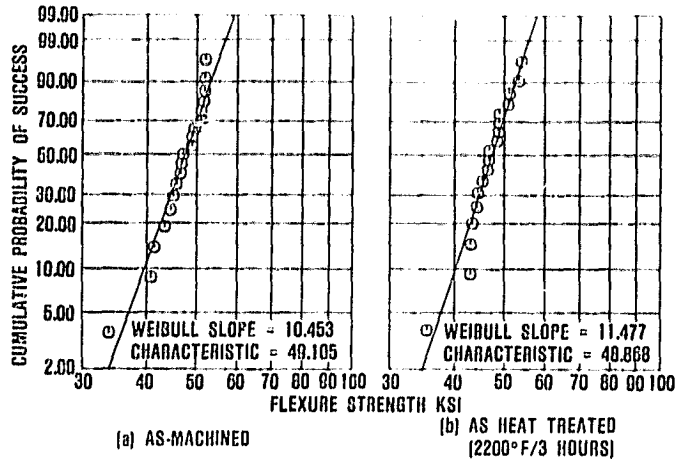

Figure 86. Weibull Flexure Results for Pure Carbon Turbine Rotor S/N 4.

and a cross head speed of 0.02 inch/minute. Weibull results are illustrated in Figure 86. Rotor microstructure was evaluated at both interior and outer region locations, as illustrated in Figure 87. Figure 87(a) shows the interior microstructure of the rotor with a typically high Si content. The SiC particles appear to be laced with smaller particles as yet unidentified, but possibly, very fine SiC. The outer region of the rotor, Figure 87(b) shows very little free Si and shows the large SiC particles; possibly bounded by very fine SiC particles.

TABLE 12. PURE CARBON REFEL ROTOR SUMMARY

S/N	Density g/cc	Visual Inspection	Dye Penetrant	Microfocus X-ray	Ultrasonic 25 MHZ	Comment
1 Batch 2	3.08	1 rim chip 1 rim crack	OK	Low in backface area	Indications top and bottom	38,000 rpm, failed at large carbon inclusion
2 Batch 1	3.09	Small bubbles on rim	Indications	OK	Indications in middle and bottom	13,000 rpm - rim fracture
3 Batch 2	3.12	Small chip on rim	OK	OK	OK	92,000 rpm - failed at hub center
4 Batch 2	3.12	Pits on shaft, non smooth back face best visual	Indications	OK	Indications on bottom	Cut up and flexure tested As machined: Characteristic Strength: 49 ksi Weibull Modules: 10 Heat Treated: Characteristic Strength: 48.9 Weibull Modulus: 11.5

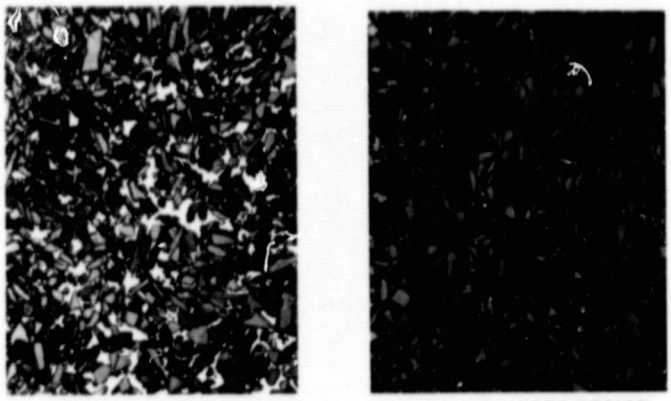

(a) ROTOR INTERIOR REGION 400x

(b) ROTOR OUTER REGION 400x

Figure 87. Refel Rotor S/N 4 Microstructure.

Spin test results showed a wide variation in rotor integrity. Rotor S/N 3, which showed no dye penetrant, X-ray, or ultrasonic indications, failed at 92,000 rpm. The degree of rotor fragmentation prohibited identification of a specific fracture origin, however, the fracture initiated from the hub center region. Rotors S/N 1 and 2 failed at 38,000 and 13,000 rpm, respectively. Both failed at previously identified defects or indications; S/N 1 from a large interior carbon inclusion shown in Figure 88, and S/N 2 from a surface dye penetrant indication.

The rotor spin tests and test bar evaluations indicate that the Pure Carbon Company Refel material will require additional development for AGT rotor application. Currently, additional AGT efforts with the Refel material have been postponed pending evaluations of ACC, Ford and Carborundum rotor developments.

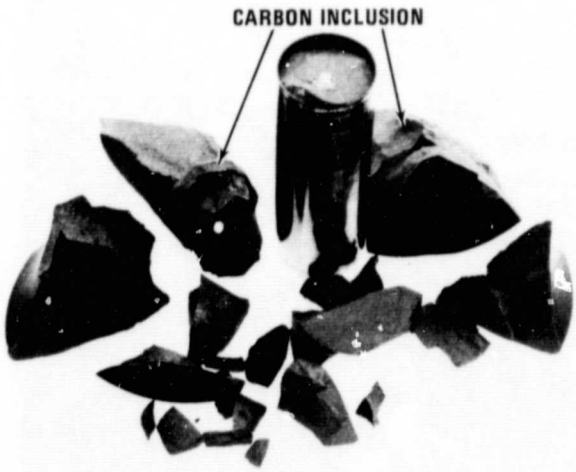

Figure 88. Refel Rotor S/N 1.

4.6.2.2 Strength of Alternate Carborundum Rotor Materials

Since current Carborundum SASC material does not meet the initial rotor strength goals (68 ksi charactristic strength with m = 12) alternate rotor materials were addressed. Work under the common effort had indicated high strength for hot-pressed α-SiC. Therefore, test bars were cut from hot-pressed cores (2-piece rotor fabrication approach, see Appendix C). Two proprietary additive systems, coded D and F, were evaluated. The flexural strength results at room temperature and 2000°F are given in Table 13. Examination of the fracture surfaces indicated that fracture initiated at inclusion type defects. A typical example is shown in Figure 89. The etched microstructure of Code D, which indicates a grain size of 1 to 2 microns, also is shown. The inclusion type defects were related to the purity of the additives and although purer material was obtained, the specific elements responsible for the low material strength could not be eliminated. As a result, hot-pressed rotor materials were dropped from further consideration.

The second alternate rotor material evaluated was reaction-sintered SiC (RSSiC) in two forms; Hexoloy KX-01,

TABLE 13. WEIBULL PARAMETERS OBTAINED FROM FLEXURAL TESTS ON BARS CUT FROM HOT-PRESSED ROTOR CORES

Code (Population)	Temperature (°F)	Characteristic Strength (ksi)	m-Value
D(12)	72	56.9	10.9
D(10)	2000	40.5	8.7
F(12)	72	40.5	6.3
F(8)	2000	25.7	12.8

Test Bar Size: 0.1 x 0.2 x 1.5 inch
Test Span: 0.5 x 1 inch

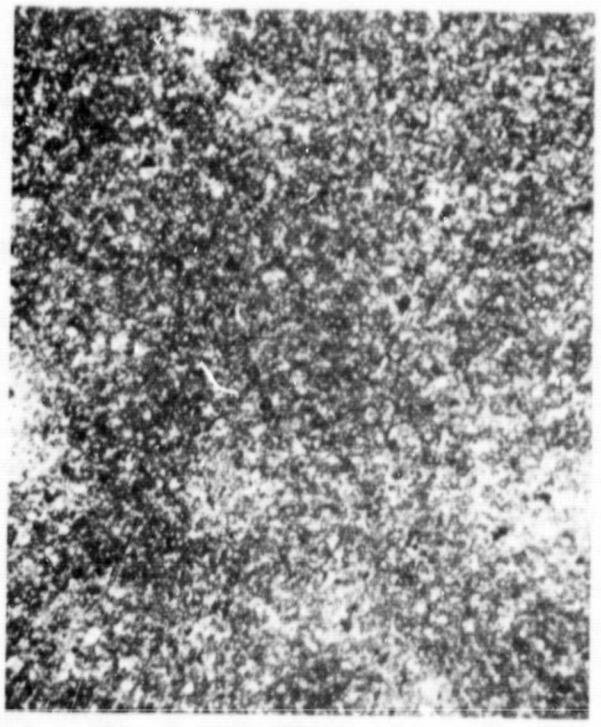

(a)

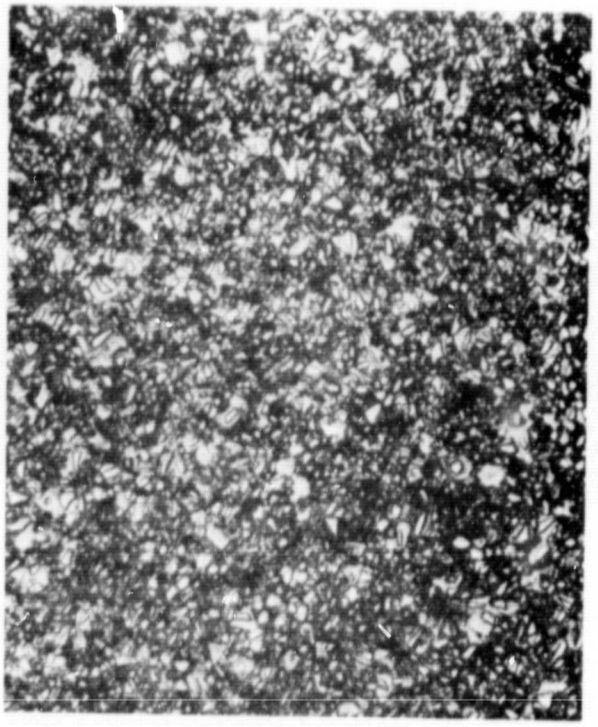

(b)

(c)

(d)

Figure 89. Carborundum Hot Pressed α-SiC Test Bar Fracture Surfaces

a fine grain material, and Hexoloy KX-02, an ultra-fine grain material with higher silicon content. Evaluation of the KX-01 material has been completed and results presented herein. Evaluation of the KX-02 material is in process and will be presented in the next semiannual report.

Thirty 0.125- x 0.25- x 2-inch test bars of Hexoloy KX-01 were 4-point bend tested using 1/4-point loading (1.5 inch outer span, 0.75 inch inner). The results are given in Table 14. Fracture surfaces were examined visually (40X) and by SEM, but the predominate flaw type could not be established. It was observed, however, that the lowest strength room temperature specimen (31.1 ksi) failed from a visible surface scratch. The removal of this data point from the test population increases the Weibull slope to 6.9. There is a large uncertainty associated with the very high Weibull slope observed at 2000°F since calculations are based on only nine data points. However, there is no question that considerable improvement has been achieved when compared with the room temperature value.

TABLE 14. WEIBULL PARAMETERS OBTAINED FROM FLEXURAL TESTS ON FINE GRAIN SILICONIZED SiC (HEXOLOY KX-01)

Material (Population)	Temperature (°F)	Characteristic Strength (ksi)	m-Value
KX-01 (20)	72	71.6	4.8
KX-01 (9)	2000	76.7	32.3
KX-01 (19)*	72	71.8	6.9

Test Bar Size: 0.125 x 0.25 x 2 inch
Test Spans: 0.75 x 1.5 inch, 1/4 point loading

*Low strength value (31.3 ksi) deleted from population

The microstructure of Hexoloy KX-01 is shown in Figure 90 in both the as-polished and etched condition. Approximately 10 micron SiC grains are imbeded in a silicon matrix. The microstructure appears to be uniform and homogeneous.

4.6.3 Subcontractor Ceramic Development

The following sections describe progress in component fabrication development by the subcontractors.

4.6.3.1 Ford Motor Company

The Ford report is included as Appendix A.

4.6.3.2 AiResearch Casting Company

The ACC report is included as Appendix B.

4.6.3.3 Carborundum Company

The Carborundum report for unique tasks is included as Appendix C.

4.7 Foil Gas Bearings

Foil gas bearing component testing was completed in December 1980. All subsequent testing of the foil gas bearings has been conducted as part of the rotor dynamics development (see Section 4.9) herein. Two foil bearing designs using 0.005 and 0.006 inch thick stainless steel foils and Teflon S coatings have been tested to rotor speeds of 97,000 rpm (rig drive speed limit). No basic problems of the foil bearings have been detected during the rotor development.

The foils presently being used have adequate temperature margin for the Mod I Build I engine environment. The Mod I and Mod II engines will require higher temperature foil materials and coatings that currently are being developed in a separately funded program.

4.8 Bearings and Seals

Development testing and evaluation of AGT101 high speed ball bearing and shaft ring seals was initiated on the rotor dynamic test rig. The rotating assembly has been successfully tested to speeds of 97,000 rpm (rig drive speed limit) during this reporting period.

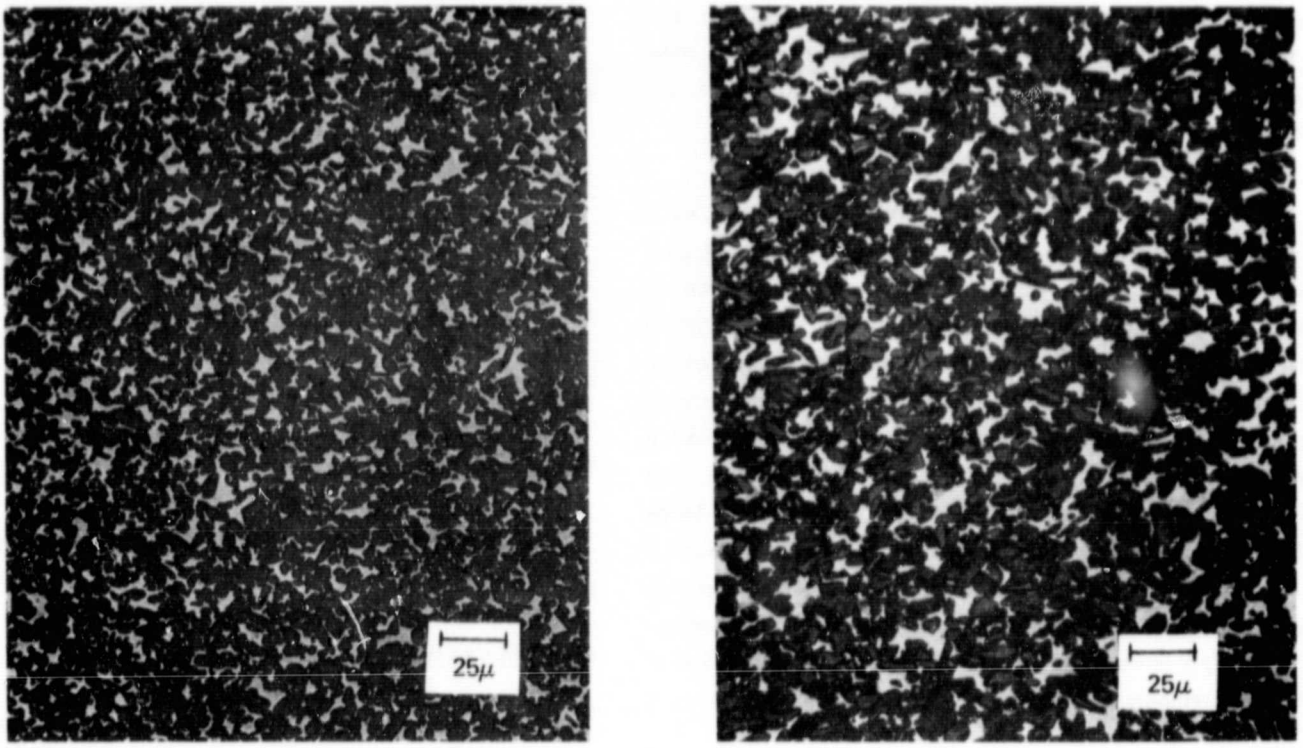

AS-POLISHED ETCHED

Figure 90. As-Polished and Etched Microstructure of Carborundum Fine Grain RSSiC (Hexoloy KX-01).

Ball bearings manufactured by Split Ball Bearing, Barden and FAG have been procured. Initial testing has been conducted using the bearings supplied by Split Ball Bearing. No evidence of bearing or lubrication problems was detected. Barden and FAG bearings will be tested later.

Fabrication of the buffered ring seal test rig was completed in March 1981. Assembly and testing of the rig was placed on hold as a result of program budget constraints. All ring seal development is being conducted on the rotor dynamic test rig.

Seal testing on the rotor dynamics rig has revealed no evidence of oil leakage, shaft burnishing, or excessive wear. Development testing using two grades of carbon rings and Mod I engine seal designs is continuing. Seals will be evaluated over the full operating envelope of the Mod I and Mod II engines.

4.9 Rotor Dynamics Development

Development testing of the AGT101 rotor system, which includes bearings, seals, lubrication, gearing, and rotor assembly, was initiated in January 1981 using the rotor dynamics test rig. Initial testing was performed without the gearbox to permit development of the hydraulic mount, curvic couplings and balance techniques for the engine rotor system. Satisfactory operation to speeds of 97,000 rpm (rig drive speed limit) has been achieved.

Testing of the engine rotor system and gearbox was initiated in April 1981. Satisfactory operation to speeds of 75,000 rpm has been demonstrated. At speeds higher than 75,000 rpm, excessive excitations occur with the present configuration hardware. The introduction of gear loads to the rotor system requires further optimization of the hydraulic mount and a change in the gearbox rotating carrier

bearing support. Work will continue into the next reporting period to resolve these problems.

Other major components undergoing development in the rotor dynamics test rig (as noted in Sections 4.7 and 4.8, herein) have not manifested any problems. The output pinion gear performs satisfactorily, and shows no sign of wear.

4.10 Controls and Accessories

During this reporting period, considerable progress has been made in all areas of the AGT control system as emphasis has progressed from design and procurement to hardware assembly and testing.

Budget constraints have resulted in deferral and deletion of a number of control software and hardware activities, particularly those related to powertrain and vehicle development. Continuing control system activities are specifically related to component and engine development.

The following sections discuss, in greater detail, significant changes, test results, and progress in the principal areas of the control system effort.

4.10.1 Systems Analysis

The logic diagram for the Mod I/Mod II vehicle-oriented engine control system was completed, and filed for future reference. This baseline logic then was revised and simplified through elimination of the vehicle-related functions to provide the present control system logic that is specifically oriented to test cell operation of the first AGT engine.

An overview of the revised engine startup and shutdown logic is presented below:

Startup

0 percent
engine speed (N_E)

- The ON position of the Electronic Control Unit (ECU) ON/OFF switch supplies dc power to the ECU power supply and lube cart power relay
- Low oil pressure protective circuit activated
- Automatic start sequencing is initiated and latched by engaging the start switch
- Ignition Unit on

10 percent N_E

- Main fuel solenoid opens
- Timed acceleration start logic begins to schedule engine acceleration rate with exhaust gas temperature (EGT) overtemperature limiting empowered
- Flame detector circuit begins testing if EGT is 100° higher than combustor inlet temperature

40 percent N_E

- Starter relay drops out
- When combustor inlet temperature exceeds 1300°F, ignition off

50 percent N_E

- Fuel/Speed Control logic transfers to proportional plus integral control, with operator controlled speed, and measured/calculated T4 temperature limiting empowered
- Underspeed shutdown limit is established at 45 percent

Shutdown

The automatic shutdown sequence is initiated by any of the following conditions:

- Speed drops below 45 percent
- Low oil pressure exceeds 10-seconds duration
- EGT in excess of 1500°F

- o Detection of flame-out condlton exceeds 3 seconds duration
- o Engine speed exceeds 107 percent
- o ECU ON/OFF switch set to OFF

After shutdown has been initiated, the following actions occur:

45 to 110 percent N_E

- o Main fuel solenoid closes
- o Fuel pump off
- o Atomizer purge solenoid opens

10 percent N_E

- o ECU power interrupted
- o All control functions disabled
- o Purge solenoid closes

4.10.2 Fuel System

4.10.2.1 Outside Supplier Inquiry

The extremes of the AGT fuel metering requirements were initially specified at 0.85 lb/hr to 45 lb/hr. These flow levels are intended to allow for 15 percent undershoot and a similar overshoot during transients. The upper limit of 45 lb/hr was subsequently reduced to 35 lb/hr to be consistent with a 100 hp engine rating. Fuel delivery pressure ranges from 0 to 600 psig. Because no gearbox pad is available, the pump is to be driven by a 12-volt dc electric motor of a size and weight suitable for automotive installation. The fuels originally specified were those considered necessary to demonstrate the multiple fuel capability of a gas turbine. These included all diesel fuels, all gasolines (including gasohol), all jet fuels, and methanol. This requirement has been reduced for the time being to include only diesel No. 2(DF-2), unleaded gasoline, and gasohol.

Consideration was given to development cost and further, long range production cost. Therefore, in parallel with Garrett development efforts, inquiries were made to suppliers that manufacture fuel control systems for the high turndown fuel delivery systems used on automotive diesel engines. An RFP and problem statement was prepared and sent to fourteen companies manufacturing controls in the United States and around the world.

Of those companies responding, all proposals intended using a gear pump with conventional metering and none proposed using existing technology unique to diesel engine systems, which was the objective of pursuing outside suppliers. In light of the significant program reductions, and the high cost associated with the outside development of the fuel control, the supplier approach was terminated for the present application.

4.10.2.2 Technical Progress

During this reporting period, development of the fuel management system involved those areas concerned with dynamic response, periodic pressure fluctuations, electric drive motor characteristics, and repeatability.

4.10.2.2.1 Dynamic Response

The AGT system dynamic analysis indicates a requirement for fuel system response at least equivalent to a first order lag with a time constant of 0.050 second for small as well as large inputs.

Torque Motor Response

Initial observations during system testing indicated excessive fuel system phase shift. Based on these observations, it was deemed necessary to establish the response capabilities of the torque motor flapper valve assembly. Initial torque motor tests showed poor response resulting from trapped air in the test system. All plumbing then was oriented such that air bubbles would rise to be purged by through flow. It is recognized that the resistance to bleeding air may be more difficult when flowing diesel versus aviation fuels due to viscosity and surface tension differences.

Following hardware modification, testing was resumed. After thoroughly bleeding the system and while supplying the torque motor flapper valve from a blow-down tank (to minimize dissolved air problems), the response at 2.5 lb/hr flow rate indicated approximately 4-degrees phase shift. These test results indicated that the torque motor flapper valve response was adequate.

Fuel System Response

Initial response to step changes of torque motor current displayed a 2-second response of the entire fuel system. This was significantly improved when it was realized that the step increase and decrease was made from and to a closed servo valve position (an unrealistic operating extreme). More reasonable results were observed by starting from and stopping at meaningful engine fuel flows such as 2 lb/hr as a minimum and 30 lb/hr at the high end. However, to achieve a more accurate dynamic definition, frequency response test techniques were utilized.

Frequency response testing revealed phase shifts as high as 110 degrees at a frequency of 3 CPS at low flows.

Fuel system flow visualization testing, between the pump exit and atomizer, showed a continuous stream of pin point bubbles (Figure 91).

Minor hardware changes were made in an effort to improve these conditions. These changes include:

- Eliminating or minimizing extraneous volumes between the servo valve and cylinder inlets
- Adding a back-pressure valve, within the fuel pump, between the torque motor servo valve and cylinder inlets. This valve was added to preclude the presence of a mixed state fluid (air/fuel), thus improving transmissivity. The valve maintains a positive pressure of 5 psi
- Adding a check valve between the fuel pump and atomizer causing entrained air to return to solution

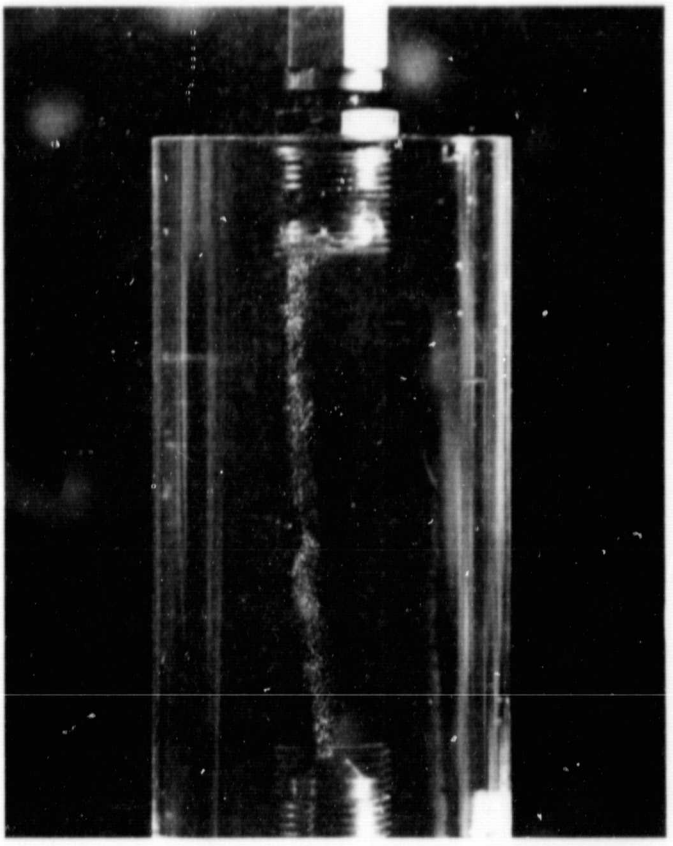

Figure 91. AGT101 Fuel Control (Breadboard Unit) High Pressure Flowstream Between Pump Discharge and Atomizer Showing Entrained Air and Trapped Air at Top of Tube.

Following these modifications, testing was resumed. Figure 92 shows no air bubbles present in the channel between the pump and atomizer. Frequency response testing showed a significant improvement. Phase shift was reduced from 110 degrees to 42 degrees at 3 CPS at low flows.

4.10.2.2.2 DC Motor Characteristics

Testing was conducted to confirm the electrical characteristics of the 12 vdc 1/8 hp motor used to drive the three-piston pump. Test data indicated that the motor tested was in good agreement with the design data received from the motor vendor. The conservative application of this motor is apparent since only 0.085 hp out of an available 0.125 hp is utilized. The motor temperature at this condition was 125°F compared to a maximum allowable supplier specification of

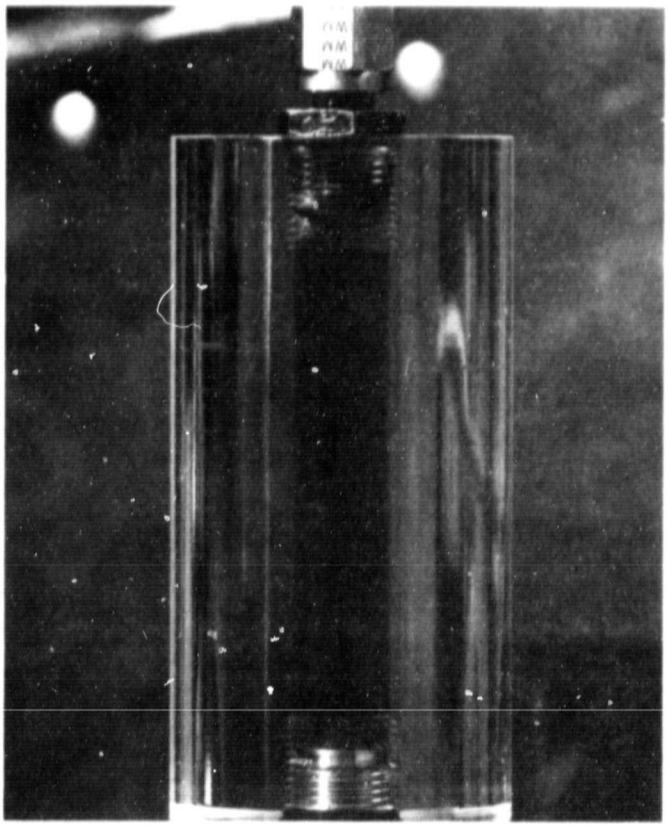

Figure 92. AGT101 Fuel Control (Breadboard Unit) High Pressure Flowstream after Incorporation of Pressurizing Valve Ahead of Atomizer Showing Disappearance of Entrained Air with a Small Bubble Remaining.

311°F; this indicates considerable margin. A somewhat smaller frame motor might be possible in this application.

4.10.2.2.3 Repeatability

Four tests were conducted to evaluate the repeatability of the fuel delivery system. The tests were started from a complete shutdown condition. Table 15 shows the forty-four data points and averages. The average deviation was 5.6 percent, which is considered acceptable.

4.10.2.2.4 Fuel System Summary

The following is a current status of the fuel system and component activities:

- Pump and metering control meet pressure and flow requirements
- Pump and control are compatible with multiple fuels
- Compatibility of pump, torque motor, and dc drive motor has been established
- Hot and cold fuel tests have been completed. No problem exists with the pump over the required automotive range
- DC motor instrumentation has established the capability of the selected 1/8 hp dc motor. Motor heating is negligible
- Low flow operation indicates no fuel heating problems

Primary development tasks which remain are:

- Mockup of fuel system in engine configuration
- Check fill times and purge characteristics
- Check compatibility with electronics
- Incorporation of centrifugal boost pump

4.10.3 Electrical Accessories

Revisions to the engine electrical harness have been accomplished to eliminate the gearbox and vehicle-related functions and consolidate the remaining engine components and lab interface. Redesign of the electrical harness to support the lab control system was completed, and fabrication of the harness is in process.

All solenoids, transducers, switches, and other electrical accessory hardware required for the first engine are being tested in preparation for the first engine run.

4.10.4 Mechanical Accessories

Mechanical accessories was the area most significantly affected by the program redirection. The main challenge originally was the design and developrnent of a vehicle-oriented lube/hydraulic system compatible with the automotive application and perfor nance requirements. This effort has been eliminated and a cart-mounted lube and hydraulic system will be utilized for all engine testing.

TABLE 15. REPEATABILITY TESTS 3-PISTON AND METERING VALVE

Milliamperes	1	2	3	4	Average	Deviation
70	2.2	2.5	2.5	2.5	2.4	5
80	4.0	2.5	4.0	4.0	3.6	15.8
90	7.0	6.0	5.7	6.0	6.2	6
100	10.7	10.0	9.5	9.5	9.9	4
110	17.0	15.5	14	14	15.1	7.7
120	21.2	19.5	19.7	19.7	20.0	2.9
130	26.2	24.7	23.5	23.5	24.5	6.9
140	31.0	29.5	27.7	27.7	19.0	4.0
150	34.0	34.0	31.5	32	33.3	3.4
160	38.2	38	35.5	35.5	36.8	3.5
170	41.7	41.7	39.7	39.7	40.7	2.4
					Average Deviation:	5.6 Percent

The AGT inlet guide vane (IGV) actuators are based on a previous Garrett design, and require no additional development. Three IGV actuators have been received, inspected, functionally tested, and released for engine use. A fourth unit was returned to the supplier for correction of excessive internal leakage.

4.10.5 Electronic Control

A test electronic control, with provisions for static (manual) and dynamic (programmable) testing of the digital circuit boards, was completed. Static testing was conducted to identify wiring shorts and misconnections on the input and output circuit boards. Dynamic functional testing, using engine oriented computer programs, of the output board and selected portions of the memory/central processing unit board has been completed. Additional test programs were developed for dynamic checkout of the memory.

Final interconnect wiring of the electronic control chassis was accomplished and design and fabrication of the ECU tester/monitor was completed.

All physical components of the electronic control, including analog and digital circuit boards, electronic control chassis and ECU tester, were individually checked out, and physical integration of the electronic control was completed. Simulated engine sensor signal inputs (speed, temperatures, pressures, etc) from the tester were received and processed by the analog control. Input signals to the digital control through the analog-to-digital converter were verified. Similarly, digital control outputs through the digital-to-analog converters were passed to the analog control and verified at the tester display panel.

Development and checkout of the digital control software is complete. Startup sequencing, fuel control startup scheduling, on-line speed control, and shutdown logic modules were completed.

APPENDIX A

FORD MOTOR COMPANY
ADVANCED GAS TURBINE (AGT) POWERTRAIN SYSTEM DEVELOPMENT PROGRAM
THIRD AGT SEMIANNUAL TECHNICAL
PROGRESS REPORT

1. Task 2.3 - Ceramic Rotor - Ford

1.1 Material Development and Characterization

References 1 and 2 discuss progress on the Ford concept for the fabrication of monolithic AGT101 ceramic turbine rotors from sintered reaction bonded Si_3N_4 (SRBSN). The first generation material, designated RM-1, contains 8-percent Y_2O_3 added as a sintering aid. Continued research on the effects of sintering parameters resulted in a significant improvement in sintered density reproducibility, which was noted as a problem in Reference 2. Late in the reporting period, a number of simulated rotors having sintered densities ranging from 3.24 to3.29 g/cm^3 [Theoretical Density (TD) = 3.33 g/cm^3] were produced at 1975°C (3587°F) and 100 atmospheres nitrogen overpressure using a new sintering furnace. Test bars are being prepared from coupons and from cut-up rotors having these high densities.

Oxidation testing of RM-1 material continued. A series of test bars (1 inch x 0.25 inch x 0.125 inch) were machined from RM-1 material. Visually, the bars were a uniform dark gray in appearance, as shown in Figure 93. Bars broken at room temperature in 4-point bending had an average strength of 596.8 MPa (86.6 ksi). At 1200°C (2192°F), strength values dropped 12 percent to 522.4 MPa (75.8 ksi).

A set of 6 samples were oxidized in a static air furnace for a total of 300 hours at 1000°C (1832°F). After 24 hours, the samples were lighter gray in color, with irregular areas of very light gray (Figure 93). Further oxidation did not appear to change the visual appearance of the samples. Most total oxidation weight gain, as shown in Figure 94, was complete after 50 hours, and there was very little weight gain after 100 hours. Total weight gains after 300 hours varied from 0.1 up to 0.43 percent. The variability in weight gain may present a problem; which, will be evaluated in subsequent work. Weight gains increased with the size of the very light

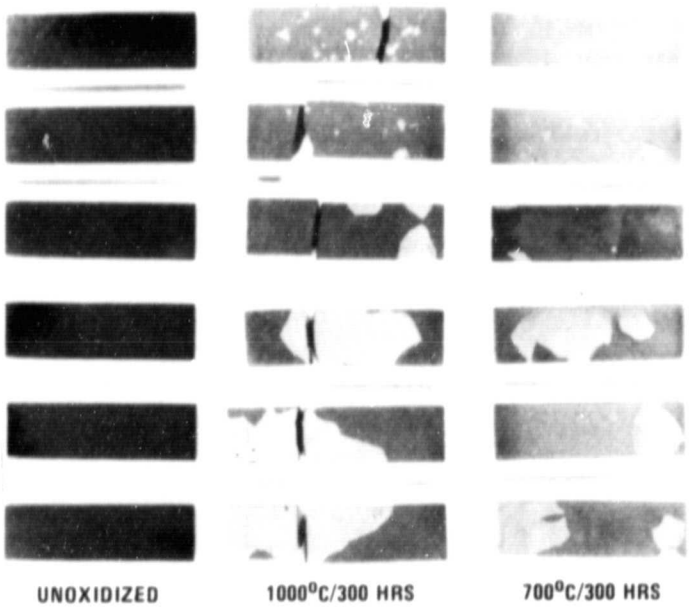

Figure 93. Test Bars of RM-1 Material Before and After Oxidation.

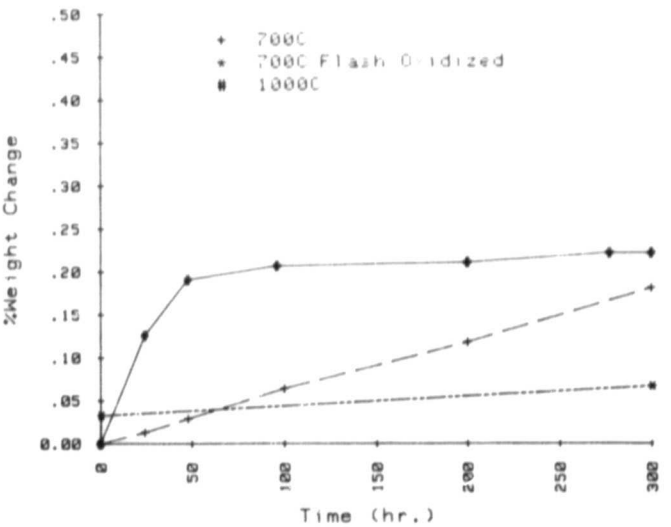

Figure 94. Oxidation Weight Gain of RM-1 Material After 300 Hours of Testing.

gray areas. The room temperature strength of these samples after 300 hours was 572.6 MPa (83.1 ksi), a decrease of only 4 percent. Considering the small sample size (6 bars), this difference may not be significant.

Since oxidation of Y_2O_3 containing Si_3N_4 had been shown (see Reference 3) to occur at lower temperatures, further oxidation testing of this material was done at 700°C (1292°F) for 300 hours. As before, after the first 24 hours, irregular light gray areas began to appear (Figure 93). However, although the rate of oxidation was slower than that seen at 1000°C (1832°F), the weight gains did not stabilize even after 300 hours as shown in Figure 94. Total weight gains averaged 0.18 percent. Room temperature strengths of these samples averaged 528.6 MPa (76.7 ksi), a decrease of 11 percent after 300 hours. Strength change versus oxidation temperature is shown in Figure 95.

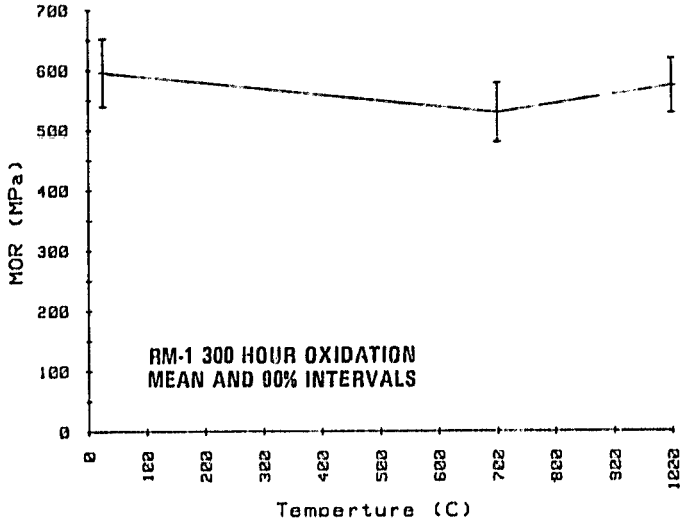

Figure 95. Strength of RM-1 Material Before and After 300 Hours of Oxidation at 700°C and 1000°C.

Another set of bars was subjected to a "flash oxidation" technique [1/2 hour at 1375°C (2481°F)] in an attempt to stabilize the 700°C (1292°F) oxidation weight gains. Although there was a small weight gain during the flash oxidation (0.03 percent), after 300 hours at 700°C (1292°F) there was only a 0.03 percent further increase in weight (Figure 94), as compared to the 0.18 percent seen without flash oxidation, showing that this technique appeared effective in reducing oxidation weight gains.

Preliminary oxidation testing on the higher density material produced late in the reporting period indicated much improved oxidation resistance at 700°C (1292°F). This material has been designated as the next generation material, RM-2.

1.2 Simulated Rotor Development

Development of the slip casting process for simulated rotors was continued with primary emphasis on reducing density gradients and internal cracking problems noted in Reference 2.

A number of changes in configuration and casting techniques were evaluated, including enlarging the shaft size, use of plaster molds at both the backface and shaft regions, and pressure casting using slip pressures up to 50 psi. None of these variations were effective in changing the previously observed density gradients.

Introduction of a small amount of organic suspending agent into the slip, combined with an increase in slip viscosity and close control of this viscosity, produced simulated rotors having markedly lower density gradients. Figure 96 illustrates that density gradients of 15 to 19 percent previously experienced within the desired nitrided density range were cut in half by these changes. The effect of this density gradient reduction is illustrated in Figures 97 and 98. Figure 97 is a photograph of a sectioned and polished simulated rotor number 198 showing uniform structure throughout. By contrast, Figure 98 is a similar photograph of a simulated rotor cast before these process changes, illustrating density variations and internal cracks. The suspending agent reduced the settling due to gravity of the silicon particles in the slip, which accounts for the improved density gradients. A beneficial side effect from the suspending agent was improved 'green' strength of the cast part.

Further improvements in simulated rotor quality were obtained by studying the drying behavior of the cast rotors. Drying experiments were run to assess vacuum, humidity, and air drying techniques. Room temperature air drying, followed by oven drying late in the process, was found to be the most satisfactory technique and is currently being used, replacing the previously used humidity drying procedure.

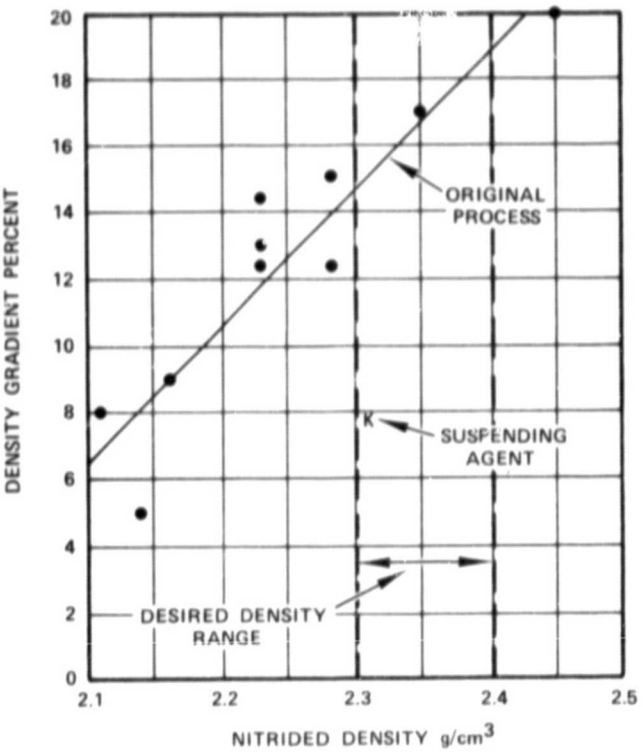

Figure 96. Effects of Using of a Slip Suspending Agent on Nitrided Density Gradients in Simulated Rotors.

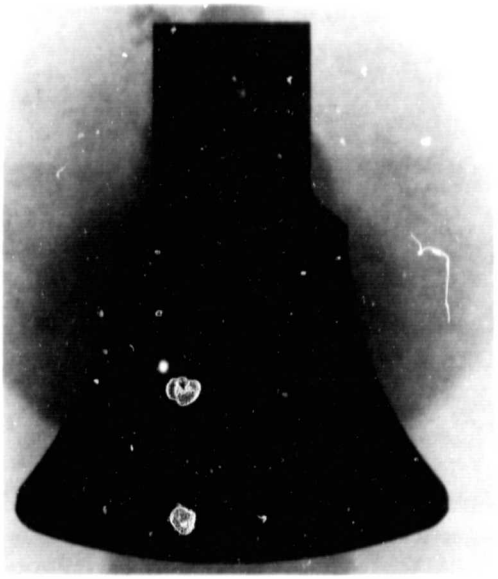

Figure 97. Sectioned Simulated Rotor Showing Uniform Structure.

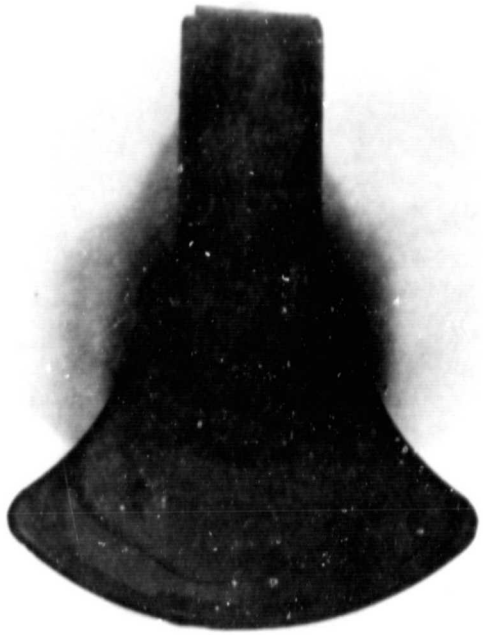

Figure 98. Sectioned Simulated Rotor Showing Non-Uniform Structures.

In summary, the use of a suspending agent in the slip, higher slip viscosity, closer control of viscosity, and improved drying have collectively contributed to a substantial improvement in simulated rotor quality. The effects of this quality are evidenced in a later section of this report covering spin testing.

1.3 Bladed Rotor Development

Later in the reporting period, work was initiated on bladed rotor fabrication. While awaiting the completion of tooling to mold wax patterns of the bladed rotor which were oversized to compensate for shrinkage, crude wax patterns were made in a rubber mold derived from an actual size metal rotor. Casting trials provided valuable experience in development of casting, mold removal, and handling techniques. It was found that the same general procedures and slip parameters developed for casting simulated rotors applied directly to these bladed rotors. No particular difficulty was experienced in casting several of these rotors, which were subsequently nitrided, with no visual cracking or distortion. Figure 99 is a photograph showing four of these bladed rotors after nitriding.

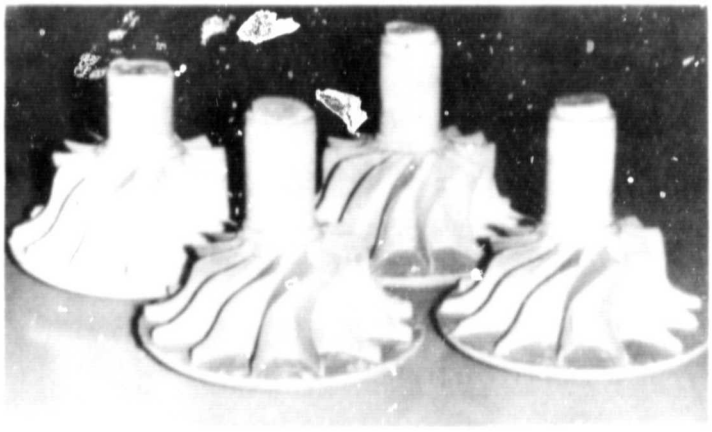

Figure 99. Bladed Rotors After Nitriding.

One of these parts has been sintered to 93 percent theoretical density (TD), and is shown in Figure 100. This part appears free of distortion and cracking.

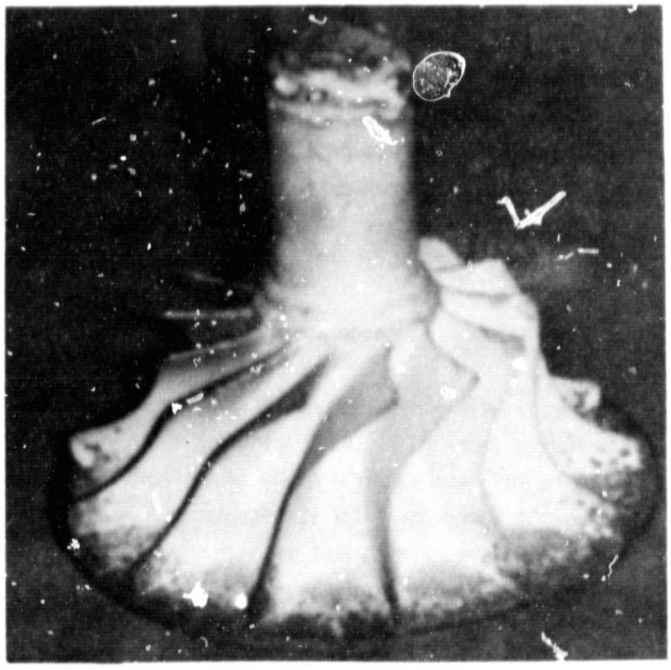

Figure 100. Sintered Bladed Rotor.

The tooling to mold oversize wax patterns was completed at the end of the reporting period. Limited experience to date using these patterns has been good; a photograph of a nitrided oversize rotor is shown in Figure 101.

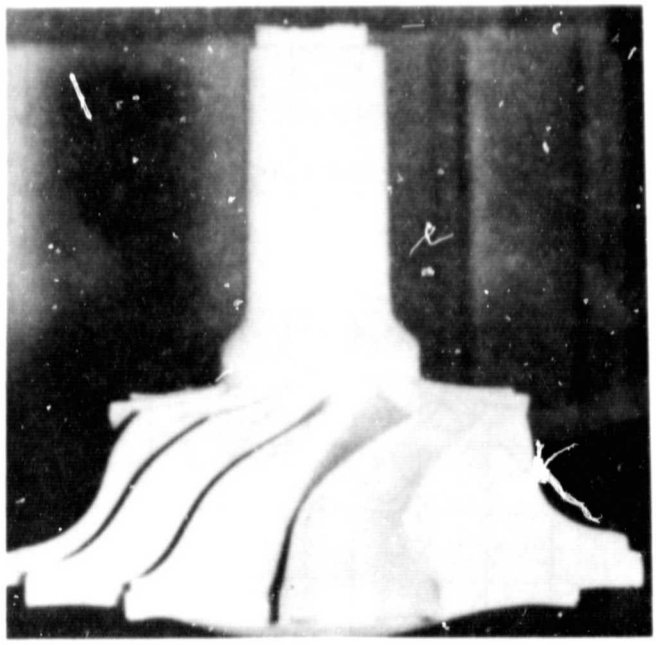

Figure 101. Nitrided Bladed Rotor Incorporating Shrinkage Allowance.

1.4 Spin Testing

Several simulated rotors were spin tested during this reporting period. All of these simulated rotors were the original, oversize design, except for rotor number 201, which was fabricated to the new (i.e., matching the hub contour of the bladed rotor) design.

Simulated Rotor Number 34

This rotor had a sintered density of 3.20 g/cm^3, and contained a large axial crack at the shaft end. Ultrasonic inspection revealed an internal defect 0.75 inches from the shaft end. This rotor was mounted, balanced, and burst at a speed of 84,630 rpm.

Simulated Rotor Number 35

This part was sintered to a density of 3.15 g/cm^3 and contained a long radial surface flaw on the back face. Ultrasonic inspection showed an internal flaw at a depth of 3.55 inches from the shaft end. This rotor burst at a speed of 80,060 rpm.

Simulated Rotor Number 59

This rotor had a sintered density of 3.11 g/cm^3, and contained a visual surface crack near the saddle. Ultrasonic inspection indicated an internal flaw at a depth of 3.5 inches from the shaft end, which appeared to line up with the surface flaw. This rotor was mounted, balanced, and spun to failure at 95,170 rpm. Figure 102 is a photograph of rotor 59 taken in the spin pit at the instant of failure. A strobe light exposing the film was triggered by a fragment of the rotor severing a wire wrapped in a coil on a paper tube surrounding the rotor; this tube is visible in the photograph.

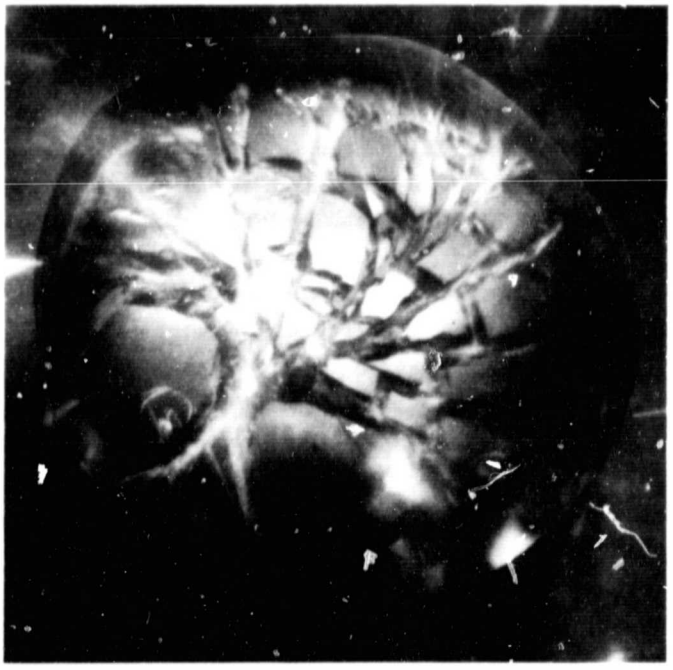

Figure 102. Burst of Simulated Rotor Number 57 at 95,170 rpm.

Simulated Rotor Number 199

This rotor was sintered to a density of 3.15 g/cm^3 and contained a visual linear indication about 3/4 inch long on the back face surface; this did not appear to be an open crack. Ultrasonic inspection revealed an internal defect 4.25 inches from the shaft end; this defect was felt to be a lamination running parallel to the back face surface. This rotor did not fail at a maximum speed of 134,000 rpm, which was the speed limit of the spin pit air turbine when spinning a component of this size and shape. Figure 103 is a photograph of this part after the spin test. Figure 104 is a stress analysis of this rotor at maximum speed, and indicates that a large volume of this part was subjected to high tensile stresses.

Simulated Rotor Number 201

This rotor was fabricated to the new design (i.e., the same size and contour as the bladed rotor hub). This part had a sintered density of 3.10 g/cm^3 and exhibited a few linear surface indications on the shaft/hub angled surface. Ultrasonic inspection located a flaw described as an axial lami-

Figure 103. Simulated Rotor Number 199 After Spin Test to 134,000 rpm.

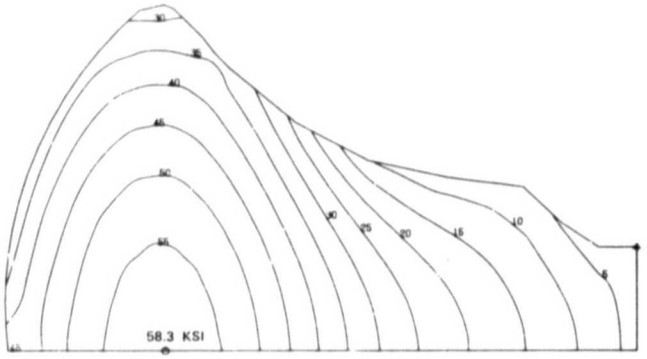

Figure 104. Principal Stresses in Simulated Rotor Number 199 at 134,000 rpm.

nation at a depth of 3 inches from the shaft end. This part did not fail at 137,000 rpm, the apparent spin pit air turbine speed limit for this part. Figure 105 is a photograph of this part after spin testing.

Figure 105. Simulated Rotor Number 201 After Spin Test to 137,000 rpm.

It is encouraging that the apparent quality improvements in simulated rotors, discussed earlier in this report, have been verified by the successful spin testing of rotors 199 and 201. These rotors were fabricated late in the reporting period, and incorporated the changes described earlier. It also is interesting to note that sectioned simulated rotor 198 (Figure 97), which contained no observed surface defects on the outer surface or the sectioned surface, also was evaluated by ultrasonic inspection and no internal defects were found. This rotor was fabricated at the same time and in the same manner as were rotors 199 and 201.

2. Task 2.7 - Stator - Ford

2.1 Molding Process Development

During this reporting period, work continued on the simulator system that takes the place of the molding machine during the development of the control programs. All the electronic components, software and equipment racks were ordered and received. The central processing unit of the simulator was checked out and is operational. Several interface chassis are in the process of being built and once checked out will be used to complete the assembly of the total simulator system.

2.2 Monolithic Stator Tool

The design of the injection molding tooling was modified to build more development flexibility into the tool. The original intent was to utilize the tool only on the vertical Tempcraft molding machine, which limited the maximum injection pressure to below 7700 psi due to clamping limitations. A minor redesign of the scroll actuating cylinder mounting system, the ejector plate access holes and a dual diameter mounting ring now makes the installation possible on both the Tempcraft and the Reed-Prentice machines. The horizontal Reed-Prentice has a much higher clamping capacity (450 vs 160 tons) and therefore a maximum injection pressure of 13,500 psi is possible.

The location of the cavity instrumentation was finalized and pressure transducers and thermocouples ordered. Pressures will be measured at the exit of the sprue/beginning of the circular runner and at two circumferential locations in the slotted shroud under both the leading edge and trailing edge ejector pins. Temperatures will be monitored at two circumferential locations in both halves of the tool at mid-radius of the vanes.

Previous experience with injection molding of complex shaped components has related cracks in the molded part to the parting of the tool and the insert removal processes. Therefore, considerable effort was spent to obtain the greatest flexibility possible in the sequencing of the parting lines/insert removal. Three sets of internal springs and five external hydraulic cylinders can be used in varying sequences during removal of the molded stator from the five surfaces which form the tool cavity.

During this reporting period the tool components were machined, hand fitted and a wax replica molded. Subsequently the tool was completely disassembled for hard chrome plating and final polishing of the die cavity.

3. Task 2.7 - Flow Separator Housing - Ford

3.1 Component Fabrication and Evaluation

Work during this reporting period encompassed the fabrication, NDE inspection, pressure testing, and strain gauging of the first flow separator housing (designated SN-8) delivered by Corning Glass Works.

SN-8 was mechanically tested, using the test fixture described in Reference 2, at 72 psi both as a partially machined casting and as a finished component. This test pressure was approximately 25 percent greater than the maximum mechanical load exerted on the component at full engine speed. No problems were encountered with either the test fixture or the component during these tests.

Following mechanical testing, SN-8 was visually inspected using dye penetrant and inspected using radiographic procedures. Visual inspection revealed two minor surface imperfections in the area of the wells formed by the double bulkhead or cross-arm. Radiographic inspection, however, did show a number of large voids in this component, particular in the lip area of the center bore. As a result of these findings, Corning was alerted and tooling changes were effected to correct this problem. Several castings were made with these tooling modifications. These castings were sectioned, and inspection revealed considerable improvement in casting quality.

The flow separator housing mechanical test fixture not only serves as a screening apparatus but also permits the correlation of 3D stress analysis with mechanical stresses encountered in engine operation. Fourteen uniaxial and seventeen triaxial strain gauges were attached to SN-8 in critical areas. Figures 106 and 107 show the component with strain gauges attached along with the mechanical test fixture and the data recording equipment. Strain gauge data were taken up to 60 psi in increments of ' psi both in air and water environments. These data currently are in the reduction process.

Figure 106. Ceramic Flow Separator Housing Showing Strain Gauges in Place.

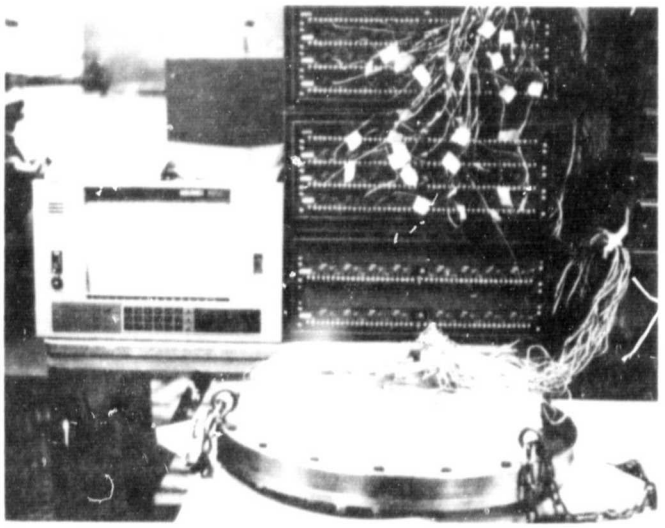

Figure 107. Ceramic Flow Separator Housing Mounted in Mechanical Test Fixture.

APPENDIX B

AIRESEARCH CASTING COMPANY (ACC)
ADVANCED GAS TURBINE (AGT) POWERTRAIN SYSTEM DEVELOPMENT PROGRAM
THIRD AGT SEMIANNUAL TECHNICAL
PROGRESS REPORT

1. TECHNICAL PROGRESS

Six simulated (bladeless) rotors were shipped to Garrett for evaluation and spin testing. The feasibility of fabricating bladed rotors by slip casting has been demonstrated. Forty-five x-ray and visually acceptable stator vanes have been processed through nitriding for delivery as engine quality hardware. Turbine shroud S/N 101 has been delivered and casting of other components has begun.

1.1 Rotor - Materials and Fabrication Development

1.1.1 Injection Molding Process

1.1.1.1 Forming Development

Late in 1980, injection molding was developed to the point where the simulated rotors could be molded with consistency and, upon immediate dissection were found to be free of voids and cracks. However, with shelf time, rotors were usually found to contain cracks. Further observation during dewax experiments showed that crack formation was occurring at the binder liquid-to-solid transition temperature during the initial cooldown, therefore, a procedure was implemented whereby all molded rotors were held at 100°F after injection (where the binder LN-266 is not brittle) which eliminated cooling cracks.

1.1.1.2 Binder and Dewax Development

Rotor fracture and/or blistering during a heated vacuum dewax cycle indicated that additional dewax study was needed. Initially, a study was performed to determine whether rotor hub size is a critical factor. For this evaluation, Configuration I crack-free molded rotors were reduced in size by lathe turning while under heat lamps to maintain them at 100°F. Configuration II and III rotors were machined and evaluated in the vacuum dewax cycle. Again, dewax cycles resulted in rotor cracking, indicating that rotor size is not a controlling variable.

Additional experiments using varied dewax cycles indicated that a nitrogen atmosphere may be superior to the vacuum cycle for LN-266 binder removal and that 10 to 12 psig of pressure may be superior to lower pressures. Under nitrogen pressure, rotor size also seems to be of secondary importance to atmosphere, pressure and temperature rates.

Additional evaluation of the injection molding process parameters has been postponed pending evaluation of more promising results in the slip casting approach. However, evaluation of binder removal parameters is continuing under ACC IR&D.

1.1.2 Slip Casting Process

1.1.2.1 Simulated Rotors

Development of slip cast simulated rotors has involved activity in four interrelated areas; casting slip stability, mold preparation, moisture removal and sintering.

1.1.2.2 Slip Stability

The basic formulation of the ACC rotor material is 88-weight percent high-purity Si_3N_4, 8-weight percent high purity Y_2O_3 and 4-weight percent high-purity Al_2O_3. When GTE SN502 Si_3N_4 powder is used, preconditioning of the many fine, needle-like crystallites is required to achieve an adequate suspension of high solids content in the slip. Additionally, the instability of Y_2O_3 powders in aqueous suspension requires the use of thermal treatments, comminution procedures and milling/suspension additives to obtain useable, stable slips. These treatments have been developed over the past several years (IR&D) efforts and have been applied to rotor fabrication; specifically to increase casting slip stability, to reduce casting time and to minimize density gradients

in the casting. Two of these procedures referred to as pre-reacted additives and as pre-calcined powder have been evaluated for rotor casting use. The pre-calcined powder method appears to yield best results to date and is the basis for the SNN-502 rotor process specification.

1.1.2.3 Mold Preparation

Mold preparation prior to the introduction of the casting slip becomes increasingly important as the size and cross-sectional thickness of the part to be cast increases. Two techniques for mold preparation have been incorporated during this reporting period. These are the use of ammonium alginate as surface treatment/release agent and controlled premoisturizing of the plaster portions of the mold.

1.1.2.4 Moisture Removal

The removal of moisture from a slip cast ceramic part is a critical step in producing a complex shape. Several drying procedures were evaluated for the simulated rotor shape during this reporting period; including vacuum drying, humidity chamber drying, dessicant drying, slow drying in vented containers, and temperature controlled stagnant air drying at various temperatures. The latter method, illustrated in Figure 108 appears to be the most satisfactory to date, because the chamber humidity can be monitored and easily adjusted via a low wattage heating system.

Knowledge gained through the use of this chamber will be used in additional studies to be performed in a microprocessor humidity controlled drying oven.

1.1.2.5 Statistical Study of Variable Interaction

A significant effort was made during the reporting period; to apply a fractional fractorial approach to the study of several steps in slip casting rotors in general, and simulated AGT rotors in particular. Discussion with Dr. Steve Sidik of NASA culminated in a parametric program plan to evaluate the interaction and influence of variables listed in Table 16. Because of practical limitations of 2 levels of variation in each of 9 selected variables, it was necessary to do some preliminary experimental extensions of process development

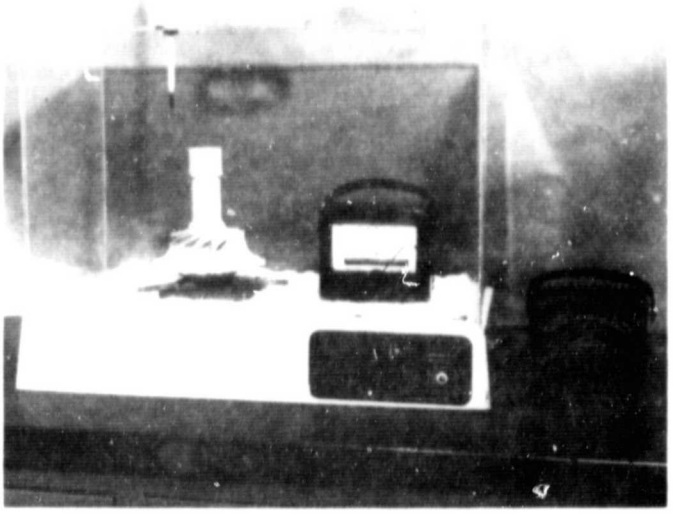

Figure 108. Stagnant Air Drying Chamber.

to have confidence that the levels selected were within range of potential success. The uncertainties were primarily in the drying conditions; atmosphere, peak temperature and heating rate. However, by the conclusion of this preliminary experiment, and prior to initiation of the matrix experiment, simulated rotors that appeared to be flaw free were being processed. Effort, therefore, was temporarily redirected at reproducing the apparent success, Figure 109. Delivery of six simulated rotors and a successful spin test, at Garrett, to 115-percent overspeed of one rotor led to a further redirection from fabrication of simulated rotors to an effort concentrating on bladed rotors. The variables associated with bladed rotors were sufficiently different from the earlier problem statement; therefore, a need for a major redesign of the experimental matrix was apparent. The acquisition of a microprocessor control system for the humidity/temperature chamber contributed to the decision to defer the statistical experiment until several programs utilizing that equipment on bladed rotors could be included.

1.1.2.6 Bladed Rotors

In April 1981, a metal version of the AGT bladed rotor, Figure 110, machined to final dimensions became available for experimental tooling development. This was used as a master from which a rubber mold could be fabricated. Subsequently, a rubber rotor pattern that duplicated the metal bladed rotor and included provision for gating was

TABLE 16. SLIP CASTING PARAMETERS TO BE EVALUATED

Process Step	Variable	Code	Level	
			- 1	+ 1
Slip	Gum Addition	A	No Gum	Gum Arabic
Slip	Powder	A	Calcined Si_3N_4 + Y_2O_3 + Al_2O_3	SI_3N_4 + $(3Y_2O_3 \cdot 5AL_2O_3)$*
Mold	Size	C	Undersize	Actual Hub
Mold	Plaster Location	D	Plaster Body	Plaster Dome
Drying	Pressure	E	Vacuum	One Atmosphere
Drying	Peak Temperature	F	150°F	200°F
Drying	Heating Rate	G	10°F/day	30°F/day
Sintering	Backfill Temperature	H	104°F	932°F
Sintering	Rate	J	6-day cycle	3-day cycle

* As YAG (Garnet structure)

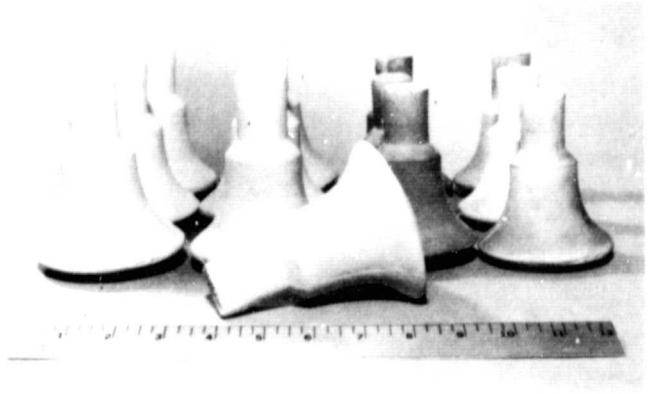

Figure 109. ACC AGT101 Simulated Rotors of SNN-522 in the Green (left) and Sintered (right) Condition.

produced. From that rubber pattern an organic investment casting shell mold, Figure 111, was prepared and subsequently, secured to a plaster-of-paris base incorporating the rotor backface shape. The two-part mold then was filled with silicon nitride slip for casting. After the casting process was completed, the shell mold was removed by dissolving in an organic solvent. On the initial casting, all blades were

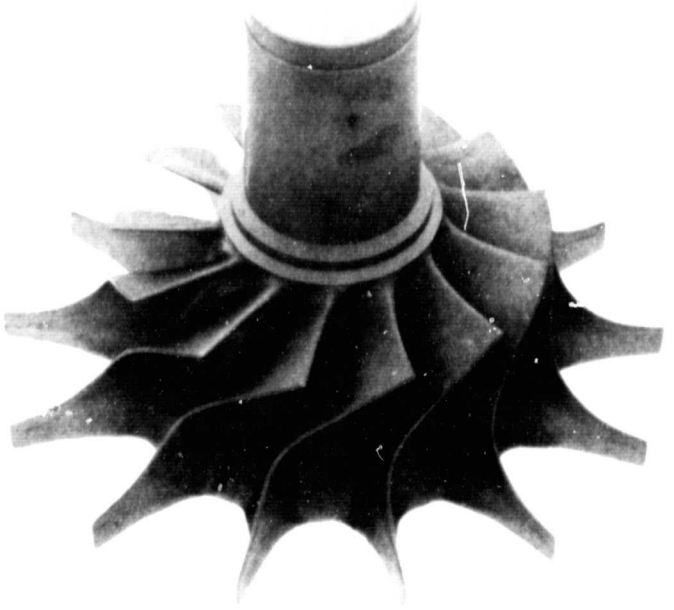

Figure 110. Metal AGT101 Turbine Rotor.

Figure 111. ACC AGT101 Bladed Rotor (left, in green state) and a Casting Shell.

intact. Many minor problems were apparent, such as parting line flash, incomplete blade fill due to lack of raisers, positives due to local wettability variations, and other common casting concerns with known cures. Additional rubber patterns were prepared so that a significant number of these rotors (although about 14 to 15 percent too small due to process dimensional shrinkage) could be produced and the casting defects resolved. By the end of this reporting period, two bladed rotors had progressed through the final sintering step illustrated in Figure 112, one of which exhibited some blade distortion and was forwarded to Garrett as a feasibility demonstration. Blade distortion will be discussed under Sintering (Section 1.1.2.7 of this appendix).

Also during this reporting period, arrangements were completed for the procurement of 20-rotor patterns molded from ACC water soluble wax in tooling that had allowance for 10-percent process shrinkage. These patterns are scheduled for delivery the week of July 6, 1981.

Dimensional measurements of sintered rotors of all configurations were compiled and plotted as a function of sintered density. From these curves a shrinkage factor for the SNN-502 process was established, allowing the preparation of documents from which tooling may be procurred. Competitive bids were obtained and a tooling procurement was initiated.

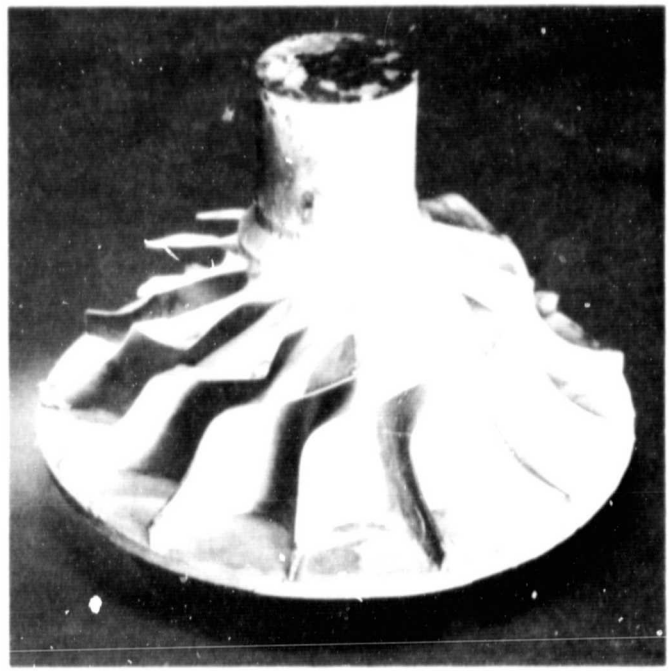

Figure 112. First Sintered ACC AGT101 SN-522 Bladed Rotor.

1.1.2.7. Sintering

Sintering of all rotor configurations during this reporting period was performed in a microprocessor controlled induction-heated furnace capable of operating with a vacuum of up to 70-psi nitrogen pressure. About 50-sintering runs were completed during this time, largely on AGT rotor hardware, confirming not only the flexibility of the control system, but also excellent reproducibility of a selected schedule so that subtle changes in loading arrangement, powder bed sintering, crucible confinement, covering techniques, etc, could be evaluated. Procedures were developed using bladeless rotor shapes to minimize weight loss, and achieve densities in excess of 3.15 g/cm^3 with good surface finish. These procedures were applied to the first bladed rotor and resulted in blade deformation. A second attempt, inverting the rotor and positioning it so that the majority of the rotor weight was supported by the shaft portion in a packed bed of Si_3N_4 powder, also resulted in blade distortion. In this case, differential shrinkage, large for rotor, virtually zero for the powder bed resulted in the distortion. This second rotor was forwarded to Garrett. Blade distortion is

not considered an insurmountable problem and additional studies are planned to optimize the bladed rotor sintering process.

1.2 BCD Ceramic Structures

1.2.1 Injection Molding Process

1.2.1.1 Turbine Stator

Tooling was received in February to injection mold individual turbine stator vanes. A parametric study was subsequently performed to establish injection procedures for this particular configuration and die. Upon completion of parametric studies, 63 stator vanes, free of visual and x-ray indications, were injected. After binder removal, forty-five of these were nitrided, Figure 113, for delivery to Garrett in July.

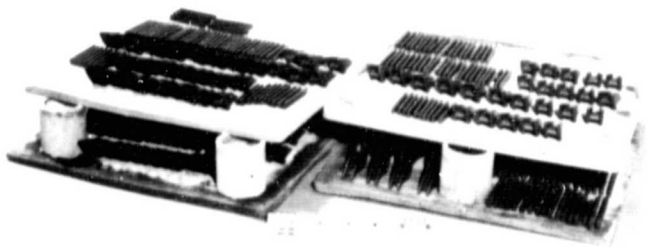

Figure 113. ACC RBSN AGT101 Stators and Test Bars in Nitriding Stack-Up.

The material originally proposed for stator vane fabrication was AirCeram RBN-126, which uses Fe as the nitriding aid. This material had a well established history, however, black spots, on the surface and interior, were often associated with this material. AirCeram RBN-124, containing Fe_2O_3, was offered as an alternate as it has a more uniform microstructure. Both materials were processed for evaluation of room temperature bend strength. Average strengths for all samples tested, more than 40 bars for each material, indicated RBN-124 was stronger than RBN-126, 39 versus 35 ksi as-nitrided. Eighty-five AirCeram RBN-124 test bars have been shipped to Garrett for further qualification.

1.2.1.2 Turbine Outer Diffuser Housing (RBN-104)

Tooling rework was completed and initial casting efforts showed that slip casting to form a reaction bonded silicon nitride component was a suitable process. A wax insert had been designed for the backside contour, but the first attempts showed that surface finish and dimensional control were not satisfactory. Temporary tooling was prepared to form a plaster-backed rubber liner of the same contour as the wax insert. This liner provided good surface finish, controlled dimensions and improved mold release.

Various levels of plaster prewetting and ammonium alginate application were evaluated. These evaluations were performed because difficulties were encountered in removing the part from the mold when the alginate layer was too wet at the time the mold was filled with casting slip. Part removal from the mold requires that a significant portion of the drying occur within the mold to provide shrinkage and release from the mold. Slow drying in the mold and increased drying time for the alginate layer have resulted in good castings using the improved rubber tooling concept. Optimization of the prewetting and alginate surface treatment should provide consistent, high quality casting of the outer diffuser and all other large, slip-cast components.

1.2.1.3 Turbine Inner Diffuser Housing (RBN-104)

Tooling was received for inner diffuser mold preparation. This tooling was fabricated according to net shape casting processes; this required significant component thickness variations. Initial casting resulted in the formation of cracks in several thinner locations in the part. Thus, mold modifications were made to provide a uniform thickness in the casting to strengthen the as-cast part. Subsequent casting trials indicated that the ring section in the lug and bolt hole region caused part-mold release difficulties in casting. Design analysis at Garrett showed this ring to be unnecessary so the tooling was reworked to remove it, parts cast in this mold were crack free but lacked material fill in the lug region as a result of casting shrinkage. An initial effort to reduce the nonfill by providing the as-cast bolt holes was only partially successful so a second modification was made to provide a reservoir for additional slip in the lug regions. These modifications currently are under evaluation.

1.2.1.4 Turbine Shroud (RBN-104)

The six-piece mold designed for the complex shroud configuration has been satisfactory in producing turbine shroud components, Figure 114. The thick cross-section, Figure 115, (0.5 to 0.75 inch) of this part provides the strength needed in this component during the critical mold removal and early handling processes.

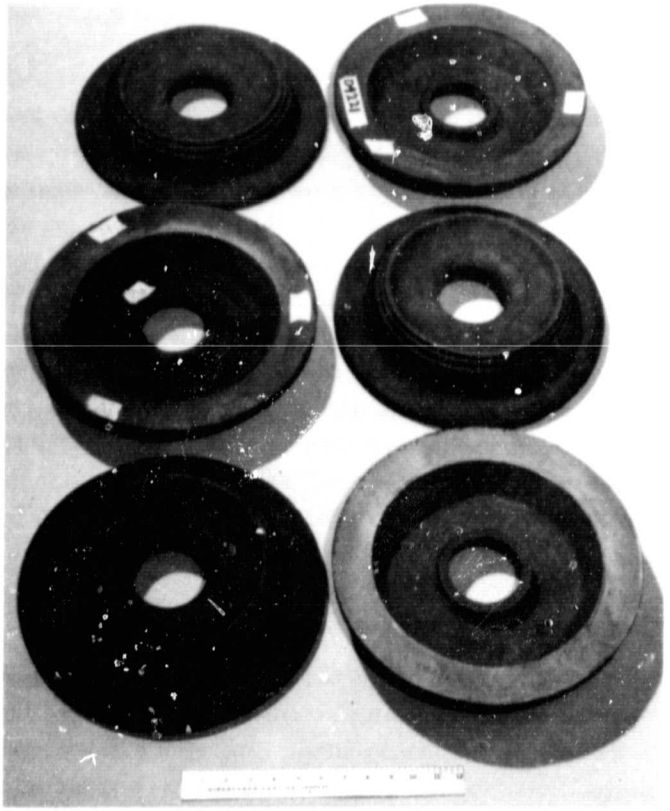

Figure 114. ACC Slip Cast RBSN AGT101 Turbine Shrouds.

Several turbine shroud castings have been nitrided to verify that the thick cross-section can be fully nitrided.

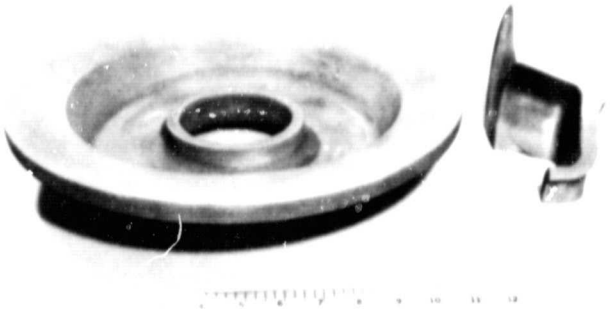

Figure 115. ACC AGT101 Turbine Shroud and Section.

Nitriding to 2.79 g/cm^3 with a 60.2 percent weight gain has been shown possible for this cross section. These results are satisfactory and demonstrate the feasibility of this aspect of processing.

Several improvements in molding technology were made during fabrication of this shroud. The first improvement incorporated the use of a reuseable rubber liner to form the backside contour. This liner simplified mold setup, mold removal, and provided improved dimensional control. A second modification to the tooling was the removal of all sharp edges from the castings which, otherwise, would act as stress concentration points and contribute to component failure in processing or in use. A final mold modification was made to provide additional machine stock based on experimental machining and handling evaluations at Garrett.

Once these modifications were completed, two shrouds were cast and pre-nitrided. S/N 101 was shipped to Garrett in June 1981 for green machining.

APPENDIX C

THE CARBORUNDUM COMPANY
(UNIQUE WORK)
ADVANCED GAS TURBINE (AGT) POWERTRAIN SYSTEM DEVELOPMENT PROGRAM
THIRD AGT SEMIANNUAL TECHNICAL
PROGRESS REPORT

1. BACKGROUND

This report summarizes work performed by The Carborundum Company during the period from January 1, 1981 to June 30, 1981 for Garrett Turbine Engine Company on the Advanced Gas Turbine Powertrain System Development Program authorized under NASA Contract DEN3-167 and sponsored by the Department of Energy (DOE).

As a major subcontractor to the program, Carborundum is required to develop silicon carbide components for the AGT hot flowpath.

To date, injection molding, slip casting, and green machining have been selected for fabrication of silicon carbide components for the program.

Ceramic fabrication technology has been successfully demonstrated to produce complex shapes economically with a high degree of precision on small items such as backshrouds, stator vanes and duct spacers and on large components such as turbine shrouds, combustor baffles and transition ducts. At the initiation of this program, maximum cross sections were limited to components not exceeding 1 inch. Recent technical process advances have significantly extended cross section capabilities so that now large and/or complex components can be successfully fabricated. In addition, two new versions of SiC designated Hexoloy KX-01 and Hexoloy KX-02 have been developed. These new materials appear to have strength properties that are applicable to a variety of components including the rotor.

The current program involved activities related to the development of a rotor and activities related to the development of static structures showing the progress being made towards producing the required deliverables using various fabrication methods.

2. ROTOR DEVELOPMENT

The early part of the rotor development program evaluated a variety of ceramic-to-ceramic bonding methods applied to the assembly of smaller components to produce an integral rotor.

2.1 Bonded Rotor Development

Further characterization of the hot pressed core material which is to be bonded to injection molded rotor shells had densities of 3.15 g/cm^3 or greater. Fracture strengths measured for test bars cut from representative core material ranged from 35,000 to 77,000 psi with an average of 54,000 psi.

Prior work had indicated that strengths in the 80,000 psi range could be achieved; however, the average core, with an overall thickness of 2.8 inches, exhibited approximately 30 percent lower strengths than projected on bars cut from 1/4-inch thick hot pressed plates. An evaluation indicated the existence of high density inclusions scattered throughout the bars. Further analysis showed that these inclusions consisted of agglomerates rich in Fe and Ni.

It is presumed that the inclusions originate from impurities. Earlier work, from which the 1/4-inch thick plates were produced using the same lot of material, and densification aiding showed no high density inclusions.

Although not yet confirmed, it is presumed that a migration mechanism exists which allows the inclusions to dissipate from relatively thin cross-sections but becomes increasingly difficult as part thickness increases. In view of these findings, mutual agreement was reached by Carborundum and Garrett whereby rotor development using this method was halted until additional work was justified.

2.2 Solid Rotor

Development activities emphasized the fabrication of a solid injection molded rotor. The tool modifications necessary to produce a void-free injection molded one-piece rotor were completed. The plate containing the spherical bottom detail was attached to a separate hydraulic system. After packing during the molding cycle, a secondary compaction was initiated and held during cooling.

The first molding used the compound that was used at the outset of the program, and from which shapes were formed containing voids. The process modification that involved a secondary compaction sequence resulted in a dense void-free mold. The technique, therefore can be used to produce thick injection molded shapes that otherwise would have internal defects and/or sink marks. Subsequent baking of the molded shapes indicated problems in baking and resulted in cracked components.

A second molding run, using a new molding compound, was conducted. Dense, void-free moldings were produced and were baked out successfully. Densification during sintering was achieved but the components exhibited cracking. The sintering cycle has to be optimized for injection molded thick shapes.

Because of the significant advantages discovered in the development of a solid simulated rotor, future rotor development will include the use of the new molding compound and will use molds designed for a secondary compaction step.

2.3 Rotor Materials

The approach to rotor development was to investigate several fabrication techniques which were to be narrowed down until a process having a high probability of success could be identified. To date, the process has been identified (i.e., injection molding using the new binder composition). The material with the performance potential needed for a rotor must be selected. A list of candidate silicon carbide materials evaluated for the program is shown in Table 17. Garrett's initial requirements for a rotor material is characterized by a strength of 68,000 psi and a Weibull of 12. From Table 17, the materials which approach these initial requirements are Hexoloy KX-01 and Hexoloy KX-02.

TABLE 17. SILICONE CARBIDE MATERIALS EVALUATED FOR SIMULATED ROTOR

Material	Trademark	77°F		2012°F		2192°F	
		Average MOR (Population)	m	Average MOR (Population)	m	Average MOR (Population)	m
Sintered Alpha SiC(2)	Hexoloy SA	61.5 (30)	5.8	--	--	57.5 (30)	6.0
Hot Pressed SiC(1)	--	54.0 (30)	--	--	--	--	--
Thixocast RBSiC(2)	Hexoloy KT	36.9 (30)	3.1	--	--	57.7 (30)	17.0
Fine Grain RBSiC(2)	Hexoloy KX-01	68.6 (9)	6.6	69.5 (10)	17.5	--	--
Ultra Fine Grain RBSiC(1)	Hexoloy KX-02	53.6 (10)	--	--	--	105.6 (10)	--

Results for 4 Point Flexure Test, 1.5 inch outer span, 0.75 inch inner span

(1) Test Bar Cross Section: 0.1 x 0.2 Inches

(2) Test Bar Cross Section: 0.250 x 0.125 Inches

3. STATIC STRUCTURES

3.1 Turbine Stator

The injection molding process was selected for the development of the stator segments from Hexoloy SA, a sintered alpha silicon carbide material.

After receipt of the injection molding tool, a program was carried out to evaluate the effect of key molding variables; such as temperatures, pressures, and injection velocities; on the molded part quality. Completion of molding parameter optimization, a series of vanes were molded to process through the baking and sintering steps. The baking was accomplished satisfactorily. Trial sintering runs produced parts with shroud distortion when the segments were free standing in the furnace.

The major thrust of the development activity during this period consisted of designing, building, and evaluating support fixtures to prevent shroud distortion during sintering. Six fixtures were tested. The most effective was one that used a fixed spacer at the trailing edge of the airfoil between the shroud tips.

During the molding and sintering development phase, the design and fabrication of a fixture for use in grinding was initiated. This work progressed to the point where ceramic hardware was required to complete the job. Two sets of sintered vanes were used for the completion of the fixture and to commence the grinding development activity.

3.2 Turbine Shroud

Injection molding was selected to produce the turbine shroud in Hexoloy SA since the part has a variable wall and precise contours. Since the finished part weighs approximately 10 pounds, it represents the largest single piece ever injection molded in this material. To fill the mold, a flow molding sequence on a 300-ton press was used. The flow molding technique uses the machine screw for partial filling followed by forward screw motion for final packing. The technique allows a large part to be formed in a relatively small press.

The initial molding trials were conducted using a microprocessor equipped 300-ton machine. Machine conditions were determined to produce parts that were completely filled. The best shrouds produced initially had a high incidence of flow and weld lines that could not be eliminated.

The injection molding tool was reworked to enlarge the gate and to provide a larger sprue bushing. Subsequent molding trials were conducted using the same flow molding technique. Results indicated that tool modifications were beneficial in reducing the flow and weld lines; however, the flow and weld liner could not be completely eliminated.

Subsequent baking and sintering steps showed that the weld lines were sites at which cracking was initiated. A decision was made to abandon the flow molding technique and to seek a press with single shot capacity. A 800-ton, 145-ounce press was located and arrangements were made to conduct future molding.

3.3 Combustor Baffle

Slip casting was selected as the fabrication method appropriate to produce the combustor baffle in Hexoloy SA.

At the start of the AGT program, the normal slip casting process produced a fairly consistent and uniform wall thickness of up to 0.25 inch. Thicker walls were achieved but were frequently non-uniform. Since the combustor baffle has a designed wall thickness of 0.400 inch, a major development effort was required to increase the casting thickness capability to produce the part to print.

Several casting procedures and formulations were evaluated. Those showing the most promise consisted of bimodal grain size distributions. Slip compositions were optimized and shrinkage rates were established.

The original model used to fabricate the mold was reworked to accommodate the new shrinkage obtained with the bimodal slips. Approximately 30 pieces were cast and successfully processed through the drying step. These pieces currently are being used for machining studies and determining optimum sintering conditions.

3.4 Regenerator Shield

Nine regenerator shields were completed and delivered. Green machining isopressed tubes and finish grinding after sintering was the fabrication method selected for this component.

3.5 Turbine Backshroud

Six turbine backshrouds were delivered. These articles were produced by green machining isopressed billets followed by finish grinding after sintering.

3.6 Transition Duct

The initial fabrication procedure selected to produce the transition duct was slip casting. Difficulties encountered in achieving dimensional requirements on the inner surface and on the tab projections suggested that the alternate fabrication method be implemented. The alternate method uses green machining of an isopressed billet. During this reporting period, special bags were procured for the isopressing operation, templates were procured for machining contours and a special mandrel was obtained.

REFERENCES

1. Garrett Turbine Engine Company, "Advanced Gas Turbine (AGT) Powertrain System Development for Automotive Applications", Semiannual Progress Report Number 1 (October 1979 through June 1980), Report No. NASA CR-165175, November 1980, Contract No. DEN3-167.
2. Garrett Turbine Engine Company, "Advanced Gas Turbine (AGT) Powertrain System Development for Automotive Applications", Semiannual Progress Report Number 2 (July 1980 through December 1980), Report No. NASA CR-165329, June 1981, Contract No. DEN3-167.
3. K. W. Benn. W. D. Carruthers, "3500 Hour Durability Testing of Commercial Ceramic Materials", Third Quarterly Progress Report, Report No. 31-2857(09) December 15, 1976, Contract No. DEN3-27, Garrett Turbine Engine Company, Phoenix, AZ.